Numerical Study of Oil Displacement by Three Hydrocarbon Phases

by

Zhongguo Xu

A thesis submitted in partial fulfillment of the requirements for the degree of

Master of Science

in

Petroleum Engineering

Department of Civil and Environmental Engineering
University of Alberta

Abstract

Solvent injection is a widely used method to enhance oil recovery (EOR). Mixtures of reservoir oil and solvents can exhibit complex multiphase behavior at temperatures typically below 120°F, in which a third solvent-rich liquid (L_2) can coexist with the oleic (L_1) and gaseous (V) phases. Reliable design of such gas injection requires a detailed understanding of oil recovery mechanisms in three-hydrocarbon-phase flow.

In prior research, three-hydrocarbon-phase displacement exhibited a higher level of miscibility with leaner gas (i.e. at a higher level of methane dilution), which resulted in a nonmonotonic trend of oil recovery with respect to gas enrichment. However, no theoretical explanation was given as to why oil displacement was more efficient at a lower level of gas enrichment. Details of oil recovery in three-hydrocarbon-phase flow are not fully understood.

This research is concerned with details of oil recovery in three-hydrocarbon-phase flow by use of compositional simulation. First, the mass transfer on multiphase transitions between two and three phases is studied for oil displacement by three hydrocarbon phases. Simple conditions are derived for the multiphase transitions that yield high local displacement efficiency by three hydrocarbon phases. A nonmonotonic trend of oil recovery can occur when local oil displacement by three hydrocarbon phases becomes more efficient, but slower, with decreasing pressure or decreasing gas enrichment.

Secondly, an improved method for robust phase identification is developed and implemented in a 1D convective flow simulator with no volume change on mixing. This part of research is important for further confirmation of the oil-displacement mechanisms identified for three-hydrocarbon-phase flow at different flow conditions (e.g., different relative permeabilities). The new method uses tie triangles and their normal unit vectors tabulated as part of the simulation input information. The method can properly recognize five different two-phase regions surrounding the three-phase region; the two two-phase regions that are super-CEP, and the three different two-phase regions that originate with the corresponding edges of the three-phase region in the sub-CEP region.

Finally, the displacement mechanisms of three-hydrocarbon-phase flow derived in a preceding part are confirmed by use of different relative permeability models for various oil displacements. Simulation results confirm that the effect of relative permeability on displacement efficiency diminishes as the miscibility level increases. The distance parameters derived before can properly represent the interaction of phase behavior and mobilities since they are derived from mass conservation, not only from thermodynamic conditions.

Acknowledgments

I would like to express my sincerest love to my family, my parents, my sister, for their unflagging support and endless love, throughout my studies.

I am very thankful to my supervisor, Dr. Ryosuke Okuno, for having faith on me, for giving me an opportunity to work on this project, for all of his encouragement and support. I would like to thank Dr. Ergun Kuru and Dr. Juliana Leung, my examining committee members.

This research is supported by research grants from the Natural Sciences and Engineering Council of Canada (RGPIN 418266) and Japan Petroleum Exploration Co., Ltd. I has received a scholarship from the China Scholarship Council. These supports are gratefully acknowledged. I also thank Dr. Kamy Sepehrnoori for providing the UTCOMP simulator. Flow simulations in this research were conducted using the computational facility of Compute Canada.

I am thankful to Cui Wang, Bo Zhang, and Arun Venkat Venkatramani for their valuable guidance and suggestions that are helpful in improving my reservoir engineering skills. Finally, I would like to thank all those who helped and inspired with me throughout my research.

Table of Contents

List of Tables

List of Figures

Chapter 1: Introduction

In this chapter, the practical significance of three-hydrocarbon-phase displacement is first presented. Then, the methods to model three-hydrocarbon-phase behavior and their corresponding observations are summarized. Next, types of research problems addressed in this research are given. Finally, main objectives of this research are listed.

1.1 Three-Hydrocarbon-Phase Displacement

Solvent injection is a widely used method for enhanced oil recovery (EOR) (Lake 1989; Orr 2007). Mixtures of oil with solvent can exhibit three-hydrocarbon-phase behavior at reservoir conditions, where the solvent-rich liquid (L_2) phase coexists with the gaseous (V) and oleic (L_1) phases. This three-hydrocarbon-phase flow has been observed in the displacements for a wide variety of oil reservoirs: in West Texas (Tanner et al. 1992), in Alaska (McGuire et al. 2001), in Canada (Malik and Islam 2000), and in the North Sea (Varotsis et al. 1986).

The three-hydrocarbon-phase equilibrium on 1D displacement of oil by solvent is rarely detrimental (Henry and Metcalfe 1983; Creek and Sheffield 1993; DeRuiter et al. 1994). Recovery at 1.2 pore volume injected (PVI) is more than 90% in the slim tube test. Shelton and Yarborough (1977) also showed that the oil recovery is around 90% in the corefloods involving three-hydrocarbon-phase flow. Creek and Sheffield (1993) speculated that the L_2 phase acts as a cosolvent by displacing the oil efficiently.

The main difference between two- and three-phase displacements is that the latter involves multiphase transitions between two and three phases. However, the phase transition between one and two phases in two-phase displacement is comparably simple. Since the three-hydrocarbon-phase displacement is complex,

different methods were used to model three-hydrocarbon-phase behavior and to investigate the mechanisms of three-hydrocarbon-phase displacement, such as slim tube test and numerical simulation with an equation of state (EOS).

1.2 Modeling of Three-Hydrocarbon-Phase Behavior

Multiphase behavior of solvent and oil mixtures is conventionally presented with a pressure-composition (P-x) diagram (Orr and Jensen 1984; Creek and Sheffield 1993). Three-phase equilibrium occurs within a pressure range at high solvent concentrations on a P-x diagram at temperature typically less than 120°F. Two-liquid phases can coexist at higher pressures above the three-phase region. A P-x diagram represents a cross section of phase behavior along the mixing line between two compositions at a fixed temperature. Thus, a P-x diagram shows only a small portion of phase behavior that spans pressure-temperature-composition (P-T-x) space.

In composition space, a three-phase region can be considered to be bounded by a lower critical endpoint (LCEP) and an upper critical endpoint (UCEP). A critical endpoint (CEP) is a critical state where two of the three equilibrium phases become critical (Uzunov 1993). The LCEP is the CEP where the L_1 and L_2 phases merge in the presence of the V phase (L_1=L_2-V), and the UCEP is the CEP where the V and L_2 phases merge in the presence of the L_1 phase (L_1-L_2=V). **Appendix A** presents a schematic for such a bounded three-phase region for four components (Okuno et al. 2011). A CEP is a tie line, instead of a point, as shown in **Fig. A-1.** Therefore, a CEP is sometimes called a CEP tie line to avoid potential confusion in this research.

A number of authors presented experimental phase behavior studies for these heavy oils; the West Sak oil (Shu and Hartman 1988; Sharma et al. 1989; Roper 1989; Hornbrook et al. 1991; Okuyiga 1992;

DeRuiter et al. 1994; Mohanty et al. 1995; McGuire et al. 2005), the Schrader Bluff oil (Reid 1994; Inaganti 1994; McKean et al. 1999; Khataniar et al. 1999; Wang and Strycker 2000; Madarapu et al. 2002), and the Kuparuk oil (Godbole et al. 1995). The primary recovery and waterflooding were relatively inefficient in these heavy-oil reservoirs due mainly to high oil viscosity. Conventional thermal methods were considered to be impractical because of high well costs, large well spacing, and thick permafrost (McGuire et al. 2005). Solvent injection has been studied because Prudhoe Bay artificial lift gas and Prudhoe Bay natural gas liquid are both available as solvent. Mixtures of heavy oils and solvent can exhibit complex multiphase behavior at the low reservoir temperature (50-100°F). Multiphase behavior involving the L_1, L_2, and V phases was observed in their static experiments and slim-tube tests.

Modeling of the complex three-phase behavior has been also conducted using various EOSs; e.g., the van der Waals EOS (van Konynenburg 1968; Scott and van Konynenburg 1970; van Konynenburg and Scott 1980; Bluma and Dieters 1999), the Redlich-Kwong EOS (Deiters and Schneider 1976; Deiters and Pegg 1989), the Peng-Robinson (PR) EOS (Gauter 1999; Gauter et al. 1999; Mushrif 2004; Yang 2006; Mushrif and Phoenix 2008), and the Soave-Redlich-Kwong (SRK) EOS (Gregorowicz and de Loos 1996). Their results show that a cubic EOS is capable of predicting three-phase behavior (van Konynenburg 1968).

1.3 Investigation of Oil Displacement by Three Hydrocarbon Phases

Reliable design of solvent injection requires detailed understanding of oil displacement mechanisms. Displacement theory for solvent injection has been established for conventional two hydrocarbon phases (Orr 2007). Multicontact miscibility (MCM) between two phases can be developed through vaporizing, or condensing, or combined condensing/vaporizing mechanisms (Johns 1992; Dindoruk 1992). An important

design parameter for solvent injection is the thermodynamic minimum miscibility pressure (MMP). The thermodynamic MMP is the minimum displacement pressure at which complete miscibility is developed along a composition path from the injection gas composition to the reservoir oil composition for one dimensional (1-D) flow in the absence of dispersion. Efficient methods have been developed for MMP calculation, where phase behavior and flow are effectively decoupled (e.g., Johns and Orr 1996; Ahmadi and Johns 2011).

However, oil displacement by three hydrocarbon phases is difficult to interpret even for 1-D flow with no gravity (DeRuiter et al. 1994). As mentioned before, theory has been well established for gas floods involving simple two-phase equilibrium (Orr 2007). An MCM composition path goes through a two-phase critical point, and is interpreted as the limit of two-phase displacements. However, the mechanism for MCM development is unknown for three-hydrocarbon-phase displacement.

Okuno et al. (2011) presented a detailed study of three-phase behavior predictions and displacement efficiency for low-temperature CO_2 floods using the UTCOMP simulator. The UTCOMP simulator is an EOS compositional multiphase reservoir simulator developed at the University of Texas at Austin. They used four components to conduct a systematic investigation of oil displacement mechanisms involving three phases bounded by the UCEP and LCEP tie lines. Results showed that high efficiency of low-temperature oil displacements by CO_2 occurs when the composition path traverses near the UCEP and LCEP tie lines. Oil components are efficiently extracted by the L_2 phase because of near-LCEP behavior at the leading edge of three phases. Near-UCEP behavior at the trailing edge of three phases then allows the L_2 phase to efficiently merge into the V phase. That is, the L_2 phase serves as a buffer between the immiscible V and L_1 phases

within the three-phase region. They also confirmed this displacement mechanism for multicomponent systems based on west Texas oils.

Although nearly piston-like displacements were simulated with three phases bounded by the CEP tie lines, it was uncertain how MCM can be developed through the CEP behavior. They used the distance between the L_1 and L_2 phase compositions $d_{L1-L2} = \left\| \underline{x}_{L1} - \underline{x}_{L2} \right\|_2$ as a proximity measure for the LCEP tie line, where $\underline{x}_j$ is the composition vector of equilibrium phase j. Similarly, $d_{L2-V} = \left\| \underline{x}_{L2} - \underline{x}_{V} \right\|_2$ was used as a proximity measure for the UCEP tie line. While $d_{L2\text{-}V}$ monotonically decreased as oil recovery at 2.0 hydrocarbon-pore-volumes injected (HCPVI) became higher, $d_{L1\text{-}L2}$ did not exhibit the same trend. Even though 500 gridblocks were used in most of their 1-D simulations using an implicit-pressure explicit-concentration (IMPEC) simulator, numerical dispersion effects were significant near the leading edge of three phases. This likely explains the non-monotonic trend of $d_{L1\text{-}L2}$ with respect to displacement efficiency in their research.

1.4 Problem Statement

Prior studies showed that 1-D oil displacement with three hydrocarbon phases can exhibit the displacement efficiency that is non-monotonic with respect to gas enrichment at a given throughput. DeRuiter et al. (1994) and Mohanty et al. (1995) conducted slim-tube experiments for the West Sak oil with enriched gas. Their results showed that oil recovery at 1.2 pore-volumes injected (PVI) first decreased, then increased, and finally decreased again with decreasing gas enrichment. Oil recoveries at 1.2 PVI were 97%, 87%, 89%, 93% and 65% at 32%-, 42%-, 51%-, 62%-, and 70%-methane dilution, respectively. A maximum of 93% at 62%-methane dilution was substantially higher than 87% at a lower methane dilution of 42%.

DeRuiter et al. (1994) speculated that the nonmonotonic trend was associated with the coexistence of three hydrocarbon phases and its effects on the front mobility. The improvement in mobility ratio can improve sweep efficiency in multidimensional floods (Mohanty et al. 1995). However, the effect of miscibility (i.e., compositional phase behavior) would dominate over the fractional flow effect in terms of local displacement efficiency in this partially miscible (PM) flow with significant mass transfer among phases. Mohanty et al. (1995) later explained that oil recovery at 1.2 PVI was higher at 62%-methane dilution than at 51%-methane dilution because (1) the L_2 phase was nearly miscible with the L_1 phase at the three-phase displacement front, (2) oil became less viscous at the front, and (3) the front moved fast enough to exit the slim tube by 1.2 PVI.

The existing theory of gas injection does not explain a nonmonotonic trend of PM displacement efficiency. The length of the shortest tie line monotonically decreases as pressure or gas enrichment increases in the conventional two-phase displacement when the fluid is properly characterized (Ahmadi 2011). Thus, the efficiency of the conventional two-phase displacement tends to increase monotonically until MCM is approached. A question then arises as to why the efficiency of three-hydrocarbon-phase displacement can decrease as gas enrichment (or displacement pressure) increases, because no detailed theoretical explanation has been given in the literature as to what causes gas enrichment to decrease oil recovery. The main novelty of this research is to perform a detailed and systematic investigation of oil displacement in three-hydrocarbon-phase flow by use of numerical simulation.

1.5 Research Objectives

This research aims to explain details of oil displacement in three-hydrocarbon-phase flow in a systematic

manner. To achieve the objective, the following tasks are set:

1. Explain why oil recovery can exhibit a nonmonotonic trend with respect to displacement pressure and enrichment.

   For this task, simulations are performed at different gas enrichments and non-monotonic oil recovery are reproduced. The interaction between phase behavior and flow is analyzed by use of the mass conservation equations on multiphase transitions.

2. Develop a 1-D convective flow simulator with no volume change on mixing for three-hydrocarbon-phase flow

   Appropriate mass conservation equations are solved by a finite-difference method. The main complexity is the flash calculation module, in which three phases should be robustly calculated and phases should be properly identified.

3. Confirm the mass transfer mechanisms in the 1-D convective simulator by use of different relative permeability parameters for various oil displacements.

   The robust algorithm for phase identification is important for this task. The theory developed in part 1 is confirmed for a wider variety of conditions.

Chapter 2: Mass Transfer on Multiphase Transitions in Three-Hydrocarbon-Phase Displacement

In this chapter, the performance of nonmonotonic oil recovery is first introduced by use of a simple quaternary system. Then, mass transfer across phase transitions is analytically analyzed. Next, nonmonotonic oil recovery is explained for the preceding quaternary system and a multicomponent system.

2.1 Nonmonotonic Oil Recovery by use of a Quaternary System

This section describes the nonmonotonic oil recovery using a quaternary fluid, which is based on the Schrader Bluff Oil model in Guler et al. (2001). Fine-scale compositional simulations are performed for linear oil displacement with no gravity. The UTCOMP simulator (Chang et al. 1990) with the PR EOS (Peng and Robinson 1976) is used for all flow simulations in this research. The UTCOMP simulator has been used in various papers on gas injection theory (e.g., Mohanty et al. 1995; Johns et al. 2000, 2004; Solano et al. 2001).

The four components consist of one light pseudo component (PC1), one intermediate pseudo component (PC2), and two heavy pseudo components (PC3 and PC4). This heavy quaternary fluid is referred as HQ oil in this research. This oil will be used again in the next chapters of this thesis. Their properties are given in **Tables 2.1 and 2.2.** The oil gravity is calculated to be approximately 10°API. The injection gas consists of 20% PC1 and 80% PC2.

Fig. 2.1 shows the P-T diagrams calculated for the quaternary oil and injection gas using the PVTsim software. The bubble-point pressure at the reservoir temperature of 86°F is 1953 psia for the oil. The bubble-

and dew-point pressures at 86°F are 658 psia and 334 psia, respectively, for the injection gas. The critical point of the injection gas is calculated to be 144.88°F and 836.38 psia.

Fig. 2.2 gives the P-x diagram calculated for mixtures of the oil and the injection gas at 86°F using the PVTsim software. Two immiscible liquid phases are present at a wide range of solvent concentrations. Three phases exist between the L_1-L_2 region and the L_1-V region. Mixing of a small amount of the oil with the injection gas causes three-phase behavior at pressures between 211 psia and 658 psia. Similar phase behavior was presented for Alaskan North Slope heavy oils and solvents in Okuyiga (1992), Godbole et al. (1995), Khataniar et al. (1999), McKean et al. (1999), Guler et al. (2001), and Wang et al. (2003).

Table 2.3 shows the reservoir properties used in simulations in this research. The relative permeability is based on the Corey model. The number of gridblocks is 1000 with a uniform gridblock size of 1 ft in the displacement direction. The initial water saturation is at the residual saturation of 0.4, and water does not flow in all simulations in this study. Gas injection is continued until the trailing edge of the three-hydrocarbon-phase region reaches the outlet when three phases are present. The quaternary oil displacements are performed at different pressures 500 psia, 600 psia, 700 psia, 800 psia, 1000 psia, 1500 psia, 1750 psia, and 2500 psia.

Fig. 2.3 presents that the displacement efficiencies at 2.0 HCPVI are 71.76%, 72.18%, 78.42%, 78.69%, 78.39%, 69.59%, 62.30%, and 59.27% at 500 psia, 600 psia, 700 psia, 800 psia, 1000 psia, 1500 psia, 1750 psia, and 2500 psia, respectively. A maximum of 78.69% is observed at 800 psia, and the oil recovery at 2.0 HCPVI becomes substantially lower at higher pressures. Three phases are present for the displacements at pressures from 500 psia to 1750 psia, but not at 2500 psia. The 1-D oil recovery at 800 psia is 19% more efficient than that at 2500 psia at 2.0 HCPVI.

Local displacement efficiency at PM conditions depends on the level of miscibility, which affects propagation rates of components. Phase behavior during the displacement is then determined by the resulting compositional variation at the operating pressure and temperature. Fig. 2.3 also shows oil recovery at breakthrough of the trailing edge of the three-phase region to see the local displacement efficiency by three phases. The trailing edge of the three-phase region reaches the producer at 1.13 HCPVI at 700 psia, 0.95 HCPVI at 800 psia, 0.89 HCPVI at 1000 psia, 0.73 HCPVI at 1500 psia, and 0.64 HCPVI at 1750 psia. Since the trailing edge of the three-phase region is extremely slow at 500 psia and 600 psia, it is not shown for these pressures. Fig. 2.3 indicates that the local displacement by three phases becomes less efficient, but propagation of three phases becomes faster with increasing pressure between 700 psia and 1750 psia. For example, even though propagation of three phases is faster at 1750 psia than at 800 psia, the local displacement by three phases is less efficient at 1750 psia than at 800 psia. As a result, the displacement efficiency at a fixed throughput of 2.0 HCPVI is 16% higher at 800 psia than at 1750 psia as shown in Fig. 2.3.

Fig. 2.4 presents the composition path and phase behavior in the displacement at 700 psia. As the pressure is below the bubble point (1953 psia at 86°F), the initial oil is in the V-L_1 region. The tie triangle at the leading edge of the three-phase region is elongated, and the L_1 and L_2 phases are close to each other. The distance between the L_1 and L_2 compositions is 0.0547 at the leading edge. The tie triangle changes its size and shape in the three-phase region as shown by a few shaded tie triangles in Fig. 2.4. The tie triangle at the trailing edge of the three-phase region shows that the coexisting phases are highly immiscible with each other. On this tie triangle, the distance is 0.6875 for $\left\|\underline{x}_{L_1} - \underline{x}_V\right\|_2$, 0.3956 for $\left\|\underline{x}_{L_2} - \underline{x}_V\right\|_2$, and 0.6835 for

$\left\| \underline{x}_{L_1} - \underline{x}_{L_2} \right\|_2$, where $\underline{x}_j$ is the composition of equilibrium phase j. The tie lines in the two-phase regions on the upstream and downstream sides also show their immiscibilities.

Figs. 2.5-2.8 show the profiles of component concentrations, phase mole fractions, phase saturations, and phase densities at 0.33 HCPVI at 700 psia. In Fig. 2.5, the PC4 concentration is significantly reduced at the three-phase leading edge, and the PC3 concentration becomes essentially zero in the three-phase region. As a result, the amount of the L_1 phase rapidly decreases at the three-phase leading edge in Figs 2.6 and 2.7. The efficient oil displacement is achieved because of the high concentration of the denser injection component PC2 in the three-phase region as shown in Fig. 2.5. Fig. 2.8 shows that the densities of the L_1 and L_2 phases are close to each other at the three-phase leading edge.

Fig. 2.9 presents the overall molar flow $\sum_{j=1}^{N_P} \rho_j x_{ij} f_j$ for component i, where ρ_j is the molar density of phase j and x_{ij} is the concentration of component i in phase j. The overall molar flow of PC2 is higher than that of PC1 upstream of the three-phase leading edge. The fast propagation of the denser injection component yields efficient oil displacement by rich gas as presented in Figure 2.8.

Figures 2.10-2.13 show the profiles of component concentrations, phase mole fractions, phase densities, and overall molar flows at 0.33 HCPVI at 1000 psia. The same set of figures is given for the displacement at 1750 psia in **Figs. 2.14-2.15.** The displacement of PC4 at the three-phase leading edge becomes less efficient with increasing pressure as shown in Figs. 2.5, 2.10, and 2.14. Also, the PC3 concentration upstream of the trailing edge of the three-phase region increases with increasing pressure.

The L_2 phase is important in transporting solvent components. However, Figs 2.9, 2.13, and 2.15 shows that the overall molar flow of PC2 becomes lower compared to that of PC1 in the three-phase region as pressure increases. The solvent that contacts the L_1 phase at the three-phase leading edge becomes leaner as

pressure increases. This solvent propagation behavior with respect to pressure not only reduces the level of miscibility between the L_1 and L_2 phases, but also makes the propagation of the three-phase region faster.

At 2500 psia, three phases are not present, and the L_2 phase displaces the oil. This immiscible two-phase flow results in a low displacement efficiency of 59.27% at 2.0 HCPVI. The oil recovery decreases when the three-phase region disappears as pressure increases.

As mentioned before, the non-monotonic trend of oil recovery at a given throughput occurs when the local oil displacement by three hydrocarbon phases becomes less efficient with increasing pressure in the cases considered in this section. The next section presents simple conditions to quantify the local displacement efficiency by three hydrocarbon phases based on mass conservation for multiphase transitions.

2.2 Mass Transfer on Multiphase Transitions

Our investigation in this section is focused on phase transitions between two and three phases in three-hydrocarbon-phase displacement. An analysis of mass conservation is presented for multiphase transitions in three-hydrocarbon-phase displacements. Material balance equations for 1-D dispersion-free compositional flow are discretized in **Appendix B** for a multiphase transition between N_P^U and N_P^D phases, where N_P^U and N_P^D are the numbers of phases on the upstream and downstream sides, respectively.

Equations B-5 and B-7 state that a multiphase transition between N_P^U and N_P^D phases occurs through an intersection between the extensions of the two tie simplexes defined by $\underline{x}_j^U$ ($j = 1, 2, \ldots, N_P^U$) and $\underline{x}_k^D$ ($k = 1, 2, \ldots, N_P^D$), where $\underline{x}_j$ is the composition of equilibrium phase j. A phase transition between two and three phases occurs through an intersection between the tie line extension and the tie triangle extension plane. Redistribution of components on the phase transition then satisfies the material balance for the two and three

phases. The two non-oleic phases can collectively achieve a high displacement efficiency if two conditions are satisfied on the phase transitions between two and three phases. The first condition is that the appearance of the non-oleic phase at the leading edge should occur by splitting the L_1 phase in the downstream two-phase region into the L_1 and the non-oleic phases in the three-phase region. The second condition is that the two non-oleic phases in the three-phase region should merge into one non-oleic phase in the upstream two-phase region.

It is easy to derive mathematical expressions for these conditions. The first condition is

$$\left\| \gamma_{N_1}^{U} \underline{c}_{N_1}^{U} - \gamma_{N_1}^{D} \underline{c}_{N_1}^{D} \right\|_2 < \varepsilon \tag{2.1}$$

such that

$$\gamma_{N_2}^{U} \underline{c}_{N_2}^{U} + \gamma_{L_1}^{U} \underline{c}_{L_1}^{U} \cong \gamma_{L_1}^{D} \underline{c}_{L_1}^{D}, \tag{2.2}$$

where N_1 is the non-oleic phase that appears at the leading edge of the downstream two-phase region and N_2 is the non-oleic phase that appears at the leading edge of three-hydrocarbon-phase region. Substitution of Equation (2.1) into Equation B-5 yields Equation (2.2). Equation (2.2) states that redistribution of components must occur between the L_1 and the non-oleic phases. Similarly, the second condition is

$$\left\| \gamma_{L_1}^{D} \underline{c}_{L_1}^{D} - \gamma_{L_1}^{U} \underline{c}_{L_1}^{U} \right\|_2 < \varepsilon \tag{2.3}$$

such that

$$\gamma_{N_1}^{D} \underline{c}_{N_1}^{D} + \gamma_{N_2}^{D} \underline{c}_{N_2}^{D} \cong \gamma_{N_3}^{U} \underline{c}_{N_3}^{U}, \tag{2.4}$$

where N_3 is the non-oleic phase in the upstream two-phase region. Summation of Equations (2.3) and (2.4) yields Equation B-5 for the trailing edge of the three-phase region. Equation (2.4) states that the two

non-oleic phases in the three-phase region should merge into a non-oleic phase in the upstream two-phase region.

Equations (2.1) and (2.3) can be rewritten using phase compositions as follows:

$$\delta^L = \left\| \Gamma_{N_1}^U \underline{x}_{N_1}^U - \Gamma_{N_1}^D \underline{x}_{N_1}^D \right\|_2 < \varepsilon \tag{2.5}$$

$$\delta^T = \left\| \Gamma_{L_1}^U \underline{x}_{L_1}^U - \Gamma_{L_1}^D \underline{x}_{L_1}^D \right\|_2 < \varepsilon. \tag{2.6}$$

The Γ_j (j = 1, 2,…, N_P) parameters determine the relative location of the N_P-phase tie simplex and an intersection involved in the phase transition. The conditions specific to the quaternary displacements in the previous section are as follows: $\delta^L = \left\| \Gamma_V^U \underline{x}_V^U - \Gamma_V^D \underline{x}_V^D \right\|_2 < \varepsilon$ and $\delta^T = \left\| \Gamma_{L_1}^U \underline{x}_{L_1}^U - \Gamma_{L_1}^D \underline{x}_{L_1}^D \right\|_2 < \varepsilon$.

Figs. 2.16 and 2.17 give schematics for the phase transitions at the leading and trailing edges of the three-phase region, respectively. These schematics indicate that a phase transition between two and three phases involves an intersection of the tie-line extension and the tie-triangle extension as described in Appendix B. Once the tie line and tie triangle involved in a phase transition (e.g., the tie line downstream and the tie triangle upstream in Fig. 2.16) are given, we can calculate an intersection of them. The location of the intersection relative to the tie line then gives the Γ_j (j = V and L_1) parameters on the tie line extension. Thus, $\underline{z}^{\text{int}} = \Gamma_V^D \underline{x}_V^D + \Gamma_{L_1}^D \underline{x}_{L_1}^D$, where $\Gamma_V^D + \Gamma_{L_1}^D = 1.0$ and $\underline{z}^{\text{int}}$ is the intersection composition. Similarly, the location of the same intersection relative to the tie triangle gives the Γ_j (j = V, L_1, and L_2) parameters on the tie triangle extension. Thus, $\underline{z}^{\text{int}} = \Gamma_V^U \underline{x}_V^U + \Gamma_{L_1}^U \underline{x}_{L_1}^U + \Gamma_{L_2}^U \underline{x}_{L_2}^U$, where $\Gamma_V^U + \Gamma_{L_1}^U + \Gamma_{L_2}^U = 1.0$. Calculation of δ^L and δ^T will be conducted using this procedure for the quaternary displacements and for the West Sak oil displacements in the subsequent section.

2.3 Case Studies

Nonmonotonic and monotonic oil recovery at a given throughput with respect to gas enrichment has been reported for the oil displacements by three hydrocarbon phases. However, the detailed mechanism is uncertain in the literature. In this section, the distance conditions derived in the previous section are applied to the West Sak (WS) oil and Bob Slaughter Block (BSB) oil displacement with enriched gas.

In this chapter, simulations are conducted by the UTCOMP simulator that has been used in various papers on gas injection theory (e.g., Mohanty et al. 1995; Johns et al. 2000, 2004; Solano et al. 2001). The UTCOMP is a systematic and robust simulator for multicomponent multiphase flow. The operation scheme of UTCOMP can be obtained from Chang (1990).

2.3.1 Nonmonotonic oil recovery for West Sak oil displacement

The West Sak oil is characterized using the Peng-Robinson EOS based on data available in Okuyiga (1992) (Xu 2012). The 15-component model given in **Table 2.4** includes eight pseudo components for the C_{7+} fraction. The oil gravity is calculated to be approximately 21˚API. The saturation pressure is 1197 psia at the reservoir temperature of 65˚F. The injection gas consists of two gaseous mixtures; the rich gas mixture of 35 mol% ethane, 34 mol% propane, and 31 mol% n-butane, and the lean gas mixture of 84 mol% methane, 9 mol% ethane, 6 mol% propane, and 1 mol% n-butane. The reservoir properties used are given in Table 2.3. The displacement pressure is 1500 psia.

Fig. 2.18 presents oil recovery at different gas enrichments at 1.0 HCPVI, 1.5 HCPVI, and 2.0 HCPVI. Three hydrocarbon phases are present in the displacements at methane concentrations in the injection gas between 50% and 70%.

As discussed in section 2.2, equations (2.1) and (2.3) cannot be calculated when simulations are performed by UTCOMP, since the effect of volume change on mixing is considered in the UTCOMP simulator. Therefore, in this chapter, the distance parameters at the leading and trailing edges of three phases are calculated using mole-based formulation (i.e. equations (2.5) and (2.6)) based on the relative location of the intersection point in phase transitions to tie line and tie triangle. This way to calculate the mole-based distances is called indirect method that has been illustrated in section 2.2.

Fig. 2.19 shows the distances given in Equations 2.5 and 2.6 for the displacements at 50%, 53%, 55%, and 60% methane concentrations. The distances decrease for leaner injection gas. These results indicate that the local displacement by three hydrocarbon phases becomes more efficient with decreasing gas enrichment. The injection gas with the methane concentration of 60% gives the maximum efficiency of three-phase local displacement. Oil recovery at breakthrough of the three-phase trailing edge is 90.4% at 50% methane, 92.0% at 53% methane, and 97.4% at 60% methane.

However, propagation of three phases is slower at higher methane concentrations. The trailing edge of three phases reaches the outlet at 2.15 HCPVI, 2.34 HCPVI, 2.73 HCPVI, and 14.94 HCPVI at the methane concentrations of 50%, 53%, 55%, and 60%, respectively. Local displacement by three phases is more efficient, but propagation of three phases is slower, for leaner injection gas for these three-phase displacements. These two factors determine a maximum in oil recovery at a given throughput in Fig. 2.16. A maximum recovery at a give throughput will occur at a different dilution level when different reservoir and/or fluid properties are used.

We also calculate the distances, $\delta^L$and δ^T, for quaternary displacements with different gas enrichment levels and pressure levels. Reservoir properties are given in Table 2.3. Three phases are present for

displacements within a certain enrichment ranges and pressure ranges. Three-phase displacement with less enrichment or lower pressure achieves higher local displacement efficiency, but it becomes slower. Oil recovery at a given throughput depends not only on local displacement efficiency by three phases, but also on the propagation rate of three phases.

2.3.2 Monotonic oil recovery for Bob Slaughter Block oil displacement

The Bob Slaughter Block fluid model developed by Khan et al. (1992) is used as presented in **Table 2.5.** The injection gas consists of 95% CO_2 and 5% methane as used in Okuno et al. (2011). The reservoir temperature is 105°F. Oil displacements are simulated at 1150 psia, 1200 psia, 1250 psia, and 1350 psia. Three phases are present in all these displacements. Details of phase behavior for these displacements are given in Okuno (2009) and Okuno et al. (2011), and not duplicated here.

Oil recovery at a given throughput monotonically increases with pressure as presented in **Fig. 2.20. Figs. 2.21** shows the distance parameters given in Equations 2.5 and 2.6 calculated for the leading and trailing edges of three phases. The distance at the trailing edge monotonically decrease indicating a more efficient displacement as pressure increases, which is different from the nonmonotonic scenario. In addition, the trailing edge of three-phase region arrives at the producer at 1.50 HCPVI, 1.33 HCPVI, and 1.17 HCPVI for 1150 psia, 1250 psia, and 1350 psia, respectively. The more efficient three hydrocarbon phases result in the monotonic oil recovery as pressure increases.

However, unlike the distance at the trailing edge, the distance at the leading edge does not decrease as the displacement becomes more efficient. Even though 1000 gridblocks are used in the 1-D simulations by UTCOMP, numerical dispersion effects are significant near the leading edge of three phases because the CO_2

concentration has a sharp increase. This should be one factor that impacts the accuracy of the distance at the leading edge. As mentioned before, the distance parameters cannot be calculated directly by use of analytical solution (i.e. equations (2.1) and (2.3)) for simulations by UTCOMP. The idea of indirect method is to determine the distances based on the relative location of intersection point to the tie-simplex. However, it is theoretically conceivable that the round error in the determination of the intersection point can be amplified when the tie line becomes nearly parallel to the tie triangle. Small round error may lead to large error of the location of the intersection point. The numerical dispersion and the indirect method both contribute to the inaccuracy of the distance parameter at the leading edge of three phases.

2.4 Conclusions

This chapter mainly investigated the local efficiency of three-hydrocarbon-phase displacement of oil. Mathematical conditions were derived for efficient redistribution of components on multiphase transitions between two and three phases. These conditions were used to explain non-monotonic oil recovery at a given throughput with respect to gas enrichment and monotonic oil recovery at a given throughput with respect to displacement pressure. Conclusions are as follows:

1. Oil recovery in a partially miscible displacement depends on two factors; local displacement efficiency and components' propagation rates. Non-monotonic oil recovery at a given throughput can occur when local displacement by three hydrocarbon phases becomes more efficient, but slower, with decreasing pressure or decreasing gas enrichment. This was confirmed using fine-scale simulations of quaternary displacements and the West Sak oil displacements. A maximum in oil recovery at a given throughput occurs as a consequence of the balance between the local displacement efficiency and the propagation

rate of three hydrocarbon phases.

2. Similar to conventional two-phase displacement, monotonic oil recovery at a given throughput can also occur when local displacement by three hydrocarbon phases becomes more efficient with increasing pressure or increasing gas enrichment. This was confirmed using fine-scale simulations of oil displacements for west Texas, such as Bob Slaughter Block oil.
3. Local displacement efficiency by three hydrocarbon phases depends significantly on how components are redistributed on multiphase transitions between two and three phases. At the leading edge of the three-phase region, the second non-oleic phase should appear from the oleic phase of the downstream two-phase region. At the trailing edge of the three-phase region, two non-oleic phases of the three-phase region should merge into the non-oleic phase of the upstream two-phase region.
4. The distances defined in Equations 2.5 and 2.6 for efficient multiphase transitions can correctly identify the local displacement efficiency by three hydrocarbon phases. The distances were successfully used to explain the quaternary displacements and the West Sak oil displacements that exhibit nonmonotonic oil recovery and the Bob Slaughter Block oil displacements that exhibit monotonic oil recovery.
5. Partially miscible displacement of oil by two non-oleic phases can be collectively efficient, even if they are individually immiscible with oil. The West Sak oil displacement with enriched gas studied in this research showed a displacement efficiency of 84.29% at 1.0 HCPVI, 90.18% at 1.5 HCPVI, and 91.53% at 2.0 HCPVI at 53% methane dilution. With this methane dilution, the three-phase displacement was locally efficient and fast enough to exhibit a high oil recovery.

Table 2.1 Properties of The Quaternary Fluid

	Oil (Mole %)	Gas (Mole %)	Molecular Weight	Tc (ºR)	Pc (psia)	Acentric Factor	Vc (ft^3/lb-mol)
PC1	37.22	20	17.268	357.77	666.48	0.0193	1.6763
PC2	10.63	80	40.288	630.32	656.22	0.1402	2.9740
PC3	30.11	0	352.25	1318.1	240.31	0.5574	21.572
PC4	22.04	0	1052.0	1967.3	94.80	1.1313	83.571

Table 2.2 Binary Interaction Parameters for The Quaternary Fluid

Components	PC1	PC2	PC3	PC4
PC1	0			
PC2	0.0052	0		
PC3	0	0.0050	0	
PC4	0.1822	0.1336	0	0

Table 2.3 Reservoir Properties for Simulations of One-Dimensional Oil Displacements

		Relative Permeability	Corey Model			
Dimensions	10 x 1 x 10 ft^3		W	L_1	V	L_2
Number of cells	1 x 1000 x 1	Residual Saturation	0.4	0.2	0.05	0.05
Porosity	0.2	Endpoint Relative Permeability	0.35	0.5	0.65	0.65
Permeability	1000 mD	Exponent	3	3	3	3
		Initial Saturation	0.4	0.6	0	0

W: Aqueous phase, L_1: Oleic phase, V: Gaseous phase, L_2: Solvent-rich liquid phase

Table 2.4 Properties of The West Sak Oil (Xu 2012)

Components	Oil (Mole %)	Rich Gas (Mole %)	Lean Gas (Mole %)	Molecular Weight	Tc (^{o}R)	Pc (psia)	Vc (ft^3/lb-mol)	Acentric Factor	Binary Interaction CO_2	Binary Interaction C_1
CO_2	0.22	0.0	0.0	44.01	547.56	1069.87	1.51	0.2250	0.00	0.180
C_1	27.47	0.0	84.0	16.04	343.08	667.20	1.59	0.0080	0.18	0.000
C_2	0.66	35.0	9.0	30.07	549.72	708.35	2.37	0.0980	0.18	0.010
C_3	0.15	34.0	6.0	44.10	665.64	615.76	3.25	0.1520	0.18	0.010
C_4	0.27	31.0	1.0	58.12	765.36	551.10	4.08	0.1930	0.18	0.010
C_5	0.19	0.0	0.0	72.15	845.28	489.38	4.87	0.2510	0.18	0.010
C_6	0.29	0.0	0.0	86.18	913.32	430.59	5.93	0.2960	0.18	0.010
C_{7-9}	3.22	0.0	0.0	105.65	1060.48	418.62	8.29	0.3697	0.05	0.007
C_{10-14}	17.95	0.0	0.0	157.72	1220.50	323.21	8.41	0.5389	0.05	0.007
C_{15-18}	13.21	0.0	0.0	210.19	1349.89	274.12	14.54	0.6992	0.05	0.007
C_{19-23}	10.91	0.0	0.0	259.06	1424.95	251.96	19.02	0.8373	0.05	0.007
C_{24-27}	5.84	0.0	0.0	302.85	1493.37	242.09	22.88	0.9500	0.05	0.007
C_{28-33}	6.60	0.0	0.0	344.37	1550.96	230.14	22.74	1.0453	0.05	0.007
C_{34-40}	4.42	0.0	0.0	389.77	1629.48	223.31	44.05	1.1345	0.05	0.007
C_{41+}	8.60	0.0	0.0	600.00	1914.78	182.82	53.57	1.2120	0.05	0.007

Table 2.5 EOS Parameters for The Bob Slaughter Block Oil (Khan et al. 1992)

Components	Oil (Mole %)	Gas (Mole %)	Molecular Weight	Tc (ºR)	Pc (psia)	Vc (ft^3/lb-mol)	Acentric Factor	BIC CO_2
CO_2	3.37	95.0	44.01	547.56	1069.87	1.506	0.2250	0.000
C_1	8.61	5.0	16.04	288.00	667.20	1.586	0.0080	0.055
C_{2-3}	15.03	0.0	37.20	619.57	652.56	2.902	0.1305	0.055
C_{4-6}	16.71	0.0	69.50	833.80	493.07	4.914	0.1404	0.055
C_{7-15}	33.04	0.0	140.96	1090.35	315.44	9.000	0.6177	0.105
C_{16-27}	16.11	0.0	280.99	1351.83	239.90	17.100	0.9566	0.105
C_{28+}	7.13	0.0	519.62	1694.46	238.12	32.500	1.2683	0.105

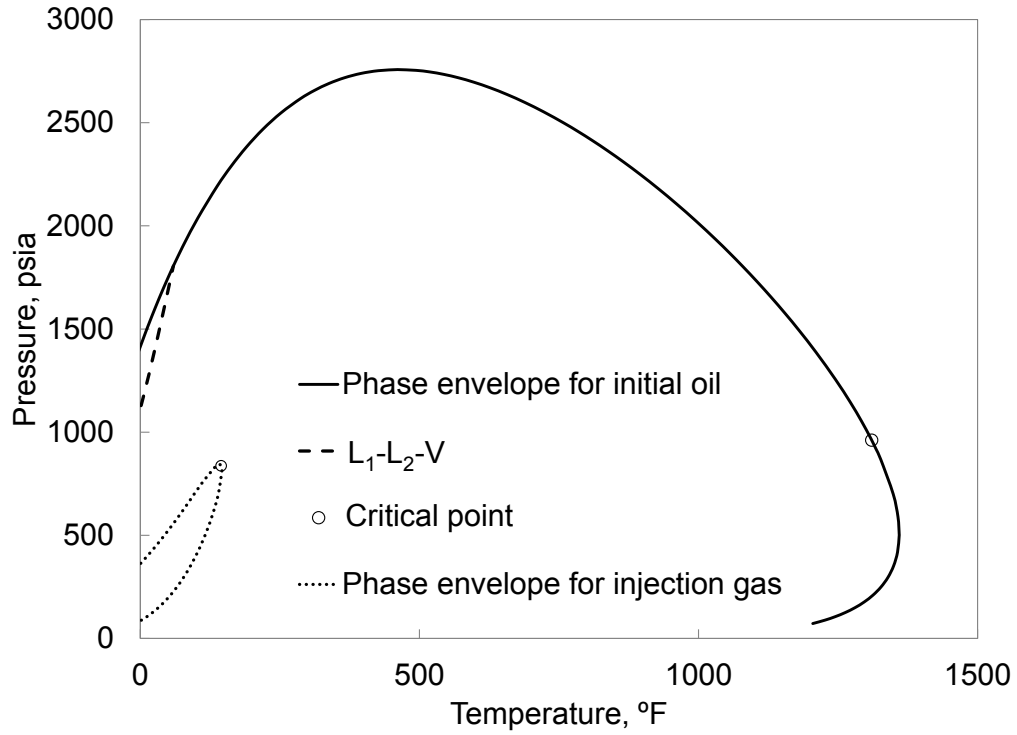

Figure 2.1 P-T diagrams of the quaternary oil and injected gas given in Tables 2.1 and 2.2.

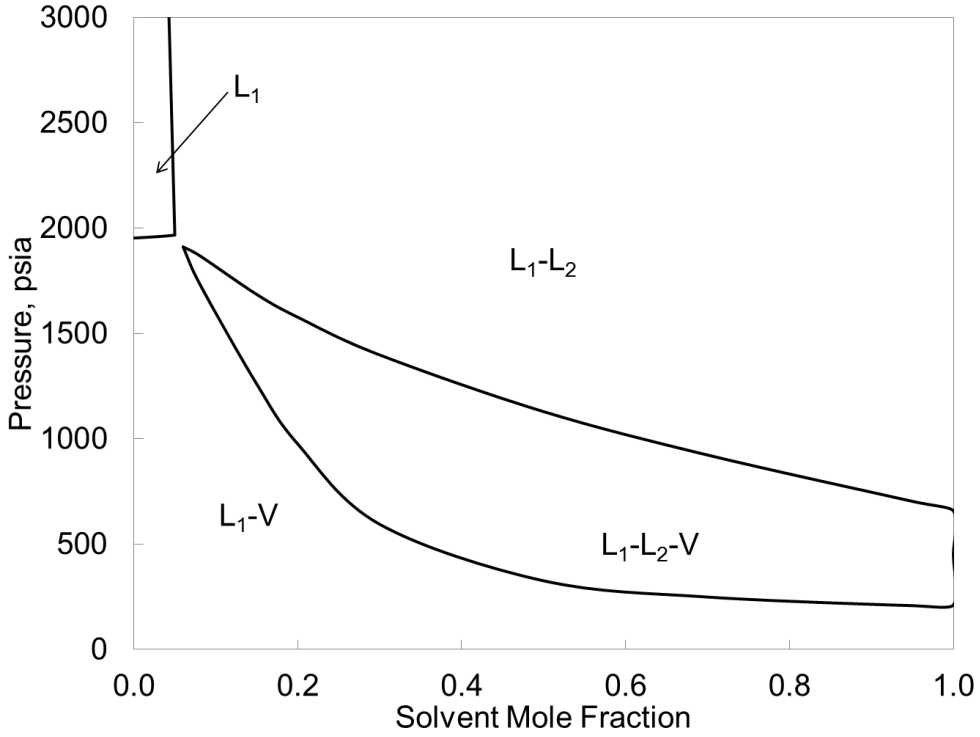

Figure 2.2 P-x diagram at 86°F for mixtures of the quaternary oil and the injection gas given in Tables 2.1 and 2.2.

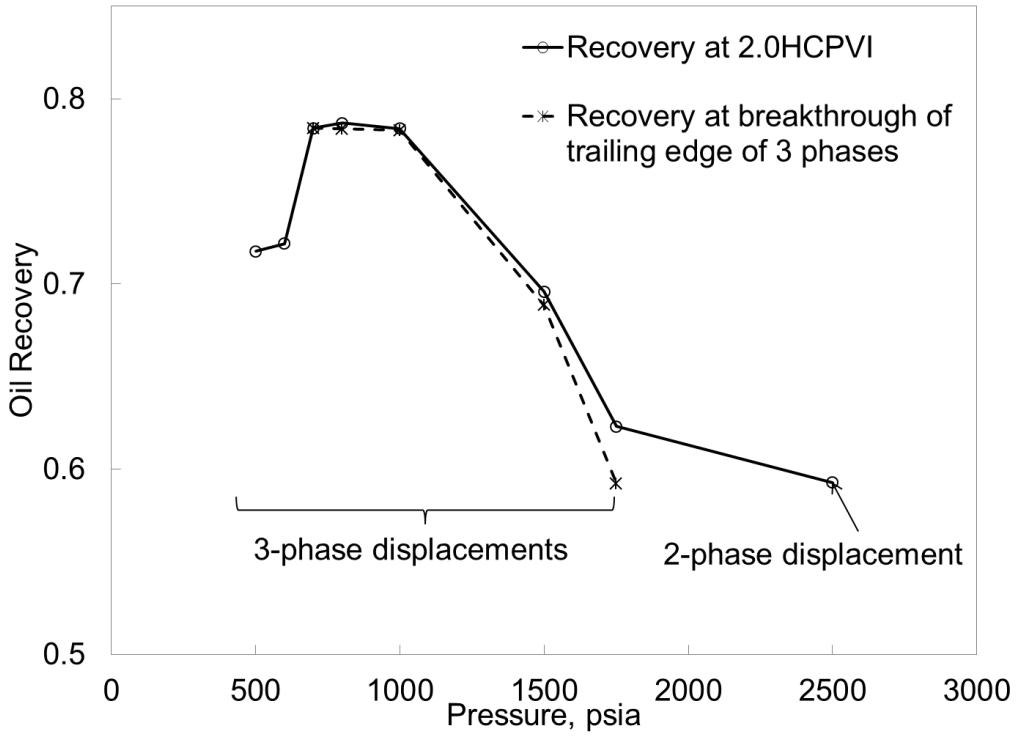

Figure 2.3 Oil recovery simulated for the quaternary displacements at different pressures at 86°F.

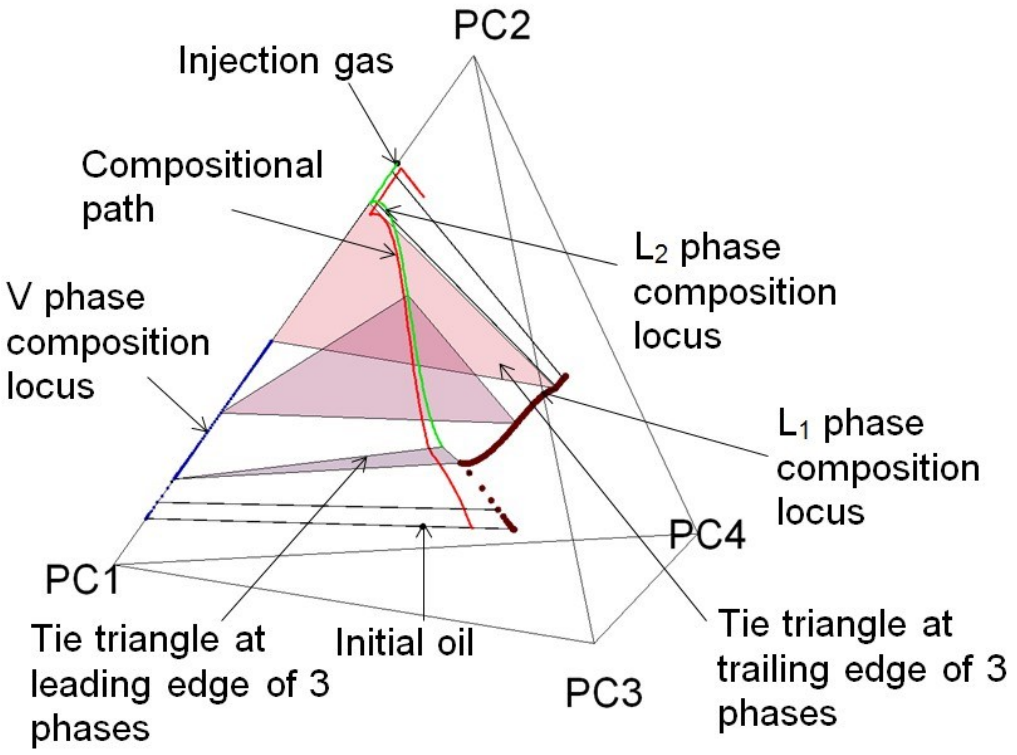

Figure 2.4 Phase behavior along the composition path in the quaternary displacement at 700 psia at 86°F.

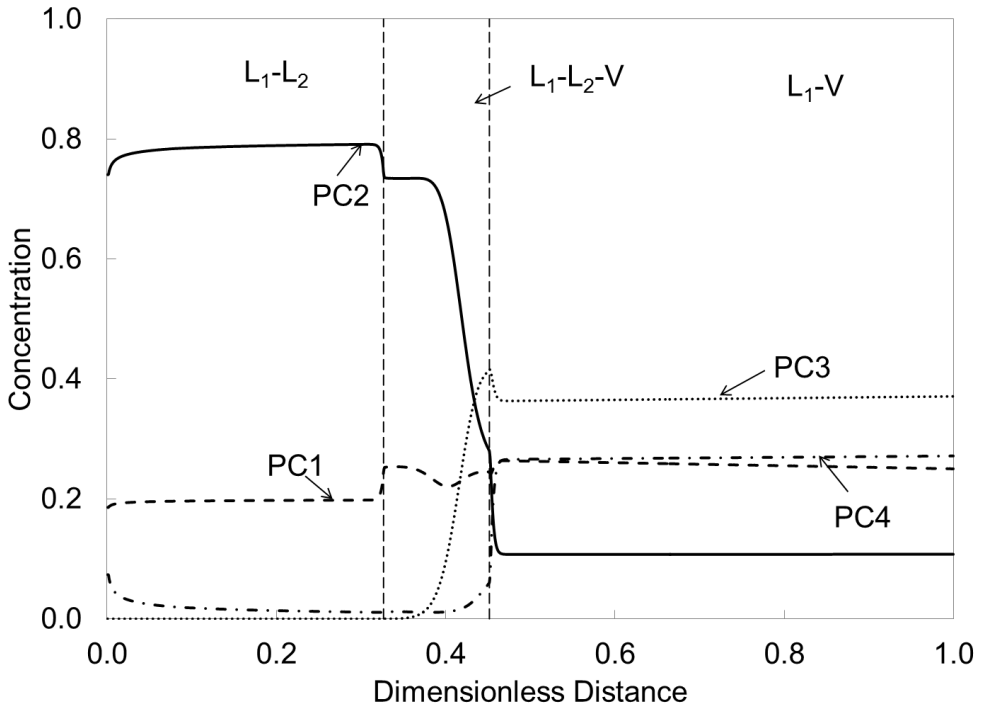

Figure 2.5 Simulated component concentrations at 0.33 HCPVI for the quaternary displacement at 700 psia at 86°F. The oil and gas properties are given in Tables 2.1 and 2.2.

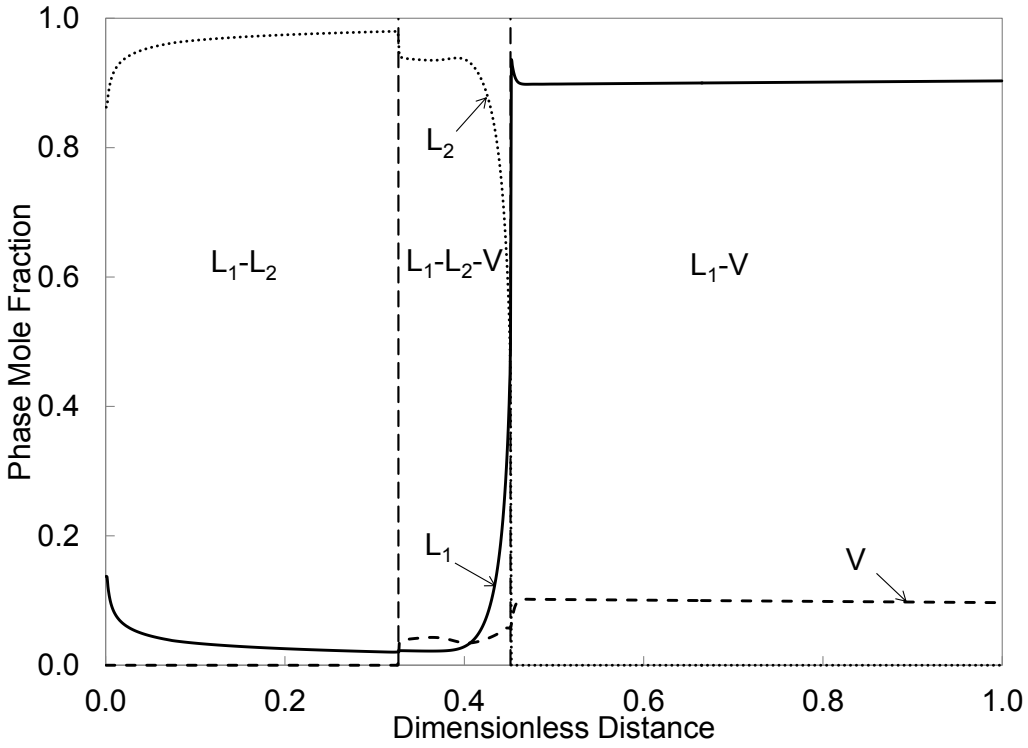

Figure 2.6 Simulated phase mole fractions at 0.33 HCPVI for the quaternary displacement at 700 psia at 86°F. The oil and gas properties are given in Tables 2.1 and 2.2.

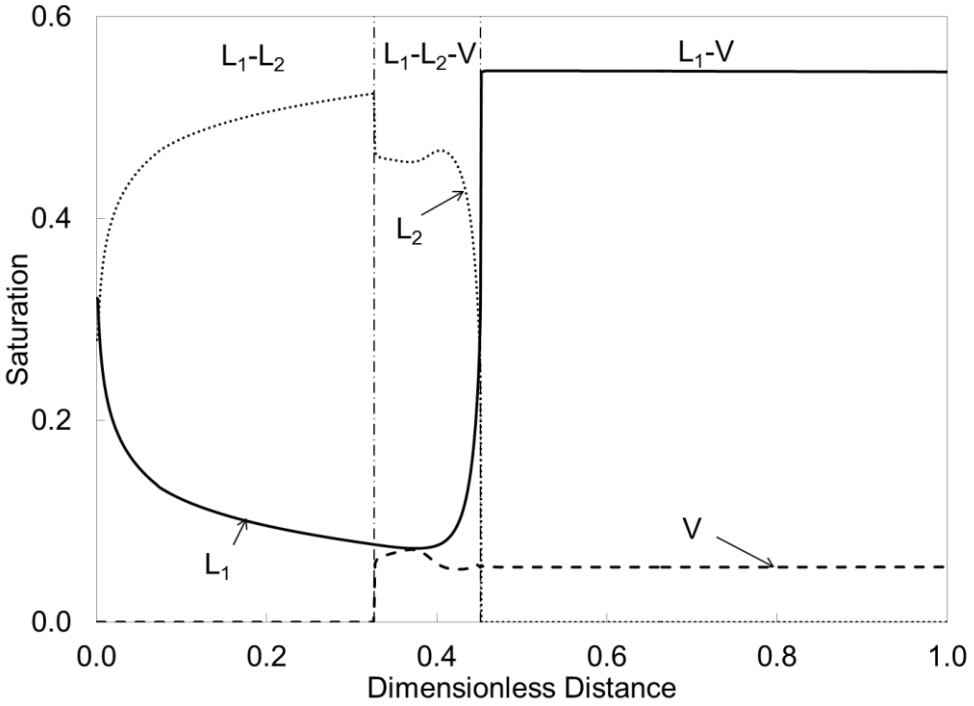

Figure 2.7 Simulated phase saturations at 0.33 HCPVI for the quaternary displacement at 700 psia at 86°F. The oil and gas properties are given in Tables 2.1 and 2.2.

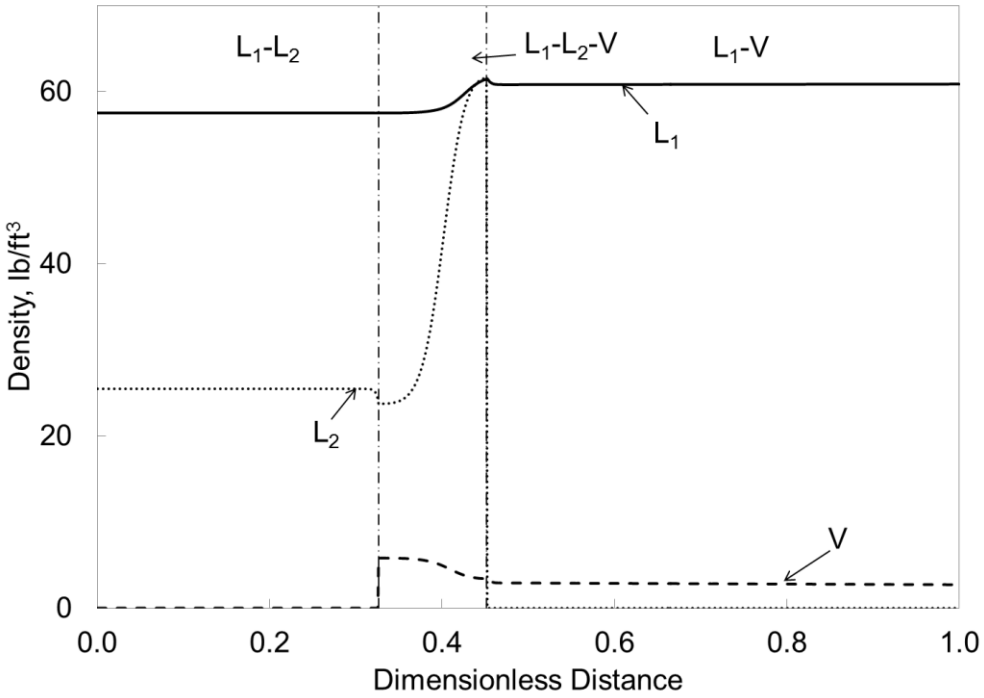

Figure 2.8 Simulated phase densities at 0.33 HCPVI for the quaternary displacement at 700 psia at 86°F. The oil and gas properties are given in Tables 2.1 and 2.2.

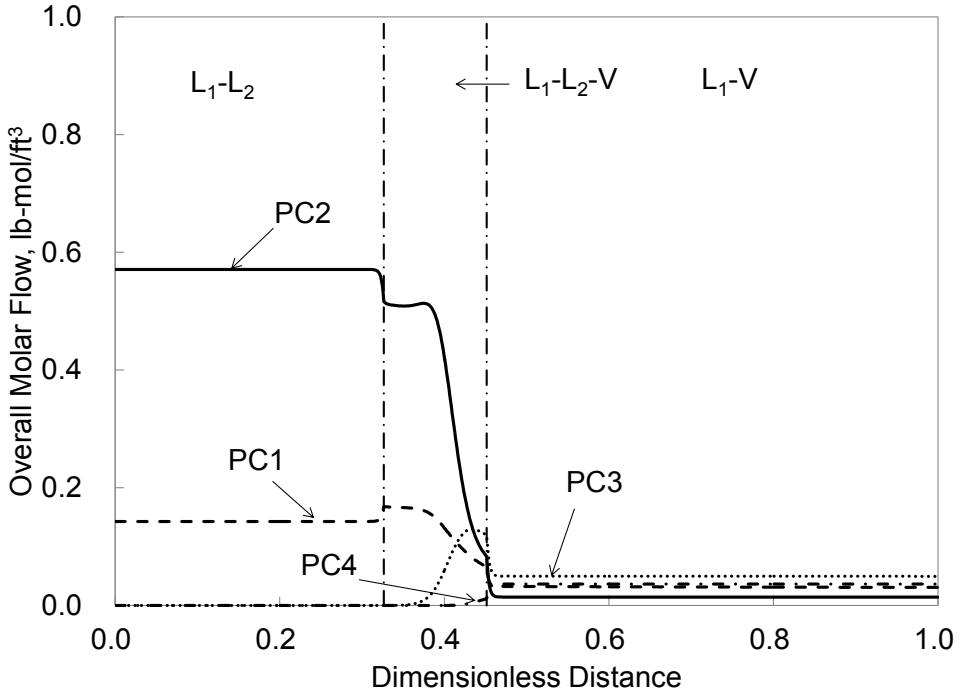

Figure 2.9 Simulated overall molar flow for each component at 0.33 HCPVI for the quaternary displacement at 700 psia at 86°F. The oil and gas properties are given in Tables 2.1 and 2.2.

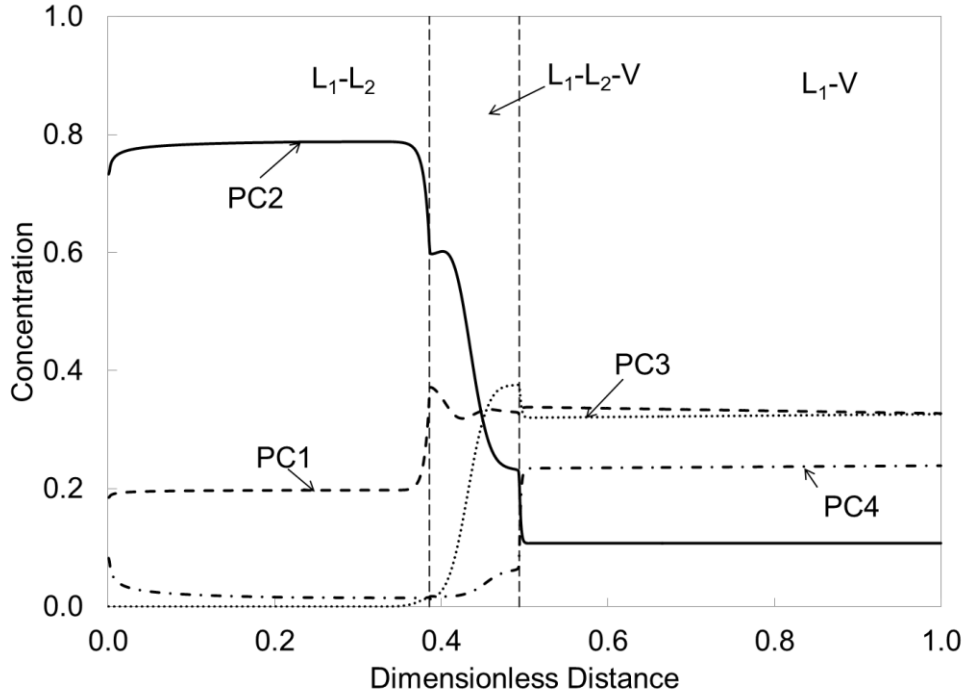

Figure 2.10 Simulated component concentrations at 0.33 HCPVI for the quaternary displacement at 1000 psia at 86°F. The oil and gas properties are given in Tables 2.1 and 2.2.

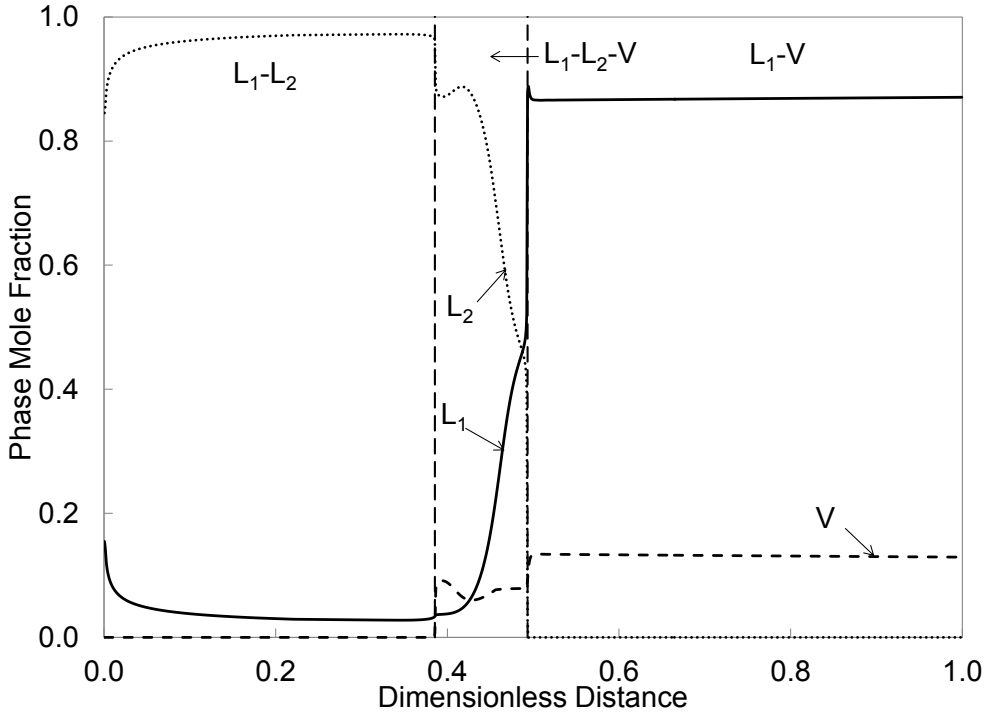

Figure 2.11 Simulated phase mole fractions at 0.33 HCPVI for the quaternary displacement at 1000 psia at 86°F. The oil and gas properties are given in Tables 2.1 and 2.2.

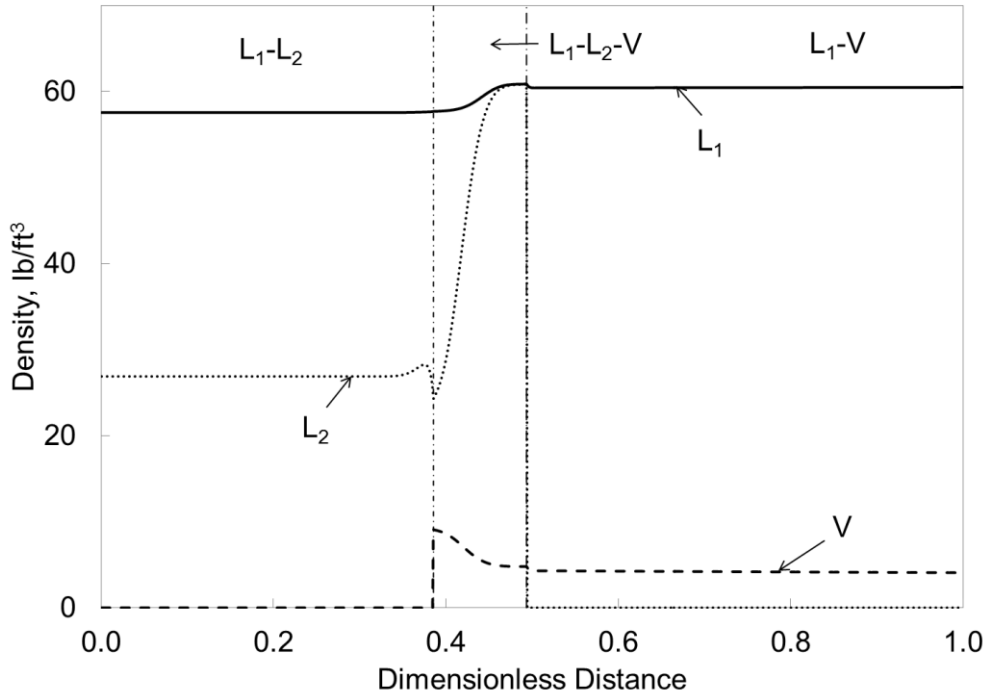

Figure 2.12 Simulated phase densities at 0.33 HCPVI for the quaternary displacement at 1000 psia at 86°F. The oil and gas properties are given in Tables 2.1 and 2.2.

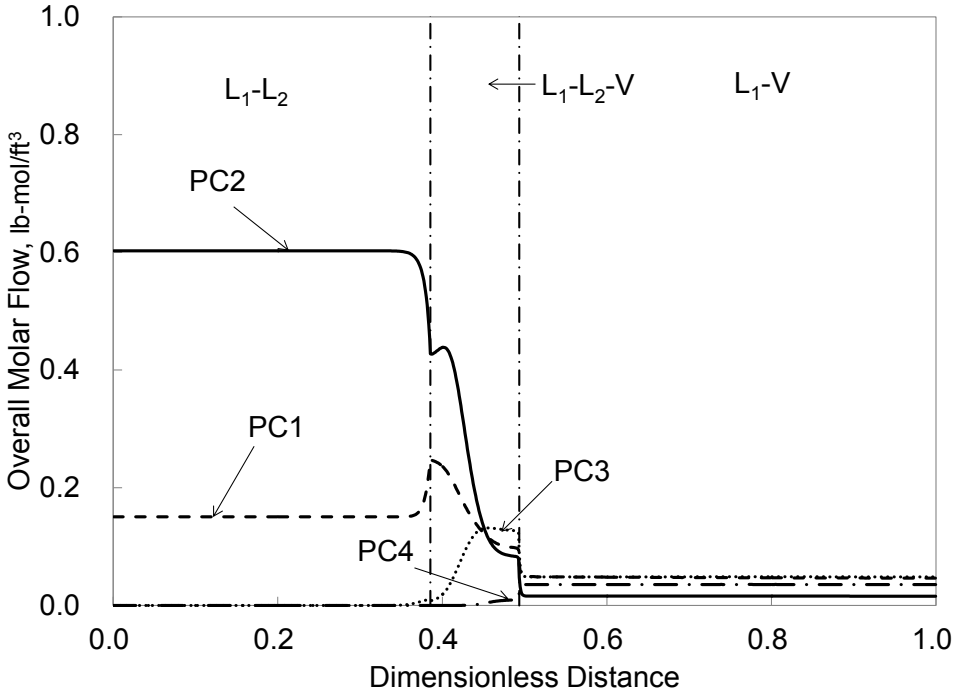

Figure 2.13 Simulated overall molar flow for each component at 0.33 HCPVI for the quaternary displacement at 1000 psia at 86°F. The oil and gas properties are given in Tables 2.1 and 2.2.

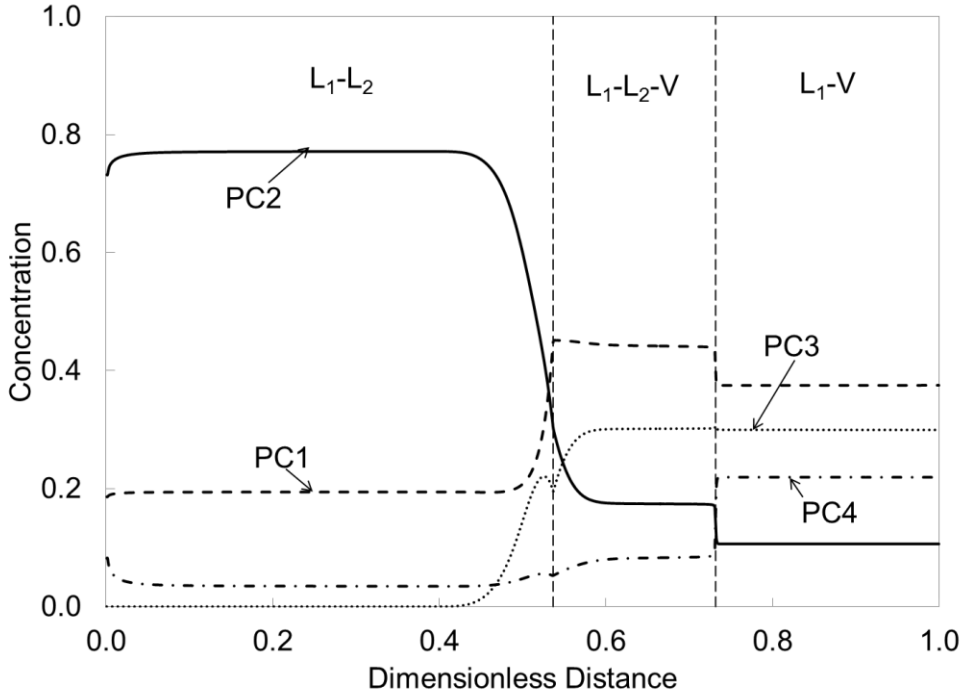

Figure 2.14 Simulated component concentrations at 0.33 HCPVI for the quaternary displacement at 1750 psia at 86°F. The oil and gas properties are given in Tables 2.1 and 2.2.

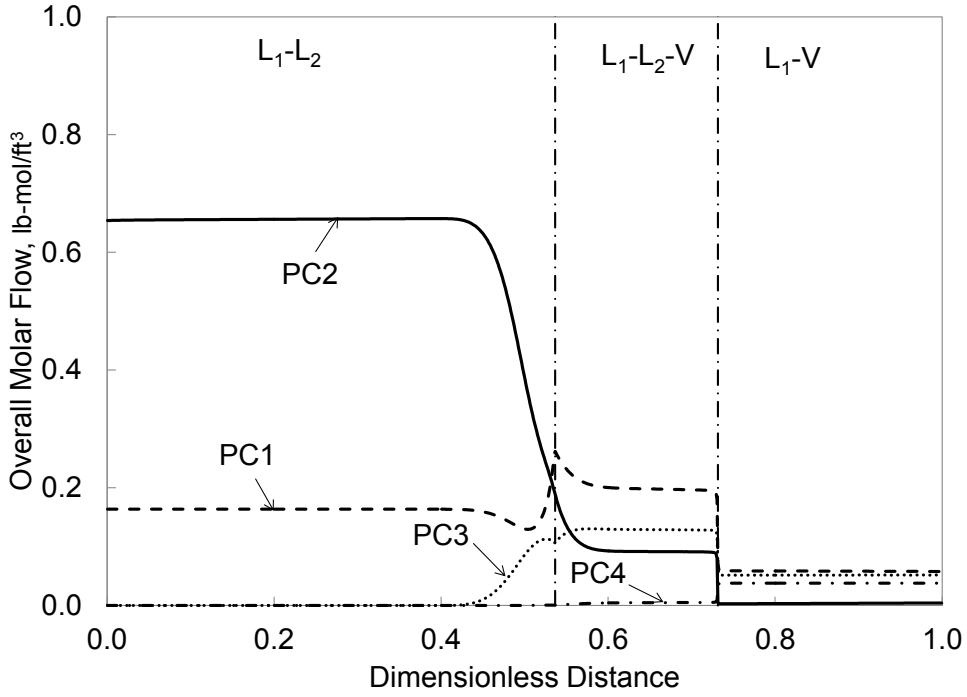

Figure 2.15 Simulated overall molar flow for each component at 0.33 HCPVI for the quaternary displacement at 1750 psia at 86°F. The oil and gas properties are given in Tables 2.1 and 2.2.

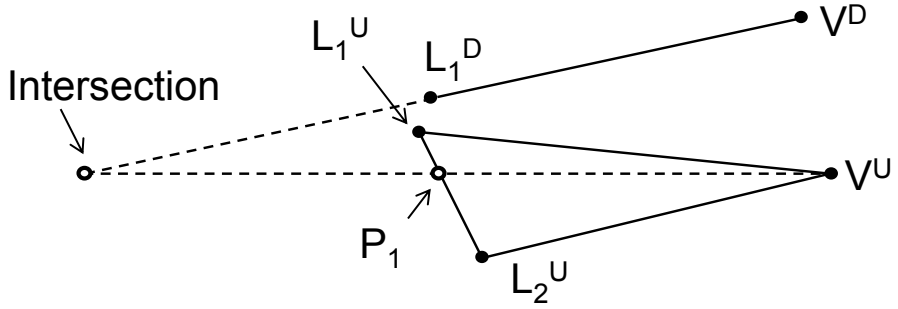

Figure 2.16 Schematic of phase transition in composition space at the leading edge of the three-phase region.

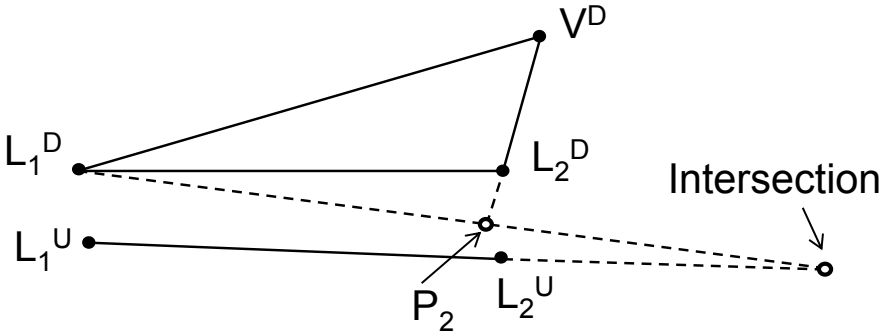

Figure 2.17 Schematic of phase transition in composition space at the trailing edge of the three-phase region.

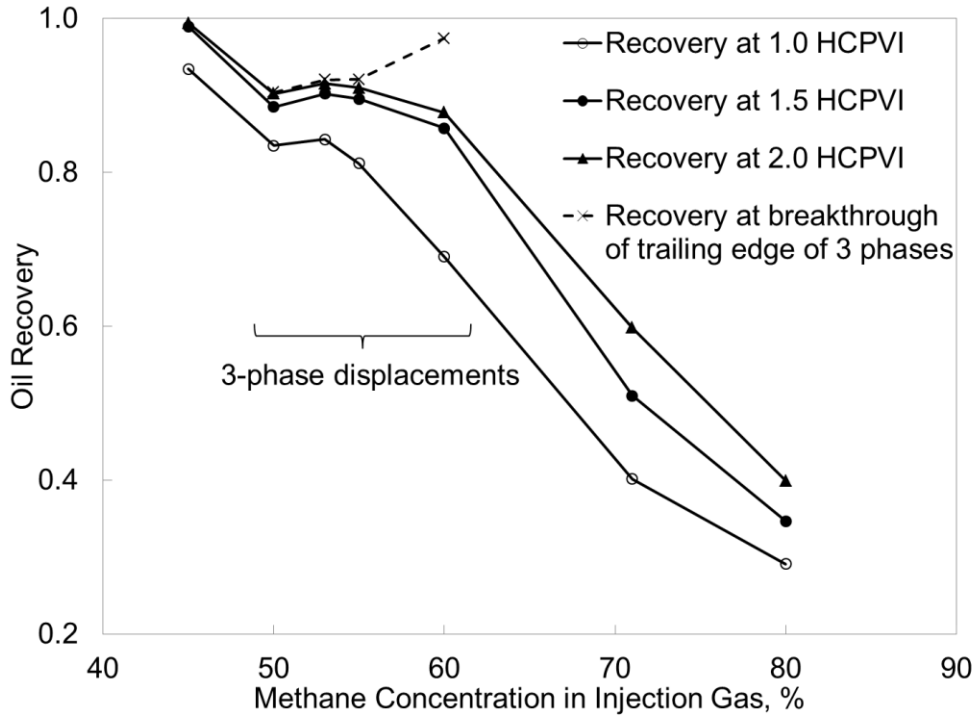

Figure 2.18 Oil recovery simulated for the West Sak displacements at different gas enrichment levels at 1500 psia and 65°F. The fluid properties are given in Table 2.4.

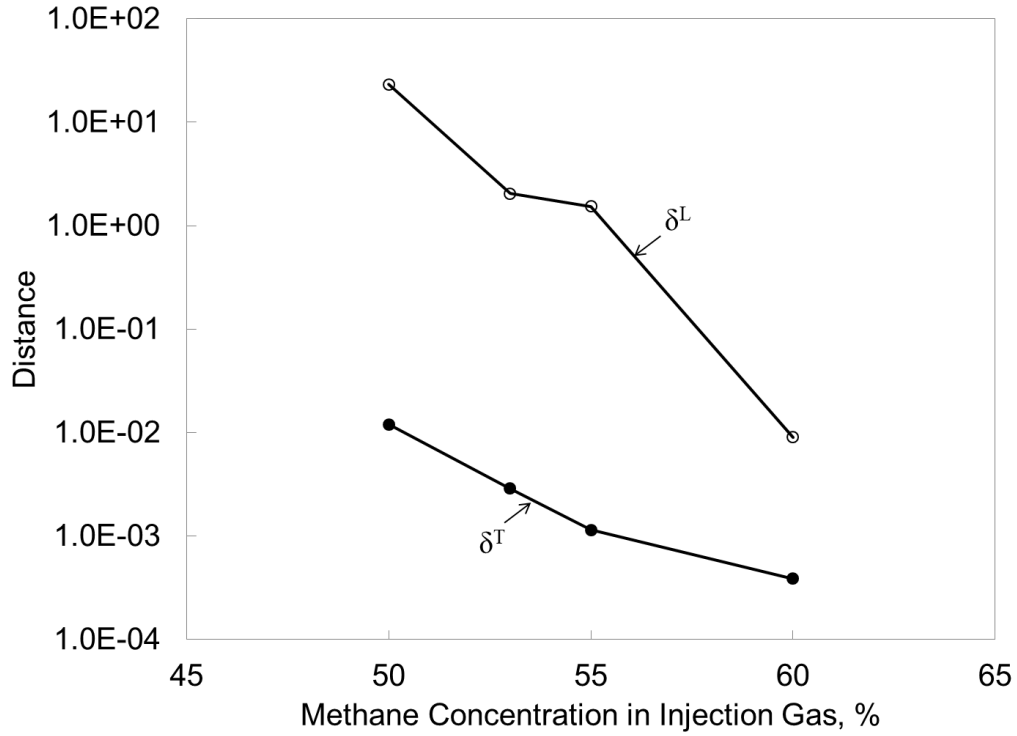

Figure 2.19 The distance parameters δ^L and δ^T (Equations 2.5 and 2.6) calculated for the West Sak displacements at different enrichment levels at 1500 psia and 65°F.

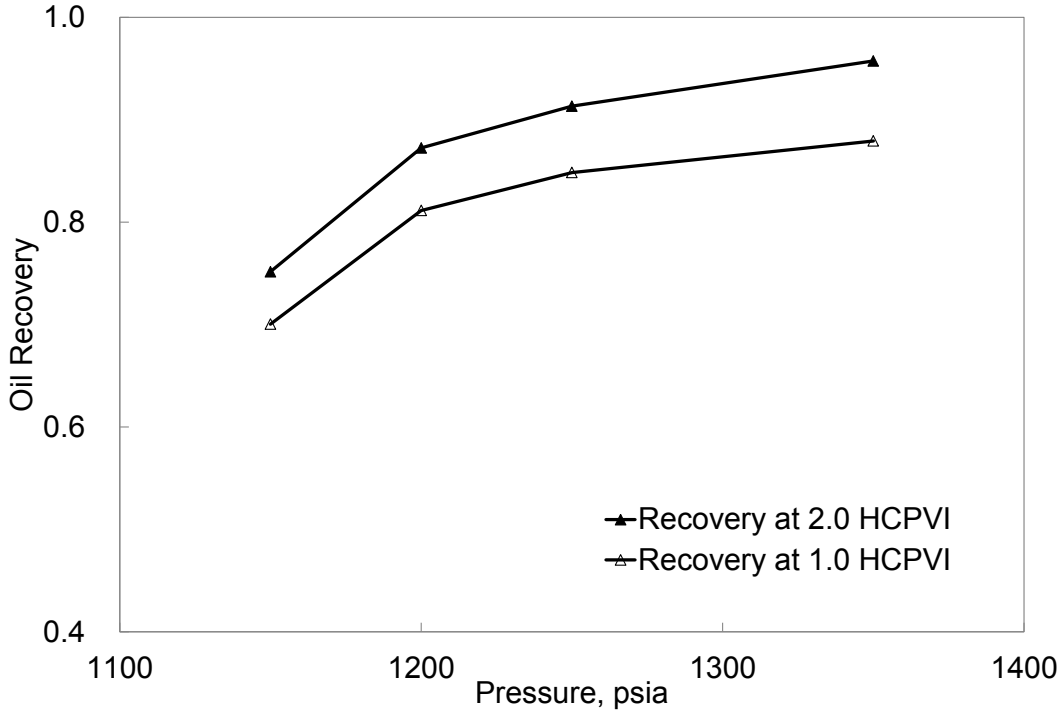

Figure 2.20 Oil recoveries for the Bob Slaughter Block oil displacements at different pressures at 105°F. Reservoir and fluid properties are given in Tables 2.3 and 2.5, respectively.

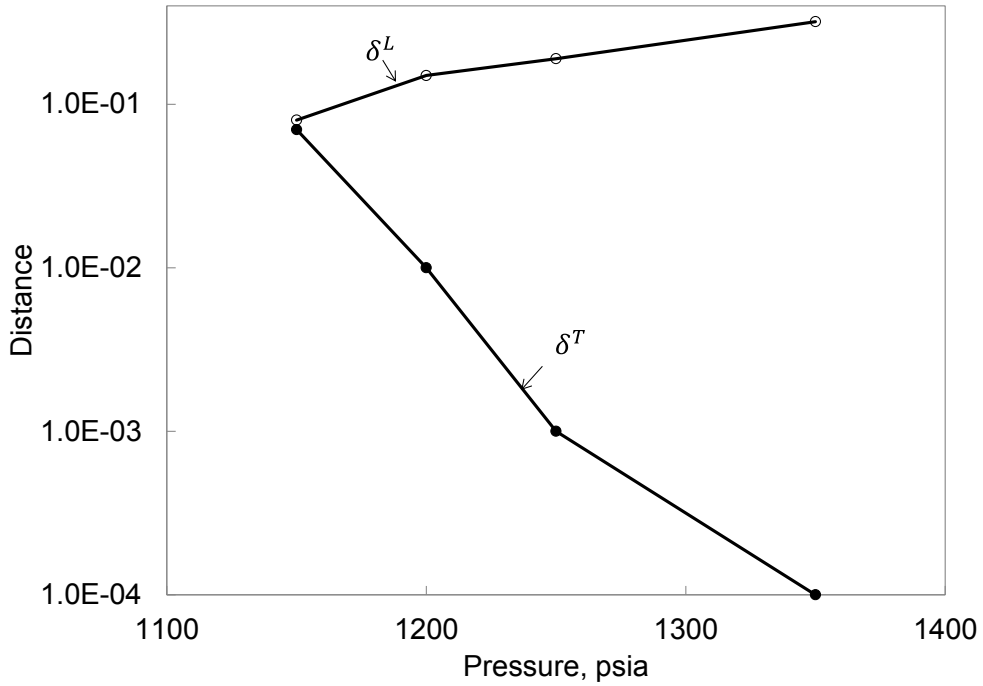

Figure 2.20 Distance parameters for the leading edge and trailing edge for the Bob Slaughter Block oil displacements at 105°F. Reservoir and fluid properties are given in Tables 2.3 and 2.5, respectively.

Chapter 3: Phase Identification in Three-Hydrocarbon-Phase Flow Simulation

In the previous chapter, we presented a detailed analysis of mass conservation on multiphase transitions between two and three phases in three-hydrocarbon-phase flow. Oil displacements were simulated by use of UTCOMP with its robust phase-behavior calculations. However, the research was limited in terms of thermodynamic and flow conditions. For example, how phase mobilities affect the interphase mass transfer was not studied in detail, due to the lack of robust phase identification in EOS compositional simulation (Mohanty et al. 1995; Yuan and Pope 2012; Beygi et al. 2014). Phase identification is always part of the solution of a multiphase flow problem, and is usually required to assign relative permeabilities to phases in simulation. To systematically understand the multiphase flow, a new method is required for robust phase identification and implemented in a 1D multiphase convective flow simulator (see **Appendix C**). This chapter is concerned with the development of an improved algorithm for phase identification in multiphase flow.

3.1 Conventional Method for Phase Identification

The conventional method for phase identification was developed by Perschke et al. (1989). In their method, the L_1 phase in a three-phase region of L_1-L_2-V was the one with the highest concentration of the heaviest hydrocarbon component. Of the two remaining phases, the denser phase was labeled as L_2, and the less dense phase was V. For two equilibrium phases, in which the L_1 phase was assumed to exist, the L_1 phase was labeled by use of the logic mentioned previously. The other phase was labeled as either V or L_2 depending on the mass density of that phase. If the mass density of the phase was lower than a specified threshold value, it was labeled as V. Otherwise, it was labeled as L_2. It was not entirely clear in their paper how to handle the

V-L_2 equilibrium that can occur near the injection composition in enriched-gas and CO_2 injection simulations at low temperature. A single phase was labeled by the user on the basis of the phase behavior data available.

The conventional method described in the preceding paragraph has been used for decades, but it has been a difficult problem to assign physically correct identities to equilibrium phases (Yuan and Pope 2012). Particularly, the use of a fixed mass-density threshold is known to be problematic for phase labeling in a two-phase region in three-hydrocarbon-phase flow simulation (Mohanty et al. 1995; Li et al. 2014; Beygi et al. 2014). The use of mass densities by Perschke et al. (1989) for three-phase labeling is less problematic. However, it is somewhat inconsistent to use volumetric predictions for identifying equilibrium phases, the compositions of which are determined by the geometry of the Gibbs free energy. This is because the two types of predictions (i.e., volumetric and compositional behavior) are not entirely coherent in the conventional phase–behavior modeling scheme based on a cubic EOS. This becomes obvious when volume shift is used to adjust volumetric predictions in fluid characterization (Kumar and Okuno 2013). It will be more robust if phase identification can be based primarily on compositional predictions in simulation. Note, however, that density information may be still useful in some special cases, such as the identification of the aqueous (condensed water) and vapor (steam) phases in steam injection simulation for dead heavy oil.

3.2 Improved Method for Phase Identification

A fundamental reason for the difficulty, especially in two-phase identification, comes from the fact that the identity of a phase is defined in comparison with other phases calculated by the thermodynamic model used. Robust phase identification requires knowledge of phase equilibria calculated away from the thermodynamic conditions of interest. In this research, three-hydrocarbon-phase flow simulation at a fixed pressure and

temperature uses a tie-triangle table that contains a few tie triangles and their normal unit vectors, as part of the simulation input information. The limiting tie triangle at a CEP, if present, is always tabulated together with its normal unit vector. For example, a tie-triangle table for composition space that contains the entire three-phase region includes the two limiting tie triangles for the UCEP and LCEP. The detailed procedure for tie triangle tabulation is shown in **Appendix D**.

The extensions of these limiting tie triangles define three different regions in composition space; i.e., the super-UCEP, super-LCEP, and sub-CEP regions. In the super-UCEP region, two equilibrium phases are considered to originate with the UCEP tie line, L_1-L_2=V, and denoted as the L_1 and (L_2V) phases. In the super-LCEP region, two equilibrium phases are considered to originate with the LCEP tie line, L_1=L_2-V, and denoted as the V and (L_1L_2) phases. In the sub-CEP region, there are three different two-phase regions; i.e., L_1-V, L_1-L_2, and L_2-V. They originate with their corresponding edges of three phases. Altogether, five different two-phase regions can be recognized around the three-phase region in composition space.

When three equilibrium phases are calculated in simulation in this research, the phase with the highest concentration of the heaviest hydrocarbon component is labeled as L_1, as in Perschke et al. (1989). The phase with the highest methane concentration is labeled as V because it is unlikely that methane/hydrocarbon mixtures form three hydrocarbon phases at realistic reservoir temperature (Peters 1994). The other phase is labeled as L_2. Unlike the method of Perschke et al. (1989), phase mass densities are not used for labeling V and L_2 in a three-phase region. Note that the L_1-V edge is not always the longest edge of a tie triangle of L_1-L_2-V in multicomponent composition space. That is, it is not robust to use lengths of tie-triangle edges for three-phase identification.

Phase identification in a two-phase region in this research is substantially different from that in Perschke

et al. (1989). N_T tie triangles are tabulated from the UCEP tie triangle through the LCEP tie triangle. The normal vectors for the N_T tie triangles point from the UCEP to LCEP in this research. Two-phase identification starts with calculation of dot products using the UCEP and LCEP tie triangles as

$$d^{\mathrm{UCEP}} = (\vec{z} - \vec{x}_{\bullet}^{\mathrm{UCEP}}) \cdot \vec{n}^{\mathrm{UCEP}} \tag{3.1}$$

$$d^{\mathrm{LCEP}} = (\vec{z} - \vec{x}_{\bullet}^{\mathrm{LCEP}}) \cdot \vec{n}^{\mathrm{LCEP}}, \tag{3.2}$$

where $\vec{z}$ is the vector of the current overall composition, and $\vec{n}$ is the unit normal vector. $\vec{x}_{\bullet}$ is the composition vector of one of the three phases, which can be either L_1, L_2, or V, but should be used consistently. Superscripts UCEP and LCEP indicate that they are associated with the UCEP and LCEP tie triangles, respectively. If the two dot products are both negative, the overall composition is in the super-UCEP region; the current two phases are the L_1 and (L_2V) phases. If the two dot products are both positive, the overall composition is in the super-LCEP region; the current two phases are the V and (L_1L_2) phases. If d^{UCEP} is positive and d^{LCEP} is negative, the overall composition is in the sub-CEP region.

If the overall composition in a two-phase region is calculated to be in the sub-CEP region, the following dot products are calculated for the other ($N_T - 2$) tie triangles tabulated:

$$d^{m} = (\vec{z} - \vec{x}_{\bullet}^{m}) \cdot \vec{n}^{m} \tag{3.3}$$

for $2 \leq m \leq (N_T - 1)$, where m is the index for the tabulated tie triangles. Note that d^1 (= d^{UCEP}) is positive and d^{N_T} (= d^{LCEP}) is negative. Then, we find two tie triangles, m+ and m-, from the table such that

$$d^{m+} = \min_m\{d^m : d^m > 0\} \tag{3.4}$$

$$d^{m-} = \max_m\{d^m : d^m < 0\}. \tag{3.5}$$

Linear interpolation of three phase compositions is conducted between the two tie triangles m+ and m- as follows:

$$\vec{x}_j = \left(|d^{m-}|\vec{x}_j^{m+} + d^{m+}\vec{x}_j^{m-}\right)/(d^{m+} + |d^{m-}|), \tag{3.6}$$

where j = {L_1, L_2, V}. Finally, negative flash by use of the algorithm of Okuno et al. (2010) with $\vec{z}$ and K values from the interpolated $\vec{x}_j$is performed to determine in which region the current overall composition is, L_1-L_2, L_1-V, or L_2-V. The negative constant-K flash indicates the phase identities of the two phases if a sufficient N_T is used. In a single-phase region, the procedure is identical with that of Perschke et al. (1989), which is based on the user's input.

If composition space does not contain the entire three-phase region, the N_T triangles to be tabulated are selected from positive composition space. For example, if the UCEP is not present in positive composition space, the first triangle is a triangle on a subspace of (N_C – 1) components. If no CEPs are present in positive composition space, the first and N_T^{th} triangles are taken from two different subspaces of (N_C – 1) components that contain subcritical three phases.

Perschke et al. (1989) also described the phase tracking technique that labels phases in simulation on the basis of the concentrations of a selected component in the tracked phases from the previous time step. The phases at the new time step are labeled such that the concentrations are closest to the values at the old time step. This phase tracking technique can offer time savings in simulation by skipping the more careful phase identification described in this section. In this research, however, no phase tracking is performed because the primary interest is in obtaining correct numerical solutions of multiphase displacements, instead of computational speed.

3.3 Case Studies

To implement and verify the improved method for phase identification, equation B-1 is solved numerically by use of the single-point upstream weighting for the flux term, as described in Johns (1992) and Orr (2007). The advantage of not having to solve for gridblock pressures is important in terms of computational robustness and costs in this research. The thermodynamic model used is the PR EOS (Peng and Robinson 1976) with the van der Waals mixing rules. Phase viscosities are calculated with the correlation of Lohrenz et al. (1964). The multiphase behavior algorithms used are based on Perschke (1988) and Chang (1990) for sequential flash and stability calculations and Okuno et al. (2010) for constant-K flash.

Simulation cases are presented to verify the improved method for phase identification in the 1D convective flow simulator with 1000 gridblocks. The gridblock size is uniform, and $\Delta t_D/\Delta x_D$ is constant at 0.05. The porosity and permeability are 20% and 1000 mD, respectively. The Corey relative permeability parameters used are taken from Yuan and Pope (2012), in which the endpoint relative permeabilities for the V and L_2 phases are markedly different from each other **(Table 3.1).** The first case uses a quaternary fluid model, the second case uses the WS model, in which displacements occur in composition space of much higher dimensions, and third case uses the North Ward Estes (NWE) oil which is also a multicomponent system. The oil EOS property has been shown in detail by Okuno (2009).

The properties of the quaternary fluid are given in Tables 2.1 and 2.2. **Fig. 3.1** depicts d^1 and d^{NT} at 0.3 PVI in the simulation at 1500 psia with the relative permeability model given in Table 3.1. The first and $N_T{}^{th}$ triangles in the table are the limiting triangles at UCEP and LCEP, respectively. Thus, $d^1 = d^{UCEP}$, and $d^{NT} = d^{LCEP}$ in this case. The two phases downstream of the three-phase region are L_1 and V. The subcritical state is

clearly indicated by the signs of d^{UCEP} and d^{LCEP}. The two phases upstream of the three-phase region are L_1 and (L_2V), as can be confirmed by the negative d^{UCEP} and d^{LCEP}.

Fig. 3.2 shows d^{UCEP} and d^{LCEP} at 0.3 PVI in the simulation for WS oil at 55%-methane-dilution with the relative permeability model given in Table 3.1. The two phases downstream of the three-phase region change their identities; L_1-V, (L_1L_2)-V, and L_1-L_2 in the direction from the producer to the injector. The algorithm developed can precisely identify phases even in this complex simulation case. The complexity of phase identification tends to increase with increasing N_C. The minimum N_T required for the West Sak oil case is seven.

Fig. 3.3 shows failures of phase identification by the conventional method when used in the WS oil displacement at 55%-methane-dilution at 0.3 PVI with the relative permeability model given in Table 3.1. The threshold mass density used is 20 lbm/ft^3. The two phases downstream of the three-phase region are labeled as L_1 and V, and no distinction is made between the sub- and super-critical states. The two-phase region upstream of the three-phase region exhibits discontinuities. This is one of the typical failures caused by using a mass-density threshold.

Fig. 3.4 shows the phase identification by the conventional method for NWE oil displacement at 0.8 PVI with the relative permeability model. The upstream two-phase region is discontinuous because the conventional algorithm for phase identification gives wrong determination. The two-phase region close to the inlet is labeled incorrectly as L_1-V because the density of the non-oleic phase is less than the density threshold (40 lb/ft^3). Ahead of this L_1-V two-phase region is L_2-V. The mislabelling of L_2-V is a result of phase tracking procedure when a phase disappears at the trailing edge of three-phase region. The tracked component is methane in this simulation. **Fig. 3.5** gives the correct phase identification for this case. The

upstream is L_1-L_2 from negative three-phase flash. The downstream two-phase is L_1-V and super-LCEP in the direction from inlet to outlet.

3.4 Conclusions

In this chapter, an improved method for phase identification is developed and applied in 1D convective flow with three hydrocarbon phases. Conclusions are as follows:

1. The phase-identification method developed in this research can correctly solve for equilibrium-phase identities, which are part of the solution for a multiphase flow problem. The robustness comes mainly from the capability of precise quantification of the location of the current overall composition relative to the three-phase region in composition space. The improved method is confirmed using simulations of a quaternary displacement and West Sak oil displacement. Compared to conventional phase identification method, the improved method can lead to more accurate and consistent phase identification results.
2. The improved phase identification method can distinguish the super-CEP states from the sub-CEP states by use of the critical tie-triangle extensions. With the developed method, five types of two-phase regions can be properly considered around the three-phase region in three-hydrocarbon-phase flow simulation.
3. 1-D convective flow simulator with no volume change on mixing for three-hydrocarbon-phase flow was developed. The advantage of using this simulator in this thesis is that the theory developed for multiphase transitions in Chapter 2 is directly applied to various simulation results based on no volume change on mixing. In this simulator, the thermodynamic model used is the Peng-Robinson (PR) EOS (Peng and Robinson 1976) with the van der Waals mixing rules. Phase viscosities are calculated with the correlation

of Lohrenz et al. (1964). The multiphase behavior algorithms used are based on Perschke (1988) and Chang (1990) for sequential flash and stability calculations and Okuno et al. (2010) for constant-K flash.

Table 3.1 Corey Relative Permeability Parameters for 1D Oil Displacement Simulations

Yuan and Pope (2012)	Phase index	L_1	V	L_2
	Residual saturation	0.2	0.2	0.2
	Endpoint	0.2	1.0	0.4
	Exponent	2	2	2
Model 1	Phase index	L_1	V	L_2
	Residual saturation	0.2	0.2	0.2
	Endpoint	0.2	1.0	1.0
	Exponent	2	2	2

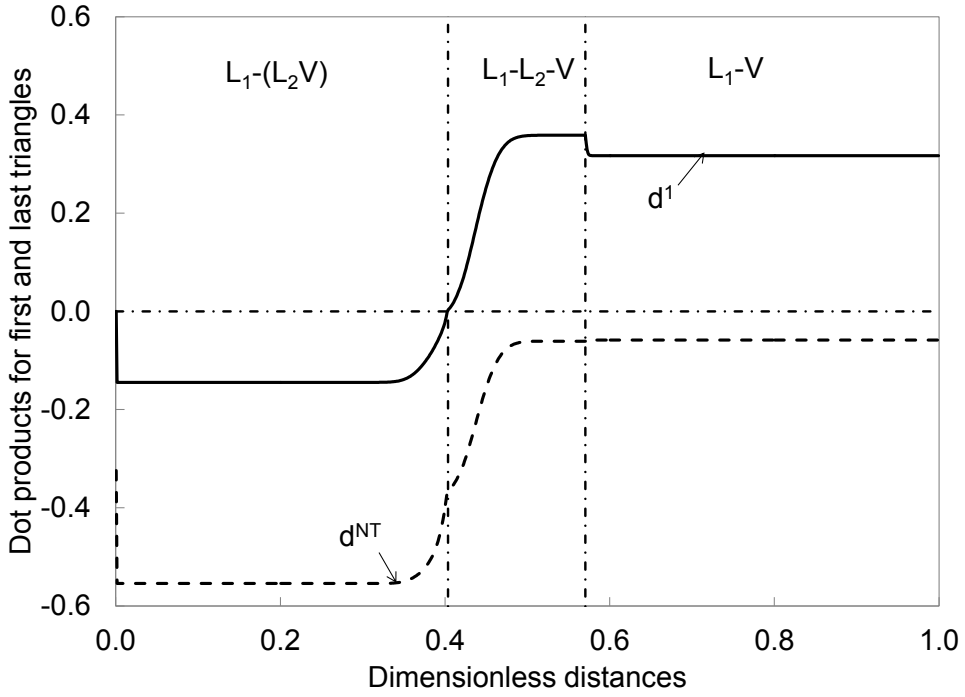

Figure 3.1 Dot products (equation 3.3) calculated at 0.3 PVI for the limiting tie triangles ($d^1 = d^{UCEP}$ and $d^{NT} = d^{LCEP}$) for the quaternary displacement at 1500 psia and 86°F with relative permeability model 1.

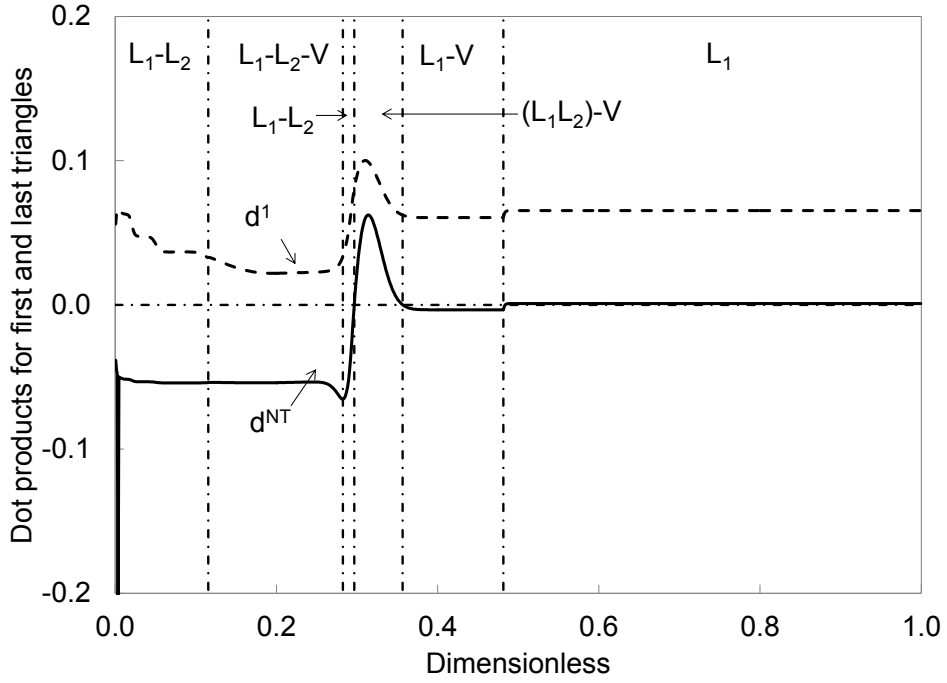

Figure 3.21 Dot products (equation 3.3) calculated at 0.3 PVI for the first and last triangles for the West Sak oil displacement at 55%-methane-dilution at 1500 psia and 65°F with relative permeability model 1.

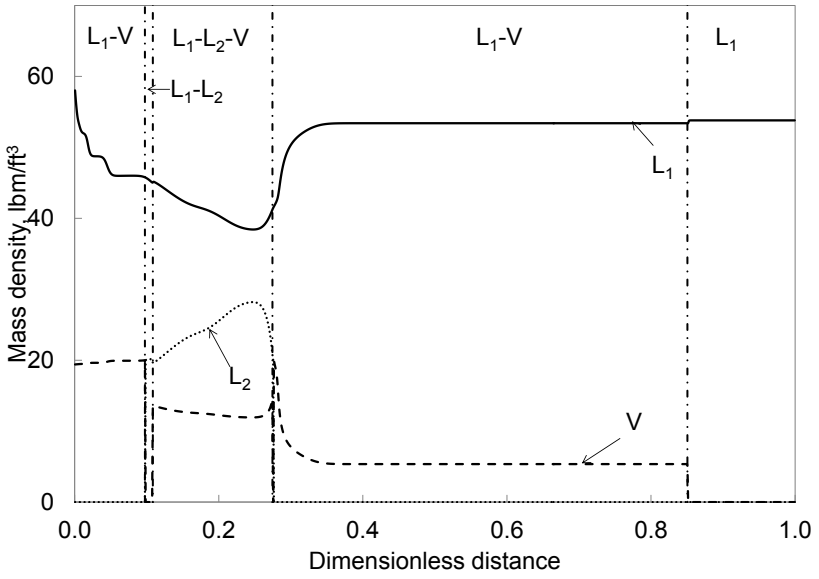

Figure 3.22 Mass density profiles at 0.3 PVI for the West Sak oil displacement at 55%-methane-dilution at 1500 psia at 65°F.

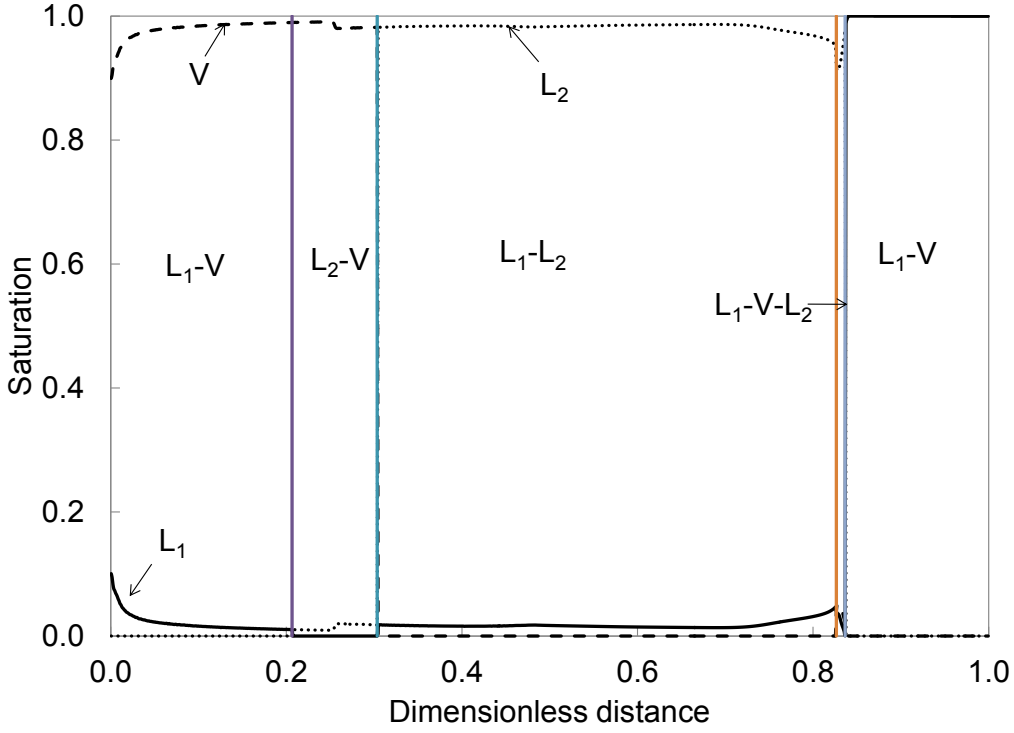

Figure 3.4 Saturation profiles at 0.8 PVI for the NWE oil displacement at 1400 psia at 83°F.

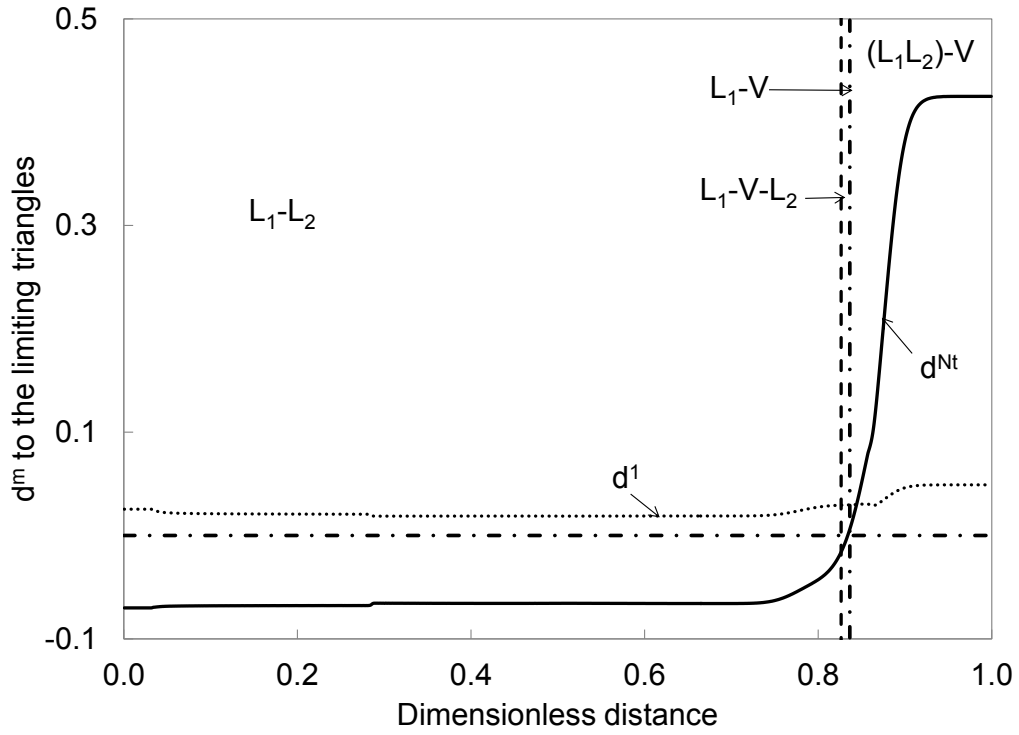

Figure 3.5 Dot products (equation 3.3) calculated at 0.3 PVI for the limiting tie triangles ($d^1 = d^{UCEP}$ and $d^{NT} = d^{LCEP}$) for the NWE oil displacement at 1400 psia and 83°F

Chapter 4: Confirmation of the Mass Transfer Mechanism in 1-D Convective Flow Simulation with No Volume Change on Mixing

In chapter 2, two analytical conditions were derived to quantify the local displacement efficiency by three hydrocarbon phases. Nonmonotonic oil recovery was explained. However, that research was limited by the flow conditions, because the conventional phase identification method implemented in UTCOMP is not entirely robust for three-hydrocarbon-phase flow. In chapter 3, therefore, an improved algorithm was developed for consistent phase identification in three-hydrocarbon-phase flow. The new phase identification algorithm was successfully implemented in a 1-D convective simulator with no volume change on mixing.

With the improved phase identification algorithm, this chapter aims to confirm that the distance parameters derived can quantify the displacement efficiency by three hydrocarbon phases, although the displacement efficiency can be affected by various factors, such as temperature, pressure, initial and injection compositions, diffusion/dispersion, fluid properties, and relative permeabilities. In this chapter, all simulations are conducted by the 1-D convective simulator with the improved phase identification algorithm, unlike in chapter 2.

Four simulation cases are presented to confirm that the distance parameters derived before can quantify the displacement efficiency by three hydrocarbon phases. The first two cases use two quaternary fluid models, but they have different recovery trends at a given throughput: nonmonotonic and monotonic trends. The last two cases use multicomponent fluid models. Similarly, the two multicomponent models exhibit nonmonotonic and monotonic oil recovery trends. The gridblock size is uniform, and $\Delta t_D/\Delta x_D$ is constant at 0.05. The porosity and permeability are 20% and 1000 mD, respectively. The Corey relative permeability parameters used are taken from Yuan and Pope (2012), in which the endpoint relative permeabilities for the V

and L_2 phases are markedly different from each other **(Table 4.1).** As shown in Table 1, two models are prepared for relative permeabilities; the L_2 phase shares the same parameter values with the V phase in model 1 and with the L_1 phase in model 2.

4.1 Case Study 1: HQ Displacement

This quaternary fluid is made after the Schrader Bluff oil model of Guler et al. (2010). The properties of fluid have been presented in Tables 2.1 and 2.2. Simulations have been performed for this fluid by use of UTCOMP in chapter 2 at different pressure and at different enrichments. The key point leading to nonmonotonic oil recovery at a given throughput is that the local displacement efficiency increases as the pressure or enrichment decreases, unlike the conventional two-phase displacement. In this section, simulations are again performed for this fluid, but by use of a simpler convective simulator with no volume change on mixing.

Fig. 4.1 presents simulated recovery of PC4 at three different pressures, 1000, 1500, and 1750 psia. The figure indicates that the miscibility level of oil displacement increases with decreasing pressure with a different set of relative permeability parameters. Use of model 2 results in higher oil recovery than use of model 1, and the difference becomes more obvious with increasing pressure. The PC4 recovery at 1750 psia at breakthrough of the three-phase trailing edge is 85.37% with model 1, which is 4.54% lower than when model 2 is used.

The degree of miscibility and phase mobilities affect oil displacements in a complicated manner. The distance parameters, δ^T and δ^L, were derived to understand the complicated interaction of flow and phase behavior through interphase mass transfer on multiphase transitions (Equations 2.5 and 2.6). However, these

two distance parameters cannot be calculated analytically in chapter 2, since the effect of volume change on mixing is considered in UTCOMP. The indirect method to calculate the two distance parameters may affect the accuracy of the numerical values. In this chapter, the two distance parameters can now be calculated analytically by

$$\delta^L = \left\| \gamma_{N_1}^U \underline{c}_{N_1}^U - \gamma_{N_1}^D \underline{c}_{N_1}^D \right\|_2, \tag{4.1}$$

$$\delta^T = \left\| \gamma_{L_1}^U \underline{c}_{L_1}^U - \gamma_{L_1}^D \underline{c}_{L_1}^D \right\|_2, \tag{4.2}$$

where $\gamma_j = \frac{\Lambda S_j - f_j}{\Lambda - 1}, \Lambda = \frac{F_i^U - F_i^D}{C_i^U - C_i^D}$. All variables in equations (4.1) and (4.2) are available in the simulations by the 1-D convective simulator with no volume change on mixing.

Figs. 4.2 and 4.3 shows the δ^T and δ^L parameters for the simulated displacements. The two parameters accurately capture the oil displacement efficiency by three phases; i.e., the oil displacement becomes more efficient as the distances decrease. The effect of relative permeability on the oil displacement is more significant with increasing pressure because the degree of miscibility decreases with increasing pressure in this displacement. As shown in Figs. 4.2 and 4.3, the lower distances in displacements by model 2 are lower than those in displacements by model 1. This also implies that the relative permeability can affect the oil recovery by changing the mass transfer on phase transitions. By use of model 2, the mass transfer on phase transitions is more efficient than that by use of model 1.

This is the first time the effect of relative permeability on three-hydrocarbon-phase oil displacement is confirmed by interphase mass transfer, which was not entirely possible without the reliable phase-identification algorithm developed in this research. The distance parameters can represent how components are redistributed on multiphase transitions in three-phase flow because they consider phase mobilities as well as phase compositions through mass conservation equations.

4.2 Case Study 2: West Sak Displacement

This multicomponent fluid is the WS oil characterized by Xu (2012). The properties of fluid have been presented in Tables 2.4. Simulations have been performed for this fluid by use of UTCOMP in chapter 2 at different enrichments. Similarly, the key point leading to nonmonotonic oil recovery at a given throughput is that the local displacement efficiency increases as the enrichment decreases. In this section, simulations are again performed for this fluid by use of the 1-D convective simulator with no volume change on mixing.

Fig. 4.4 presents simulated recovery of C_{34-40} at three different enrichments, 50%-, 55%-, and 60%-methane dilution. Similar trends were also observed for other heavy components. Use of model 2 results in higher oil recovery than use of model 1, and the difference becomes more obvious with decreasing methane dilution. **Figs. 4.5 and 4.6** show the distance parameters, δ^L and δ^T, calculated in analytical way for the simulations with relative permeability models 1 and 2. δ^T clearly indicates that the miscibility level of oil displacement increases with increasing methane dilution, which is consistent with results given in the literature (DeRuiter et al. 1994; Mohanty et al. 1995). It also shows that use of model 2 results in interphase mass transfer on the multiphase transition that is more favorable in terms of oil displacement by three phases. The difference between models 1 and 2 decreases with increasing methane dilution. These results can be confirmed in Fig. 4.4. Thus, methane dilution enables to increase the miscibility level of this West Sak oil displacement by making interphase mass transfer on multiphase transitions more favorable. The increased miscibility level can be so high that relative permeability parameters little affect oil recovery predictions. Further investigation is required to understand under what conditions methane dilution can enhance the miscibility of oil displacement.

4.3 Case Study 3: BSBQH Displacement

This quaternary fluid used was taken from Okuno (2009), which was made after the BSB oil model. For simplicity, this quaternary fluid is referred as BSBQH. The four components consist of methane (C_1), CO_2, and two heavy pseudocomponents (CH1 and CH2). Their properties are given in Okuno (2009) (i.e. the BSBQH2 in the dissertation)**.** The injection gas consists of 5 mol% C1 and 95 mol% CO_2. The reservoir temperature is 105°F. Detailed phase behavior predictions in P-T-x space for this quaternary fluid can be found in Okuno (2009), and are not duplicated here.

Fig. 4.7 presents simulated recoveries of CH2 at three different pressures, 1300, 1400, and 1500 psia. Different from the HQ displacements in section 4.1 and the WS displacements in section 4.2, the miscibility level of oil displacement increases with increasing pressure. In addition, use of model 1 results in higher oil recovery than use of model 2, and the difference becomes more obvious with decreasing pressure which indicates more immiscible displacement. The CH2 recovery at 1300 psia at breakthrough of the three-phase trailing edge is 66.41% with model 1, which is 20.24% higher than when model 2 is used.

Figs. 4.8 and 4.9 show the δ^L and δ^T parameters in an analytical way for the simulated displacements. The two parameters accurately capture the oil displacement efficiency by three phases. The effect of relative permeability on the oil displacement is more significant with decreasing pressure because the degree of miscibility decreases with decreasing pressure in this displacement.

4.4 Case Study 4: Bob Slaughter Block Displacement

This multicomponent system is the BSB oil that was developed by Khan et al. (1992) as presented in Table

2.5. The injection gas consists of 95% CO_2 and 5% methane as used in Okuno et al. (2011). The reservoir temperature is 105°F. Oil displacements are simulated at 1100 psia, 1200 psia, and 1300 psia. Three phases are present in all these displacements. Details of phase behavior for these displacements are given in Okuno (2009) and Okuno et al. (2011), and not duplicated here.

Oil recovery at a given throughput monotonically increases with pressure as presented in chapter 2. **Fig. 4.10** shows the oil recovery at the breakthrough time of the three-phase trailing edge by use of models 1 and 2. The use of model 1 results in a more efficient displacement than model 2. Although the recovery difference is small for all simulations, the difference does decrease as pressure increases. This indicates that the miscibility level of oil displacement increases with increasing pressure. The increased miscibility level can be so high that relative permeability parameters little affect oil recovery predictions. **Figs. 4.11 and 4.12** show the distance parameters, δ^T and δ^L, calculated in the simulations with relative permeability models 1 and 2. It also shows that use of model 1 results in interphase mass transfer on the multiphase transition that is more favorable in terms of oil displacement by three phases.

4.5 Conclusions

This chapter was concerned with numerical solutions of 1D three-hydrocarbon-phase convective flow problems set by temperature, pressure, initial and injection compositions, fluid properties, and relative permeabilities. In case studies, the simulator with the new phase-identification method was used to investigate the effect of relative permeability parameters on oil displacement by three hydrocarbon phases. Results confirm that the distance parameters derived in chapter 2 are capable of capturing not only the effect of miscibility (i.e., phase behavior), but also the effect of phase mobility (i.e., multiphase flow) on oil

displacement by three phases. Conclusions are as follows:

1. The equations for the interphase mass transfer on multiphase transitions presented in chapter 2 was confirmed with varying level of miscibility and relative-permeability parameters. The distance parameters can properly represent the interaction of flow and phase behavior since they were derived from mass conservation, not only from thermodynamic conditions. The direct calculation of the distance parameters that is possible with the new simulator improves the reliability of the distance parameters in quantification of oil displacement efficiency.
2. The simulation case study for the West Sak oil confirmed the experimental observation of DeRuiter et al. (1994) and Mohanty et al. (1995). The analysis of interphase mass transfer indicated that the miscibility level of oil displacement increases with increasing methane dilution in this case. The effect of relative permeability diminishes as the miscibility level increases owing to methane dilution. Further investigation is required to understand under what conditions methane dilution can enhance miscibility development in oil displacement.

Table 4.1 Corey Relative Permeability Parameters for 1D Oil Displacement Simulations

Yuan and Pope (2012)	Phase index	L_1	V	L_2
	Residual saturation	0.2	0.2	0.2
	Endpoint	0.2	1.0	0.4
	Exponent	2	2	2
Model 1	Phase index	L_1	V	L_2
	Residual saturation	0.2	0.2	0.2
	Endpoint	0.2	1.0	1.0
	Exponent	2	2	2
Model 2	Phase index	L_1	V	L_2
	Residual saturation	0.2	0.2	0.2
	Endpoint	0.2	1.0	0.2
	Exponent	2	2	2

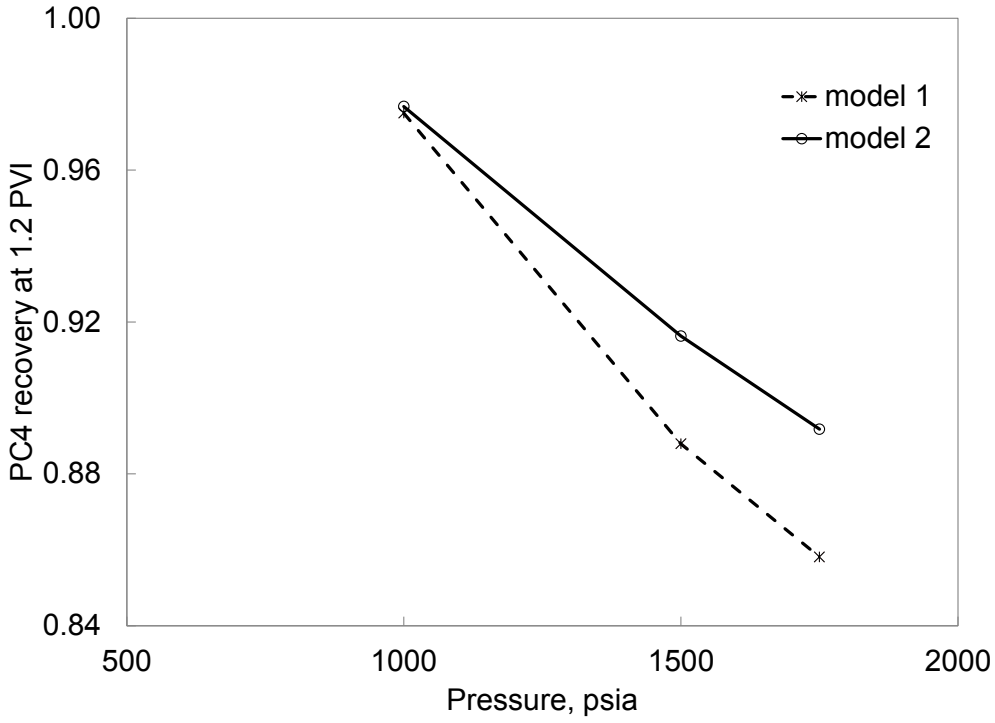

(a)

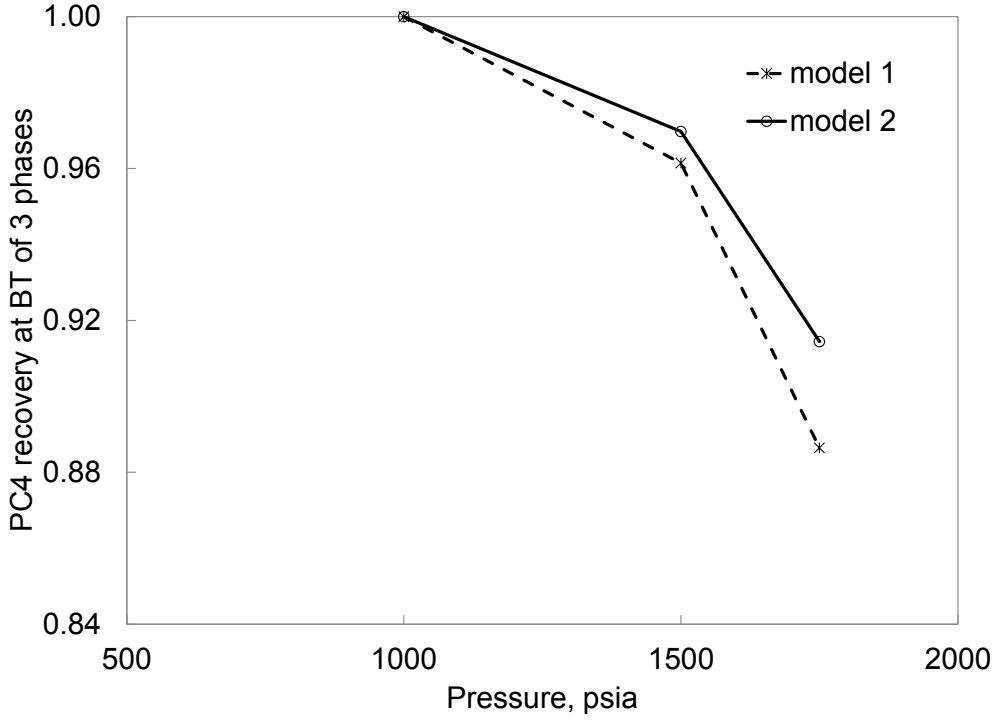

(b)

Figure 4.1 Simulated recoveries of PC4 in the HQ displacement at 86°F; (a) PC4 recoveries at 1.2 PVI; (b) PC4 recoveries at breakthrough (BT) of the trailing edge of three phases.

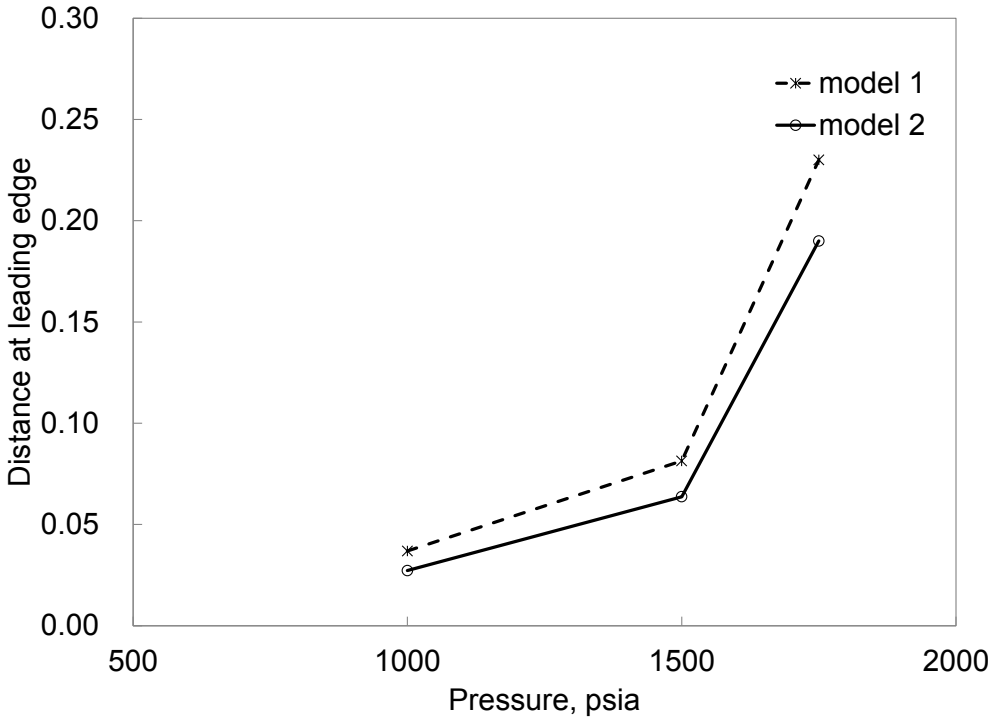

Figure 4.23 The δ^L parameter for the HQ displacements with relative permeability models 1 and 2

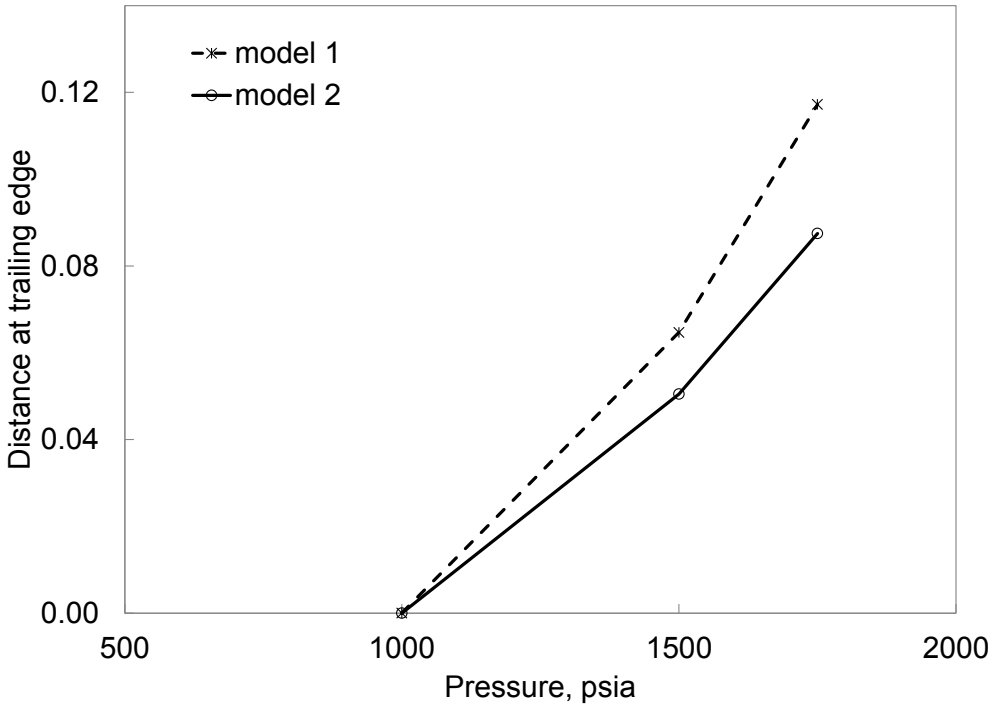

Figure 4.24 The δ^T parameters for the HQ displacements with relative permeability models 1 and 2

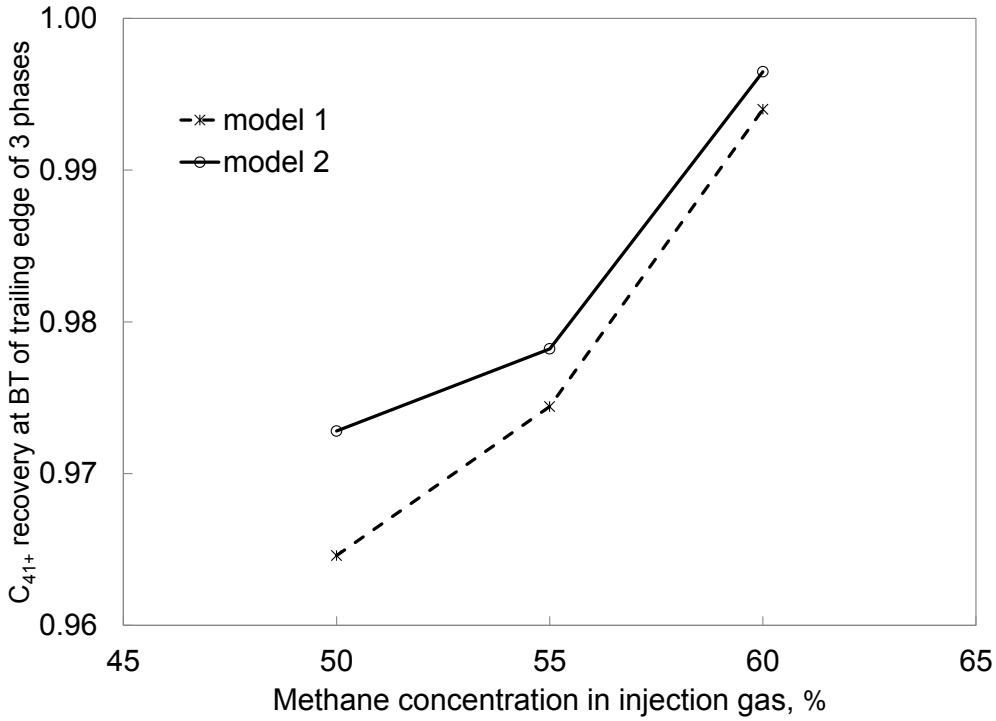

Figure 4.4 Simulated recoveries of C_{34-40} at BT for the WS displacement at 65°F by use of models 1 and 2

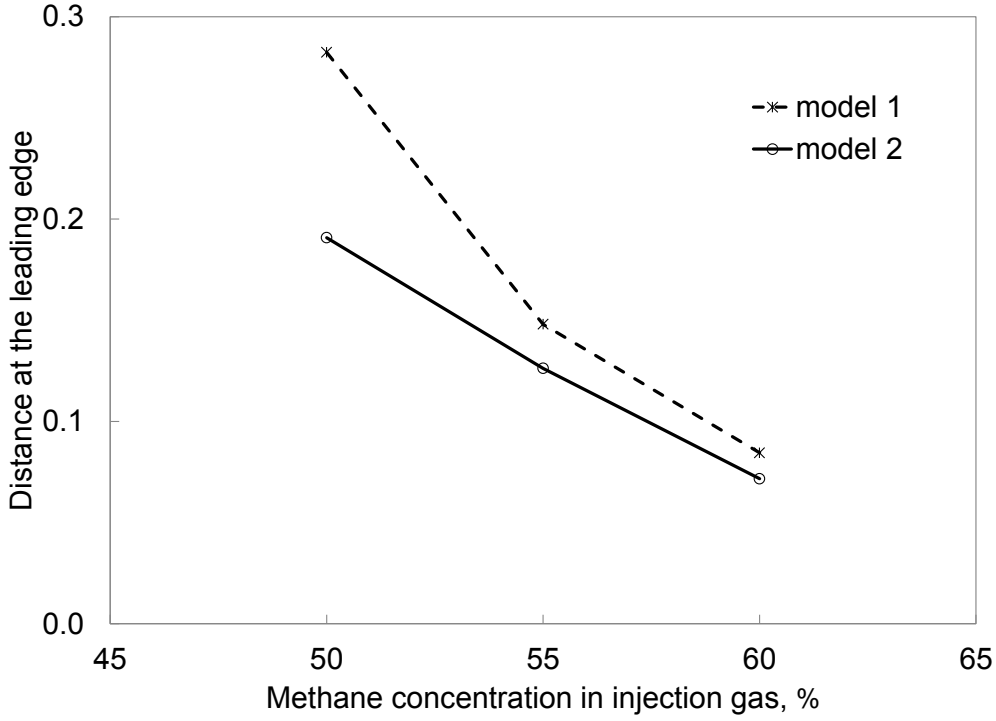

Figure 4.5 The δ^L parameter for the WS displacements with relative permeability models 1 and 2

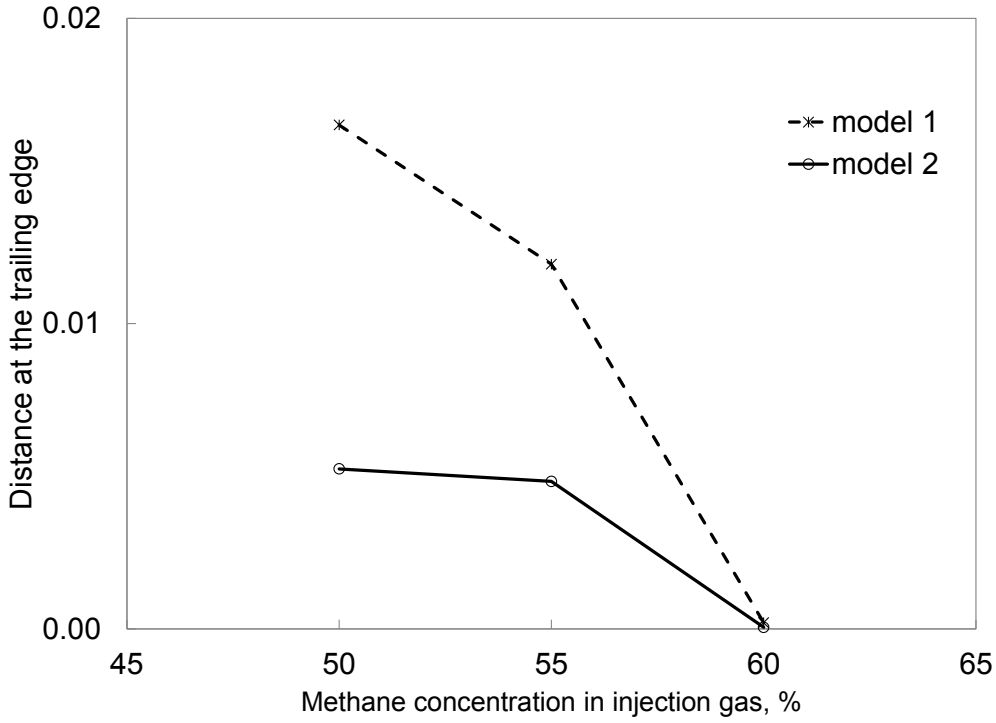

Figure 4.6 The δ^T parameter for the WS displacements with relative permeability models 1 and 2 dilution at 65°F by model 1.

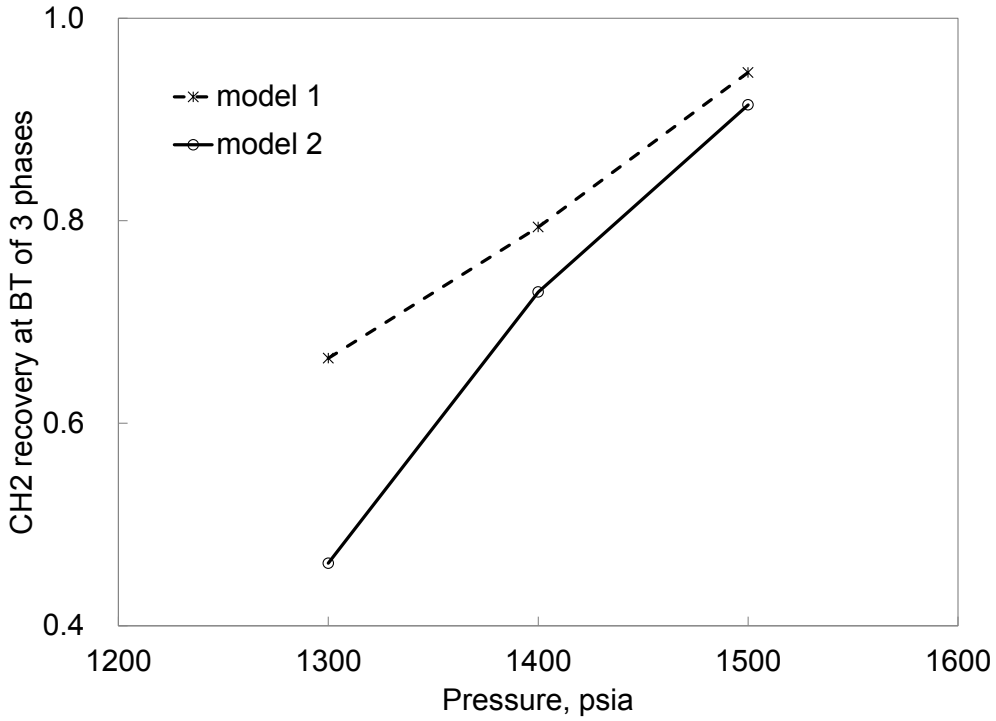

Figure 4.7 Simulated recoveries of CH2 at BT for the BSBQH displacement at 105°F by use of models 1 and 2

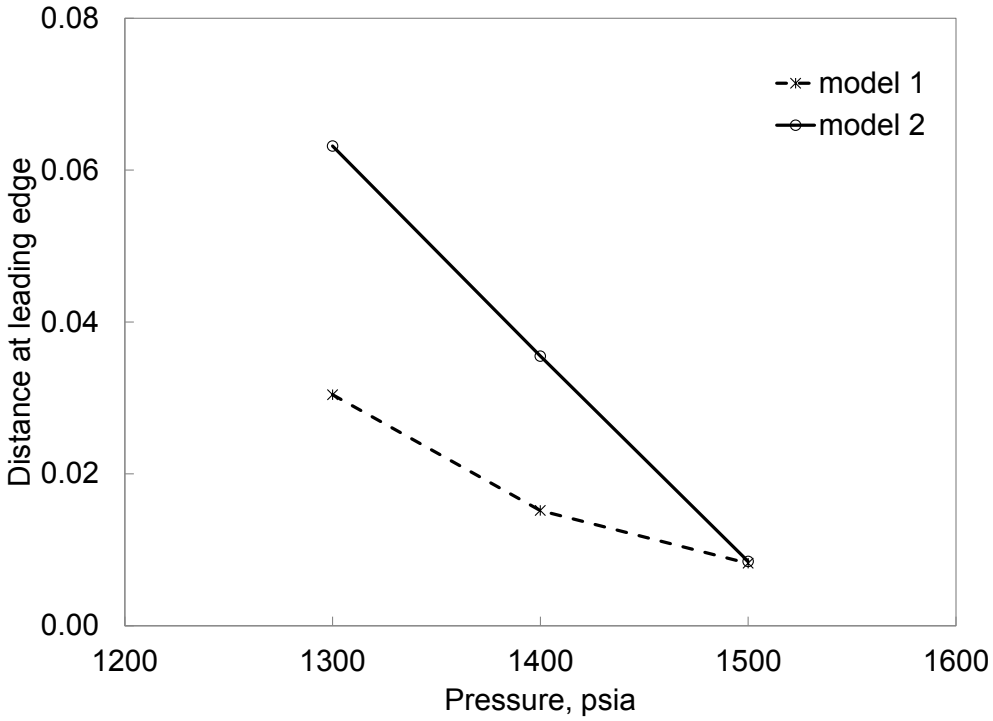

Figure 4.25 The δ^L parameter for the BSBQH displacements with relative permeability models 1 and 2

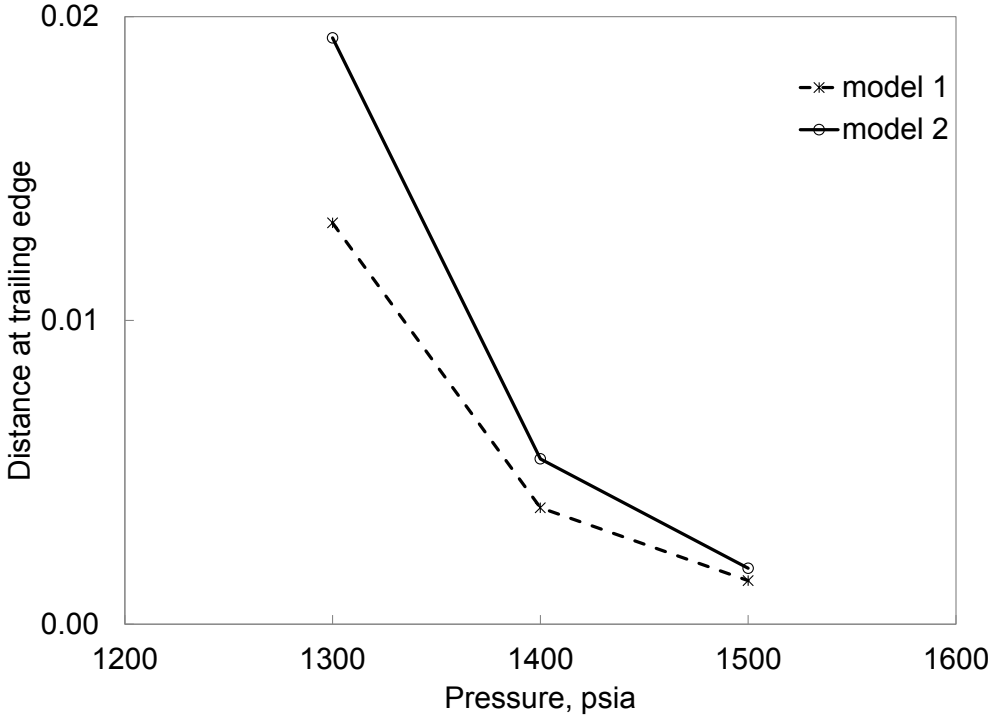

Figure 4.9 The δ^T parameter for the BSBQH displacements with relative permeability models 1 and 2

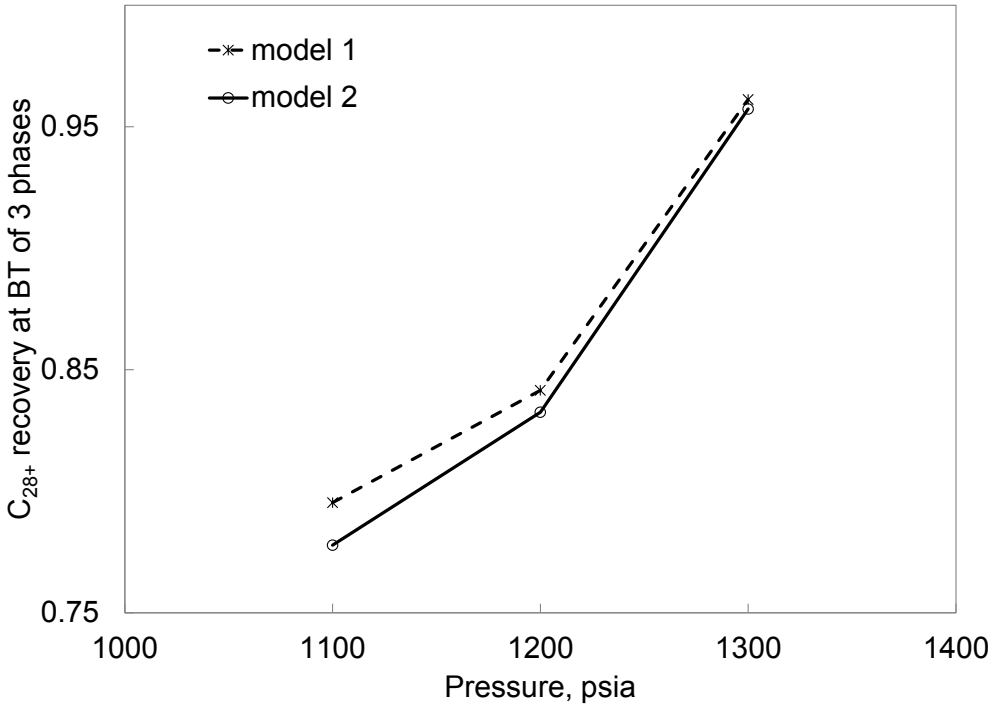

Figure 4.26 Simulated recoveries of C_{28+} at BT for the BSB displacement at 105°F by use of models 1 and 2

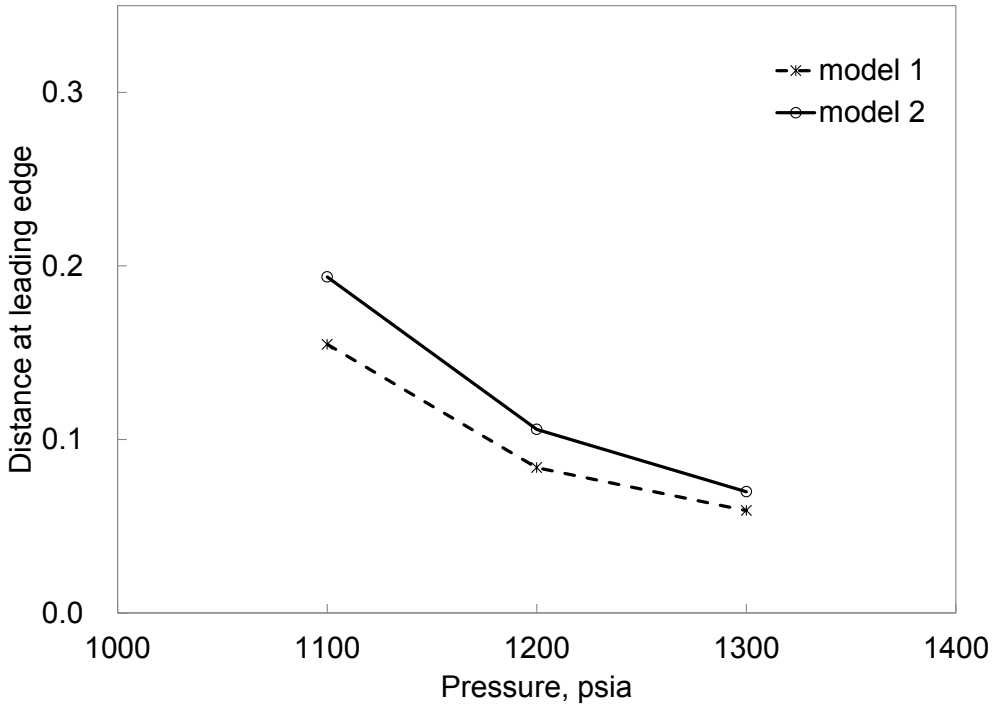

Figure 4.27 The δ^L parameter for the BSB displacements with relative permeability models 1 and 2

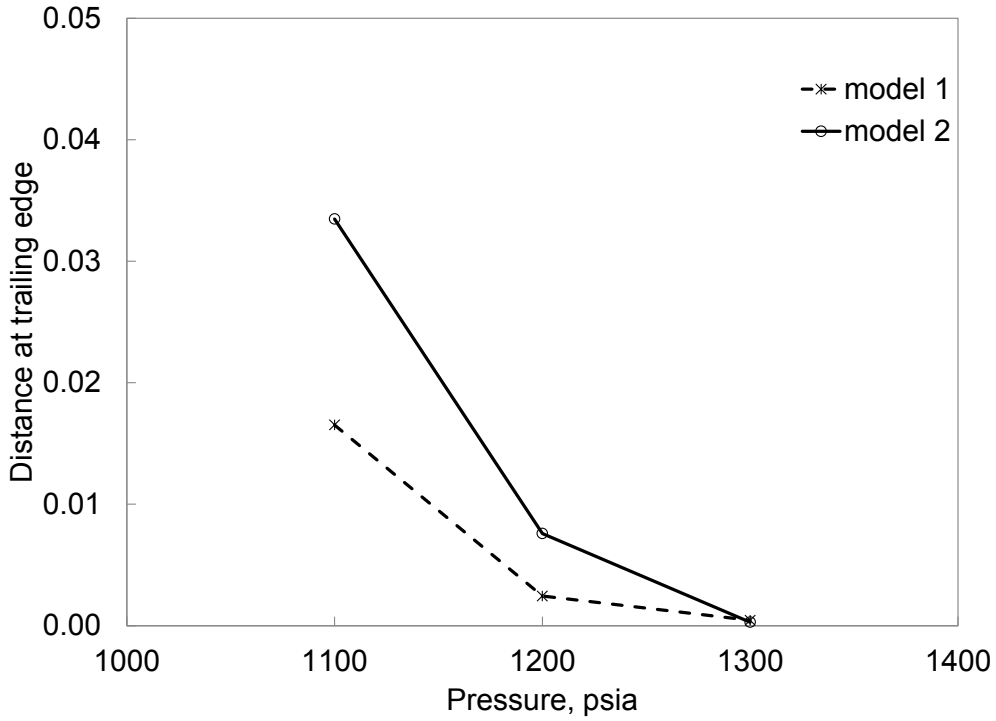

Figure 4.28 The δ^T parameter for the BSB displacements with relative permeability models 1 and 2

Chapter 5: Conclusions and Recommendations for Further Research

This thesis presented the analytical conditions to quantify the oil-displacement efficiency by three hydrocarbon phases. To confirm the mass transfer mechanisms, a 1-D convective simulator was coded with an improved phase identification algorithm by assuming no volume change on mixing. Then, various cases were used to confirm that the distance parameters derived in chapter 2 can quantify the oil-displacement efficiency by three hydrocarbon phases, although the displacement efficiency can be affected by various factors, such as temperature, pressure, initial and injection compositions, fluid properties, diffusion/dispersion, and relative permeabilities.

5.1 Conclusions

Chapter 2 mainly investigated the local efficiency of three-hydrocarbon-phase displacement of oil. Mathematical conditions were derived for efficient redistribution of components on multiphase transitions between two and three phases. These conditions were used to explain non-monotonic oil recovery at a given throughput with respect to gas enrichment and monotonic oil recovery at a given throughput with respect to displacement pressure. Conclusions are as follows:

1. Oil recovery in a partially miscible displacement depends on two factors; local displacement efficiency and components' propagation rates. Non-monotonic oil recovery at a given throughput can occur when local displacement by three hydrocarbon phases becomes more efficient, but slower, with decreasing pressure or decreasing gas enrichment. This was confirmed using fine-scale simulations of quaternary displacements and the West Sak oil displacements. A maximum in oil recovery at a given throughput occurs as a consequence of the balance between the local displacement efficiency and the

propagation rate of three hydrocarbon phases.

2. Similar to conventional two-phase displacement, monotonic oil recovery at a given throughput can also occur when local displacement by three hydrocarbon phases becomes more efficient with increasing pressure or increasing gas enrichment. This was confirmed using fine-scale simulations of oil displacements for west Texas, such as Bob Slaughter Block oil.
3. Local displacement efficiency by three hydrocarbon phases depends significantly on how components are redistributed on multiphase transitions between two and three phases. At the leading edge of the three-phase region, the second non-oleic phase should appear from the oleic phase of the downstream two-phase region. At the trailing edge of the three-phase region, two non-oleic phases of the three-phase region should merge into the non-oleic phase of the upstream two-phase region.
4. The distances defined in Equations 2.5 and 2.6 for efficient multiphase transitions can correctly identify the local displacement efficiency by three hydrocarbon phases. The distances were successfully used to explain the quaternary displacements and the West Sak oil displacements that exhibit nonmonotonic oil recovery and the Bob Slaughter Block oil displacements that exhibit monotonic oil recovery.
5. Partially miscible displacement of oil by two non-oleic phases can be collectively efficient, even if they are individually immiscible with oil. The West Sak oil displacement with enriched gas studied in this research showed a displacement efficiency of 84.29% at 1.0 HCPVI, 90.18% at 1.5 HCPVI, and 91.53% at 2.0 HCPVI at 53% methane dilution. With this methane dilution, the three-phase displacement was locally efficient and fast enough to exhibit a high oil recovery.

In chapter 3, an improved method for phase identification is developed and applied in 1D convective flow with three hydrocarbon phases. Conclusions are as follows:

1. The phase-identification method developed in this research can correctly solve for equilibrium-phase identities, which are part of the solution for a multiphase flow problem. The robustness comes mainly from the capability of precise quantification of the location of the current overall composition relative to the three-phase region in composition space. The improved method is confirmed using simulations of a quaternary displacement and West Sak oil displacement. Compared to conventional phase identification method, the improved method can lead to more accurate and consistent phase identification results.
2. The improved phase identification method can distinguish the super-CEP states from the sub-CEP states by use of the critical tie-triangle extensions. With the developed method, five types of two-phase regions can be properly considered around the three-phase region in three-hydrocarbon-phase flow simulation.
3. 1-D convective flow simulator with no volume change on mixing for three-hydrocarbon-phase flow was developed. The advantage of using this simulator in this thesis is that the theory developed for multiphase transitions in Chapter 2 is directly applied to various simulation results based on no volume change on mixing. In this simulator, the thermodynamic model used is the Peng-Robinson (PR) EOS (Peng and Robinson 1976) with the van der Waals mixing rules. Phase viscosities are calculated with the correlation of Lohrenz et al. (1964). The multiphase behavior algorithms used are based on Perschke (1988) and Chang (1990) for sequential flash and stability calculations and Okuno et al. (2010) for constant-K flash.

Chapter 4 was concerned with numerical solutions of 1D three-hydrocarbon-phase convective flow problems set by temperature, pressure, initial and injection compositions, fluid properties, and relative permeabilities. In case studies, the simulator with the new phase-identification method was used to

investigate the effect of relative permeability parameters on oil displacement by three hydrocarbon phases. Results confirm that the distance parameters derived in chapter 2 are capable of capturing not only the effect of miscibility (i.e., phase behavior), but also the effect of phase mobility (i.e., multiphase flow) on oil displacement by three phases. Conclusions are as follows:

1. The equations for the interphase mass transfer on multiphase transitions presented in chapter 2 was confirmed with varying level of miscibility and relative-permeability parameters. The distance parameters can properly represent the interaction of flow and phase behavior since they were derived from mass conservation, not only from thermodynamic conditions. The direct calculation of the distance parameters that is possible with the new simulator improves the reliability of the distance parameters in quantification of oil displacement efficiency.
2. The simulation case study for the West Sak oil confirmed the experimental observation of DeRuiter et al. (1994) and Mohanty et al. (1995). The analysis of interphase mass transfer indicated that the miscibility level of oil displacement increases with increasing methane dilution in this case. The effect of relative permeability diminishes as the miscibility level increases owing to methane dilution. Further investigation is required to understand under what conditions methane dilution can enhance miscibility development in oil displacement.

5.2 Recommendations for Future Research

Solvent injection for EOR requires a detailed understanding of oil-recovery mechanisms in multiphase displacement. The main contribution of this thesis is the derivation of analytical conditions to quantify the displacement efficiency by three phases. However, more fundamental and systematic research is required to

create useful knowledge for the oil industry.

1. In chapter 4, the effects of relative permeability on displacement efficiency were concluded for two types: model 2 was better than model 1 for HQ and WS displacements, but model 1 was better than model 2 for BSBQH and BSB displacements. The possible explanation of the two types of relative-permeability effects is that the dense injected component moves faster with model 2 than model 1 for HQ and WS displacements, but moves faster with model 1 than model 2 for BSBQH and BSB displacements.
2. Displacement pressure and enrichment can both affect the displacement efficiency by three hydrocarbon phases. For HQ and WS displacements, displacement efficiency increases as the displacement pressure or enrichment decreases. For the BSBQH and BSB displacements, displacement efficiency increases as the displacement pressure increases. However, it is unclear how pressure and enrichment impact on the displacement efficiency. The possible solution requires the fundamental study of the three-phase behavior, such as how three-phase behavior changes in pressure space.

Nomenclature

Roman Symbols:

c_{ij}: Volumetric fraction of component i in phase j

$\underline{c}_j$: Vector consisting of c_{ij} as defined in Equation B-4

C_i: Overall volume fraction of component i

d: Distance between two equilibrium-phase compositions x

f_j: Fractional flow of phase j

F_i: Overall fractional flow of component i

L_1: Oleic phase

L_2: Solvent-rich liquid phase

$\vec{n}$: is the unit normal vector

N_j (j = 1, 2, or 3): Non-oleic phase (i.e., L_2 or V)

N_C: Number of components

N_P: Number of phases

N_T: Number of tie triangles

P: Pressure or pseudo phase

P_C: Critical pressure

S: Surface area of CV

S_j: Saturation of phase j

T: Temperature

T_C: Critical temperature

t_D: Dimensionless time in pore volumes

V: Gaseous phase or volume of the CV in equation B-2

V_C: Critical volume

v_D: Dimensionless velocity of phase transition defined in Equation B-3

W: Aqueous phase

x: Composition

x_D: Dimensionless distance from the injector

$\underline{x}_j$: Vector consisting of x_{ij}

x_{ij}: Mole fraction of component i in phase j

$\underline{z}$: Overall composition vector

Abbreviations

CEP: Critical endpoint

CV: Control volume

EOS: Equation of state

LCEP: Lower critical endpoint

HCPVI: Hydrocarbon pore-volume injected

HQ: Quaternary heavy (oil)

MCM: Multicontact miscibility

MMP: Minimum miscibility pressure

MOC: Method of characteristics

PC: Pseudo component

PM: Partially miscible

PR: Peng-Robinson

PVI: Pore-volume injected

SRK: Soave-Redlich-Kwong

UCEP: Upper critical endpoint

Superscripts

D: Downstream

L: Leading edge of three phases

T: Trailing edge of three phases

U: Upstream

Greek symbols

ρ_j: Density of phase j

γ: Parameter defined in Equation B-5

Γ: Parameter defined in Equations (2.5) and (2.6)

δ: Distance defined

Λ: Dimensionless shock velocity

References

Aghbash, V.N. and Ahmadi, M. 2012. Evaluation of CO_2-EOR and Sequestration in Alaska West Sak Reservoir Using Four-Phase Simulation Model. Paper SPE 153920 presented at the SPE Western Regional Meeting, 21-23 March, Bakersfield, CA, USA.

Ahmadi K. 2011. *Advances in Calculation of Minimum Miscibility Pressure.* PhD dissertation, the University of Texas at Austin, Austin, Texas.

Beygi, M.R., Delshad, M., Pudugramam, V.S., Pope, G.A., and Wheeler, M.F. 2014. Novel Three-Phase Compositional Relative Permeability and Three-Phase Hysteresis Models. *SPE Journal* (in print). SPE-165324-PA.

Bluma, M. and Deiters, U.K. 1999. A Classification of Phase Diagrams of Ternary Fluid Systems. *Physical Chemistry Chemical Physics* **1**(18): 4307-4313.

Creek, J.L. and Sheffield, J.M. 1993. Phase Behavior, Fluid Properties, and Displacement Characteristics of Permian Basin Reservoir Fluid-CO_2 Systems. SPE Reservoir Engineering, 8(01), 34-42.

Chang. Y.-B. 1990. *Development and Application of an Equation of State Compositional Simulator.* PhD dissertation, the University of Texas at Austin, Austin, Texas.

DeRuiter R. A., Nash, L.J., and Wyrick M.S. 1994. Solubility and Displacement Behavior of Carbon Dioxide and Hydrocarbon Gases with a Viscous Crude Oil. *SPE Reservoir Engineering*. 9(02), 101-106.

Deiters, U.K. and Pegg, I.L. 1989. Systematic Investigation of the Phase Behavior in Binary Fluid Mixtures. I. Calculations Based on the Redlich-Kwong Equation of State. *The Journal of Chemical Physics* **90**(11): 6632-6641.

Deiters, U. and Schneider, G.M. 1976. Fluid Mixtures at High Pressures. Computer Calculations of the Phase Equilibria and the Critical Phenomena in Fluid Binary Mixtures From the Redlich-Kwong Equation of State. *Berichte der Bunsengesellschaft fuer Physikalische Chemie* **80**(12): 1316-1321.

Dindoruk, B. 1992. *Analytical Theory of Multiphase, Multicomponent Displacement in Porous Media.* PhD dissertation, Stanford University, Stanford, CA.

Gauter, K. 1999. *Fluid Multiphase Behavior in Ternary Systems of Near-Critical CO_2.* PhD dissertation, the Technical University of Berlin, Berlin, Germany.

Gauter, K., Heidemann, R.A., and Peters, C.J. 1999. Modeling of Fluid Multiphase Equilibria in Ternary Systems of Carbon Dioxide as the Near-Critical Solvent and Two Low-Volatile Solutes. *Fluid Phase Equilibria* **158-160:** 133-141.

Godbole, S.P., Thele, K.J., and Reinbold, E.W. 1995. EOS Modeling and Experimental Observations of Three-Hydrocarbon-Phase Equilibria. *SPE Reservoir Engineering* **10**(2): 101-108. SPE-24936-PA.

Gregorowicz, J. and de Loos, Th.W. 1996. Modeling of the Three Phase LLV Region for Ternary Hydrocarbon Mixtures With the Soave-Redlich-Kwong Equation of State. *Fluid Phase Equilibria* **118**(1): 121-132.

Guler, B., Wang, P., Delshad, M., Pope, G.A., and Sepehrnoori, K., 2001. Three- and Four- Phase Flow Compositional Simulations of CO_2/NGL EOR. Paper SPE 71485 presented at Annual Technical Conference and Exhibition, 30 September-3 October, New Orleans, Louisiana, USA.

Henry, R.L., and Metcalfe, R.S. 1983. Multiple-Phase Generation During Carbon Dioxide Flooding. *SPE Journal*, 23(04), 595-601.

Hornbrook, M.W., Dehghani, K., Qadeer, S., Ostermann R.D., and Ogbe, D.O., 1991. Effects of CO_2 Addition to Steam on Recovery of West Sak Crude Oil. *SPE Reservoir Engineering* **6**(3): 278-286. SPE-18753-PA.

Inaganti, M.S. 1994. *Miscible EOR Studies for Schrader Bluff Heavy Oil Reservoir, North Slope of Alaska: Slim Tube Displacement and Fluid Characterization.* Master thesis, University of Alaska Fairbanks, Alaska, U.S.A.

Johns, R.T. 1992. *Analytical Theory of Multicomponent Gas Drives with Two-Phase Mass Transfer.* PhD dissertation, Stanford University, Stanford, CA.

Johns, R.T. and Orr, Jr., F.M. 1996. Miscible Gas Displacement of Multicomponent Oils. *SPE Journal* **1**(1): 39-50. SPE-30798-PA.

Johns, R.T., Sah, P., and Sabramanian, S.K. 2000. Effect of Gas Enrichment Above the MME on Oil Recovery in Enriched-Gas Floods. *SPE Journal* **5**(3): 331-338. SPE-65704-PA.

Khataniar. S., Kamath, V.A., Patil, S.L., Chandra, S., and Inaganti, M.S., 1999. CO_2 and Miscible Gas Injection for Enhanced Recovery of Schrader Bluff Heavy Oil. Paper SPE 54085 presented at the SPE International Thermal Operations/Heavy Oil Symposium, Bakersfield, CA, USA.

Kumar, A. and Okuno, R. 2013. Characterization of Reservoir Fluids using an EOS Based on Perturbation from n-Alkanes, *Fluid Phase Equilibria* **358:** 250-271.

Lake, L.W. 1989. *Enhanced Oil Recovery,* Prentice-Hall, Inc., Upper Saddle River, N.J.

Lohrenz, J., Bray, B.C., and Clark, C.R. 1964. Calculating Viscosities of Reservoir Fluids from Their Compositions. *Journal of Petroleum Technology* **16**(10): 1171-1176.

Madarapu, R.R., Khataniar, S., and Dandekar, A.Y., 2002. A Simulation Study of Enhanced Recovery of Schrader Bluff Heavy Oil by Immiscible and Miscible Gas Injection. Paper SPE 76776 presented at the SPE Western Regional/AAPG Pacific Section Joint Meeting, 20-22 May, Anchorage, Alaska, USA.

Malik, Q.M. and Islam, M.R. 2000. CO_2 Injection in the Weyburn Field of Canada: Optimization of Enhanced Oil Recovery and Greenhouse Gas Storage with Horizontal Wells. Paper SPE 59327 presented at the SPE/DOE Improved Oil Recovery Symposium, 3-5 April, Tulsa, Oklahoma.

McGuire, P.L., Redman, R.S., Jhaveri, B.S., Yancey, K.E., and Ning, S.X. 2005. Viscosity Reduction WAG: An Effective EOR Process for North Slope Viscous Oils. Paper SPE 94914 presented at the SPE Western Regional Meeting, Mar 30 - Apr 01, 2005 2005, Irvine, California.

McGuire, P.L., Spence, A.P., and Redman, R.S. 2001. Performance Evaluation of a Mature Miscible Gasflood at Prudhoe Bay. *SPE Reservoir Evaluation & Engineering* **4**(4): 318-326. SPE-72466-PA.

Mckean, T.A.M., Thomas, A.H., Chesher, J.R., and Weggeland, M.C. 1999. Schrader Bluff CO_2 EOR Evaluation. Paper SPE 54619 presented at the SPE Western Regional Meeting, 26-27 May, Anchorage, Alaska.

Mohanty, K.K., Masino Jr., W.H., Ma, T.D., and Nash, L.J. 1995. Role of Three-Hydrocarbon-Phase Flow in a Gas-Displacement Process. *SPE Reservoir Engineering* **10**(3): 214-221. SPE-24115-PA.

Mushrif, S.H. 2004. *Determining Equation of State Binary Interaction Parameters Using K- and L-Points.* Master thesis, the University of Saskatchewan, Saskatoon, Canada.

Mushrif, S.H. and Phoenix, A.V. 2008. Effect of Peng-Robinson Binary Interaction Parameters on the Predicted Multiphase Behavior of Selected Binary Systems. *Industrial and Engineering Chemistry Research* **47**(16): 6280-6288.

Okuno, R. 2009. *Modeling of Multiphase Behavior for Gas Flooding Simulation.* PhD dissertation, the University of Texas at Austin, Austin, Texas.

Okuno, R., Johns, R.T., and Sepehrnoori, K. 2011. Mechanisms for High Displacement Efficiency of Low-Temperature CO_2 Floods. *SPE Journal* **16**(4): 751-767. SPE-129846-PA.

Okuyiga, M.O. 1992. Equation of State Characterization and Miscibility Development in a Multiple Phase Hydrocarbon System. Paper SPE 24937 presented at Annual Technical Conference and Exhibition, 4-7 October, Washington, D.C., USA.

Orr, Jr., F.M. 2007. *Theory of Gas Injection Processes.* Tie-Line Publications, Holte, Denmark.

Orr, Jr., F.M. and Jensen, C.M. 1984. Interpretation of Pressure-Composition Phase Diagrams for CO_2/Crude-Oil Systems. *SPE Journal* **24**(5): 485-497. SPE-11125-PA.

Peng, D.-Y. and Robinson, D.B. 1976. A New Two-Constant Equation of State. *Industrial & Engineering Chemistry Fundamentals* **15**(1): 59-64.

Perschke, D.R., Pope, G.A., and Sepehrnoori, K. 1989. Phase Identification During Compositional Simulation. SPE-19442-MS.

Peters, C.J. 1994. Multiphase Equilibria in Near-Critical Solvents. E. Kiran and J.M.H. Levelt Sengers (eds.), *Supercritical Fluids,* 117-145. Kluwer Academic Publishers.

Reid, T. 1994. *Study of Hydrocarbon Miscible Solvent Slug Injection Process for Improved Recovery of Heavy Oil From Schrader Bluff Pool, Milne Point Unit, Alaska.* Annual Report for DE-FG22-93BC14864 submitted to U.S. Department of Energy.

Roper, M. 1989. *An Experimental Study of CO_2/West-Sak-Crude-Oil Phase Behavior.* Master thesis, University of Alaska Fairbanks, Alaska, U.S.A.

Scott, R.L. and van Konynenburg, P.H. 1970. van der Waals and Related Models for Hydrocarbon Mixtures. *Discussions of the Faraday Society* **49:** 87-97.

Sharma, A.K., Patil, S.L., Kamath, V.A., and Sharma, G.D. 1989. Miscible Displacement of Heavy West Sak Crude by Solvents in Slim Tube. Paper SPE 18761 presented at the SPE California Regional Meeting held in Bakersfield, California, April 5-7.

Shelton, J.L. and Yarborough, L. 1977. Multiple Phase Behavior in Porous Media During CO_2 or Rich-Gas Flooding. *Journal of Petroleum Technology* **29**(9):1171-1178. SPE-5827-PA.

Shu, W.R. and Hartman, K.J. 1988. Effect of Solvent on Steam Recovery of Heavy Oil. *SPE Reservoir Engineering*, **3**(2): 457-465. SPE-14223-PA.

Solano, R., Johns, R.T., and Lake, L.W. 2001. Impact of Reservoir Mixing on Recovery in Enriched-Gas Drives Above the Minimum Miscibility Enrichment. *SPE Reservoir Evaluation & Engineering* **4**(5): 358-365. SPE-73829-PA.

Tanner, C.S., Baxley, P.T., Crump III, J.G., and Miller, W.C. 1992. Production Performance of the Wasson Denver Unit CO_2 Flood. Paper SPE 24156 presented at the SPE/DOE Enhanced Oil Recovery Symposium, 22-24 April, Tulsa, Oklahoma.

Uzunov, D.I. 1993. *Introduction to the Theory of Critical Phenomena.* Singapore: World Scientific Publishing.

van Konynenburg, P.H. 1968. *Critical Lines and Phase Equilibria in Binary Mixtures.* PhD dissertation, University of California, Los Angeles, California.

van Konynenburg, P.H. and Scott, R.L. 1980. Critical Lines and Phase Equilibria in Binary van der Waals Mixtures. *Philosophical Transactions of the Royal Society of London. Series A, Mathematical and Physicla Sciences* **298**(1442): 495-540.

Varotsis, N., Stewart, G., Todd, A.C., and Clancy, M. 1986. Phase Behavior of Systems Comprising North Sea Reservoir Fluids and Injection Gases. *Journal of Petroleum Technology*, **38**(12): 1221-1233.

Wang, Y., Lin, C.-Y., Bidinger, C., Muralidharan, V., and Lee, S.-T. 2003. Compositional Modeling of Gas Injection With Three Hydrocarbon Phases for Schrader Bluff EOR. Paper SPE 84180 presented at the SPE Annual Technical Conference and Exhibition, 5-8 October 2003, Denver, Colorado.

Wang, X. and Strycker, A. 2000. Evaluation of CO_2 Injection with Three Hydrocarbon Phases. Paper SPE 64723 presented at International Oil and Gas Conference and Exhibition in China, 7-10 November, Beijing, China.

Xu, Z. 2012. *Displacement Efficiency of Solvent Floods with Three Partially Miscible Phases*. M.Eng. project report, the University of Alberta, Edmonton, Alberta.

Yang, Q. 2006. *Automatic Development of Global Phase Diagrams for Binary Systems in Pressure-Temperature Space.* Master thesis, the University of Saskatchewan, Saskatoon, Canada.

Yuan, C. and Pope, G.A. 2012. A New Method to Model Relative Permeability in Compositional Simulators to Avoid Discontinuous Changes Caused by Phase-Identification Problems. *SPE Journal* **17**(4): 1221-1230. SPE-142093-PA.

Appendix A: Schematic of a Three-Phase Region Bounded by Critical Endpoint Tie Lines

A three-phase region has one degree of freedom at a given temperature and pressure for four components. Therefore, a three-phase region is a volumetric region in a quaternary diagram. The three-phase region consists of an infinite number of tie triangles. A tie triangle changes its shape and size within the three-phase region. Two tie triangles are shown to illustrate tie triangles exhibiting near-CEP behavior. A CEP is not a point in composition space, but is a tie line where two of the three phases are critical in the presence of the other noncritical phase. The UCEP typically occurs at higher solvent concentrations than the LCEP as observed for CO_2-n-alkane and n-alkane binaries. More details on three-hydrocarbon-phase behavior predictions are given in Okuno (2009).

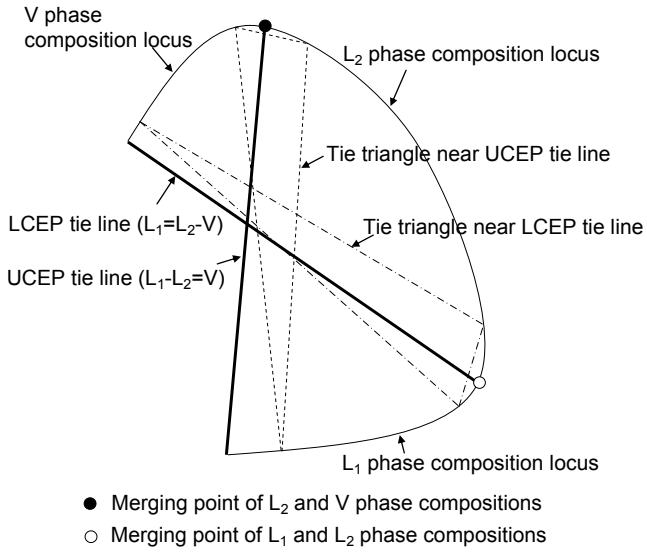

Figure A-1. Schematic of a three-phase region bounded by critical endpoint (CEP) tie lines for a quaternary system at a fixed temperature and pressure.

Appendix B: Mass Conservation on Multiphase Transitions

Conservation of mass for a component in N_P-phase flow through porous media is considered with the following assumptions:

- One dimensional flow with no gravity
- Constant temperature
- Change in pressure is small over the displacement length
- Constant porosity with time
- No diffusion/dispersion
- No chemical reaction or sorption on the solid phase
- No capillary pressure
- Local equilibrium
- Ideal mixing
- Laminar flow.

We then obtain

$$\frac{\partial C_i}{\partial t_D} + \frac{\partial F_i}{\partial x_D} = 0, \tag{B-1}$$

where t_D is a dimensionless time measured in pore volumes, x_D is a dimensionless distance from the injector, C_i is the overall volume fraction of component i, F_i is the overall fractional flow of component i, and i = 1, 2,…, (N_C - 1). C_i and F_i are given as

$$C_i = \sum_{j=1}^{N_P} S_j c_{ij}$$

$$F_i = \sum_{j=1}^{N_P} f_j c_{ij},$$

where S_j is the saturation of phase j, f_j is the fractional flow of phase j, and c_{ij} is the volume fraction of component i in phase j. A detailed derivation of Equation B-1 is given in Orr (2007).

The weak form of Equation B-1 is

$$\frac{d}{dt_D}\int C_i dV + \int n \cdot F_i dS = 0, \tag{B-2}$$

where V and S are the volume and surface area of the control volume of interest, respectively. n is the outward normal unit vector on surface S. Let us consider two consecutive gridblocks in a 1-D simulation model, where $N_P{}^U$ and $N_P{}^D$ phases are present in the upstream and downstream cells, respectively, at a given time. A uniform grid size of Δx_D is considered.

Suppose a phase transition between $N_P{}^U$ and $N_P{}^D$ propagates at a dimensionless velocity of $v_D = \Delta x_D/\Delta t_D$, where Δt_D is a certain time period in pore volumes. Discretization of Equation B-2 with Δx_D and Δt_D using the one-point upstream weighting for the flux term yields

$$v_D = \frac{\Delta x_D}{\Delta t_D} = \frac{F_i^U - F_i^D}{C_i^U - C_i^D}. \tag{B-3}$$

Rearrangement of Equation B-3 gives

$$\sum_{j=1}^{N_P^U}(v_D S_j^U - f_j^U)\underline{c}_j^U = \sum_{j=1}^{N_P^D}(v_D S_j^D - f_j^D)\underline{c}_j^D, \tag{B-4}$$

where $\underline{c}_j$ is a vector consisting of c_{ij}. Dividing Equation B-4 by (v_D-1),

$$\sum_{j=1}^{N_P^U}\gamma_j^U \underline{c}_j^U = \sum_{j=1}^{N_P^D}\gamma_j^D \underline{c}_j^D, \tag{B-5}$$

where $\gamma_j^U = \frac{v_D S_j^U - f_j^U}{v_D - 1}$ and $\gamma_j^D = \frac{v_D S_j^D - f_j^D}{v_D - 1}$. Note that $\sum_{j=1}^{N_P^U}\gamma_j^U = 1.0$ and $\sum_{j=1}^{N_P^D}\gamma_j^D = 1.0$.

Components are redistributed on a multiphase transition. Equation B-5 indicates that the redistribution of components must occur through an intersection of the N_P^U-phase tie-simplex extension and the N_P^D-phase tie-simplex extension for the phase transition between N_P^U and N_P^D phases. For example, a phase transition between two and three phases must occur through an intersection of the tie-line extension and the tie-triangle extension in composition space as shown in Figures 32 and 33.

A special case of multiphase transitions is a phase-transition shock in MOC solution of Equation B-1. The conservation equations for a shock are called the jump conditions. The jump conditions for a shock with a dimensionless velocity of Λ are

$$\Lambda = \frac{F_i^U - F_i^D}{C_i^U - C_i^D} \tag{B-6}$$

where i = 1, 2,…, (N_C - 1). Replacement of v_D in Equations B-4 and B-5 with Λ results in

$$\sum_{j=1}^{N_P^U} \gamma_j^U \underline{c}_j^U = \sum_{j=1}^{N_P^D} \gamma_j^D \underline{c}_j^D, \tag{B-7}$$

where $\gamma_j^U = \frac{\Lambda s_j^U - f_j^U}{\Lambda - 1}$ and $\gamma_j^D = \frac{\Lambda s_j^D - f_j^D}{\Lambda - 1}$. Note that $\sum_{j=1}^{N_P^U} \gamma_j^U = 1.0$ and $\sum_{j=1}^{N_P^D} \gamma_j^D = 1.0$.

Equation B-7 indicates that a shock must occur through an intersection of the tie simplex extension of (N_P^D - 1) dimensions and that of (N_P^U - 1) dimensions. For (N_P^D, N_P^U) = (1, 2), the above result reduces to the well-known result of Helfferich (1981) that a shock between one and two phases must occur on the tie-line extension. For (N_P^D, N_P^U) = (2, 3), a shock between two and three phases must occur through an intersection of the tie-triangle extension plane and the tie-line extension. Equation B-5 is of the identical form with the generalized jump conditions on multiphase transition presented in Equation B-7. The difference is that v_D in Equation B-5 is in general not the same as the shock velocity Λ in Equation B-7.

Equation B-5 is even more general, and applicable in mechanistic interpretation of mass transfer on a multiphase transition even in the presence of numerical dispersion

Appendix C: 1-D Convective Flow Simulator with No Volume Change on Mixing for Three-Hydrocarbon-Phase Flow

Mathematical Background

If the effects of dispersion and volume change on mixing can be both neglected, mass balance equation in 1-D flow reduces to equation B-1. Equation B-1 is often used for analytical and numerical solutions of gas injection problems (Helfferich 1979; Lake 1989; Johns 1992; LaForce and Johns 2005ab; LaForce et al. 2006; Orr 2007; LaForce et al. 2008ab; LaForce and Orr 2008; LaForce and Johns 2009; LaForce and Jessen 2010; LaForce 2012). In this research, the equation C-1 is solved explicitly by use of the single-point upstream weighting for the flux term, as described in Johns (1992) and Orr (2007), as follows:

$$(\mathrm{C_i})_{\mathrm{k}}^{\mathrm{n+1}} = (\mathrm{C_i})_{\mathrm{k}}^{\mathrm{n}} + (\Delta \mathrm{t_D}/\Delta \mathrm{x_D})[(\mathrm{F_i})_{\mathrm{k-1}}^{\mathrm{n}} - (\mathrm{F_i})_{\mathrm{k}}^{\mathrm{n}}], \quad \text{(C-1)}$$

where n is the time-step index and k is the gridblock index. $\Delta \mathrm{x_D}$ and $\Delta \mathrm{t_D}$ are the gridblock size and time-step size, respectively, which are uniform in this research. Equation C-1 is used in the simulations for chapter 4.

Initial and boundary conditions are required to complete the mathematical formulation. In this research, initial composition is constant throughout the reservoir with no gravity effects:

$$\underline{x_i}(x_D, 0) = \underline{x_i}^{init}, 0 \le x_D \le 1, i = 1, \cdots, N_c, \quad \text{(C-2)}$$

where $\underline{x_i}$ refers to the overall composition of component i.

The boundary conditions consist of impermeable condition, inflow condition, and outflow condition. Across the impermeable boundary, the component flux is zero:

$$\vec{n} \cdot \overrightarrow{F_{ij}} = 0, \quad \text{(C-3)}$$

where $\vec{n}$ is the unit vector normal to the boundary, $\overrightarrow{F_{ij}}$ is the flux term of component i in phase j. For the inflow condition, the injection composition is specified at a fixed pressure:

$$\underline{x_i}(0, t_D) = \underline{x_i}^{inj}, 0 \le t_D \le t_D^{end}, i = 1, \cdots, N_c, \quad \text{(C-4)}$$

where t_D^{end} is the end time of simulation. Similarly, for the outflow condition, constant bottom hole pressure is specified (Chang 1990). For the partial differential equation of equation (B-1), Orr (2007 "Theory of Gas Injection Processes" Pages 67-69 and 127-129) derived the component recovery at the outlet:

$$Q_i = C_i^{init} - C_i^{out} + t_D F_i^{out}, \tag{C-5}$$

where Q_i is the volume of component i recovered.

When the initial and boundary conditions are known, simulation starts:

Step 1: Calculate the overall composition of the first gridblock close to the injector:

$$z_i = \frac{C_i \rho_i}{\sum_{k=1}^{Nc} C_k \rho_k}, \tag{C-6}$$

where z_i is the overall composition of component i, C_i is the overall volume fraction of component i, ρ_i is the molar density of component i.

Step 2: The phase equilibrium calculation is conducted for the overall composition at a given gridblock and time step.

Step 3: When the number of equilibrium phases, their compositions and amounts are known from the flash calculation, phase properties, such as saturation, density, and viscosity can be calculated.

Step 4: Phase identification is called to label the phases.

Step 5: Assignment of phase relative permeabilities is performed.

Step 6: Calculation of the phase fractional flow is conducted.

Step 7: Calculate the component overall volume fraction for the next gridblock by use of equation (C-1).

Step 8: Calculate the overall composition for the next gridblock by use of equation (C-6).

Step 9: Repeat steps 2 to 8 until the end gridblock.

Step 10: Repeat steps 1 to 9 for the next time step until a specified ending time is achieved, such as 1.2 PVI.

As described above, phase equilibrium calculation is required to determine the number of equilibrium phases and their compositions for each gridblock at each time step. The algorithm that determines the number and compositions of phases must be robust and efficient. Phase equilibrium calculation requires the information about relationship between pressure, volume, temperature, and composition to calculate the component partial fugacity coefficients. Phase equilibrium calculation consists of stability analysis and flash calculation. The stability analysis is used to test whether the mixture of interest is stable or not. If it is unstable, a new phase is added for the subsequent flash calculation. If the stability analysis indicates that the mixture is stable, then no further calculation is performed. There are two conventional methods are for stability analysis: locations of stationary point and Gibbs free energy minimization.

If a mixture is indicated unstable, the number and compositions of phases must be calculated. As a result of phase equilibrium, the fugacity of component is equal in different phases, such as $f_i^{L1} = f_i^V = f_i^{L2}$ for three-phase equilibrium. The component fugacity is the effective pressure in accurate chemical equilibrium calculation. Two conventional methods have been developed in the literature. One is the flash formulation with successive substitution method. The other method is by use of minimization of the Gibbs free energy where the independent variables are the component mole numbers. The detailed step-by-step algorithms to implement the above methods for stability analysis and flash calculation have been presented in many publications. In this research, the thermodynamic model used is the Peng-Robinson (PR) EOS (Peng and Robinson 1976) with the van der Waals mixing rules. The multiphase behavior algorithms used are based on Perschke (1988) and Chang (1990) for sequential flash and stability calculations and Okuno et al. (2010) for constant-K flash.

Validation of 1-D Convective Simulator

In this thesis, the 1-D convective simulator is validated by comparing its simulation results for two-hydrocarbon-phase flow with the analytical solution. The first case is a ternary system that was used by Johns (1992). **Tables C-1 and C-2** show the fluid properties of this three-component system. **Fig. C-1** shows the ternary diagram for this three-component system at reservoir temperature of 160 ^{o}F and 1600 psia by use of the part of phase equilibrium calculation in the 1-D convective simulator. Johns (1992) also shows the similar diagram at page 94 of the dissertation. As shown in the figure, a wide two-phase region is observed indicating immiscible two-phase flow. **Figs. C-1 and C-2** show the CO_2 and C_{10} concentration at 0.25 PVI for the displacements of this three-component system by use of analytical solution and numerical simulations with 100, 1000, and 5000 gridblocks. As the number of gridblocks increases indicating a smaller numerical dispersion effect, the deviation between the numerical simulation and analytical solution diminishes.

Tables C-3 and C-4 shows another three-component system that has been presented by Orr (2007). Compared with the preceding ternary system, this ternary system shows a narrower two-phase region, as shown in **Fig. C-4**. This ternary diagram is created by use of the part of phase equilibrium calculation in the 1-D convective simulator. Orr (2007) also shows similar diagram at page 116 of the reference. **Fig. C-5** shows the gas saturation profiles at 0.25 PVI for the displacement of this ternary system by use of analytical solution and numerical simulations with 100, 1000, and 5000 gridblocks. As more gridblocks are used, the numerical solution approaches to the analytical solution. The effects of the numerical dispersion on simulation results are significant for the 100 blocks case.

Tables C-5 and C-6 show the fluid properties of a five-component system that was used in Johns (1992). These two tables are reflected by the table 7.1 in his dissertation. The analytical solution for the

displacement is shown in the table 7.2 in his dissertation, so it is not duplicated here.

Fig. C-6 shows the CO_2 at 0.25 PVI for the displacement of this five-component system by use of analytical solution and numerical simulations with 100, 1000, and 5000 gridblocks.. As shown in the figure, as the number of gridblock increases, the numerical result shows better agreement with the analytical solution, though some variations across the shocks are still observed.

Explanation of Simulation Files

Comp_Drop: this file is used to drop a component before phase equilibrium calculation when the mole fraction of this component is very small.

ComCompressibilityFactor: this file is used to calculate the compressibility factor of a given component.

CompViscosity: this file is used to calculate the component viscosity.

Data_Read: this file is used to read the data from the input file.

FUG_CAL: this file is used to calculate the component fugacity coefficient.

MAIN: this file is the main file where simulation starts from.

MultiPhase_Flash_SS: this file is to perform flash calculation by use of successive substitution method.

MultiphaseRachfordRice: this file is to solve the RachfordRice equation.

Partial_Lnf_nij: this file is to calculate the derivation of log(f) with respect to phase mole number.

PhaseIdentification: this file is to perform phase identification algorithm.

PhaseEquilibrium: this file is to initiate the phase equilibrium calculation.

PhaseViscosity: this file is to calculate the phase viscosity.

RelativePerm: this file is to calculate the phase relative permeability.

Z_CAL: this file is to calculate the phase compressibility factor.

Input.txt: this file is to contain the input data used for simulation.

Example of Input File

Number of component

4

Component Composition

0.3722 0.1063 0.3011 0.2204

Injection Composition

0.05 0.95 0.0 0.0

Tc

198.7611111 350.1777778 732.2777778 1092.944444

Pc

4.598297301 4.527509685 1.657989474 0.654061013

Vc

1.6763 2.9740 21.572 83.571

Acentric Factor

0.0193 0.1402 0.5574 1.1313

Molecular Weight

17.268 40.288 352.25 1052

Binary Interaction Coefficient

0.0000 0.0052 0.0000 0.1822

0.0052 0.0000 0.0050 0.1336

0.0000 0.0050 0.0000 0.0000

0.1822 0.1336 0.0000 0.0000

Tolerance for Stability Analysis

1e-7

Tolerance for Flash Splitting Calculation

1e-7

Maximum Number for Stability Analysis Iteration

1000

Maximum Number for Flash Splitting Calculation Iteration

1000

Stability Analysis Option

1

type 1: Stationary point

2: Minimization

Flash Calculation Option

1

type 1: Pure SS

2: ACSS

3: Minimization

Phase Identification Option

1

type 1: Conventional Method in UTCOMP

2: New Algorithm

Supercritical Phases

0

type 0: Supercritcal Phases are not included

1: Supercritical Phases are included

Methane Position

1

Maximum number of phases

3

Reservoir Temperature (Unit is K)

303.16

Reservoir Pressure (Unit is Mpa)

12.418

Time Step

0.0001

Size of grid block

10 1 10

Number of grid blocks in flow direction

1000

Porosity

0.4

Residual saturation

0.2 0.2 0.2

type 1: oil

2: gas

3: L2

Endpoint of each phase in Corey model

0.2 1.0 1.0

Exponent of each phase in Corey model

2.0 2.0 2.0

Tabulated pressure (Unit is Mpa)

10.3490666667 5.681

Table C-1. Fluid Properties for a Three-Component System (Johns 1992)

Component	Oil	Gas	Molecular weight	Tc (ºF)	Pc (psia)	Acentric factor	Vc (ft^3/lb-mol)
CO_2	0.0000	1.0	44.01	87.90	1071.0	0.2250	1.5060
CH_4	0.3000	0.0	16.04	-116.63	667.8	0.0104	1.5899
C_{10}	0.7000	0.0	142.29	652.10	305.7	0.4900	9.6610

Table C-2. Binary Coefficient for a Three-Component System (Johns 1992)

Kij	CO_2	CH_4	C_{10}
CO_2	0.0000	0.1000	0.0942
CH_4	0.1000	0.0000	0.0420
C_{10}	0.0942	0.0420	0.0000

Table C-3. Fluid Properties for a Three-Component System (Orr 2007)

Component	Oil	Gas	Molecular weight	Tc (ºF)	Pc (psia)	Acentric factor	Vc (ft^3/lb-mol)
CO_2	0.0000	1.0	44.01	87.90	1071.0	0.2250	1.5060
C_4	0.4759	0.0	58.12	305.65	550.7	0.2010	4.0828
C_{10}	0.5241	0.0	142.29	652.10	305.7	0.4900	9.6610

Table C-4. Binary Coefficient for a Three-Component System (Orr 2007)

Kij	CO_2	C_4	C_{10}
CO_2	0.0000	0.1257	0.0942
C_4	0.1257	0.0000	0.0080
C_{10}	0.0942	0.0080	0.0000

Table C-5. Fluid Properties for a Five-Component System (Johns 1992)

Component	Oil	Gas	Molecular weight	Tc (ºF)	Pc (psia)	Acentric factor	Vc (ft^3/lb-mol)
CO_2	0.0000	1.0	44.01	87.90	1071.0	0.2250	1.5060
CH_4	0.3000	0.0	16.04	-116.63	667.8	0.0104	1.5899
C_4	0.1795	0.0	58.12	305.65	550.7	0.2010	4.0828
C_{10}	0.2600	0.0	142.29	652.10	305.7	0.4900	9.6610
C_{20}	0.2605	0.0	282.56	920.91	161.4	0.9070	20.0000

Table C-6. Binary Coefficient for a Five-Component System (Johns 1992)

Kij	CO_2	CH_4	C_4	C_{10}	C_{20}
CO_2	0.0000	0.1000	0.1257	0.0942	0.0865
CH_4	0.1000	0.0000	0.0270	0.0420	0.0540
C_4	0.1257	0.0270	0.0000	0.0080	0.0000
C_{10}	0.0942	0.0420	0.0080	0.0000	0.0000
C_{20}	0.0865	0.0540	0.0000	0.0000	0.0000

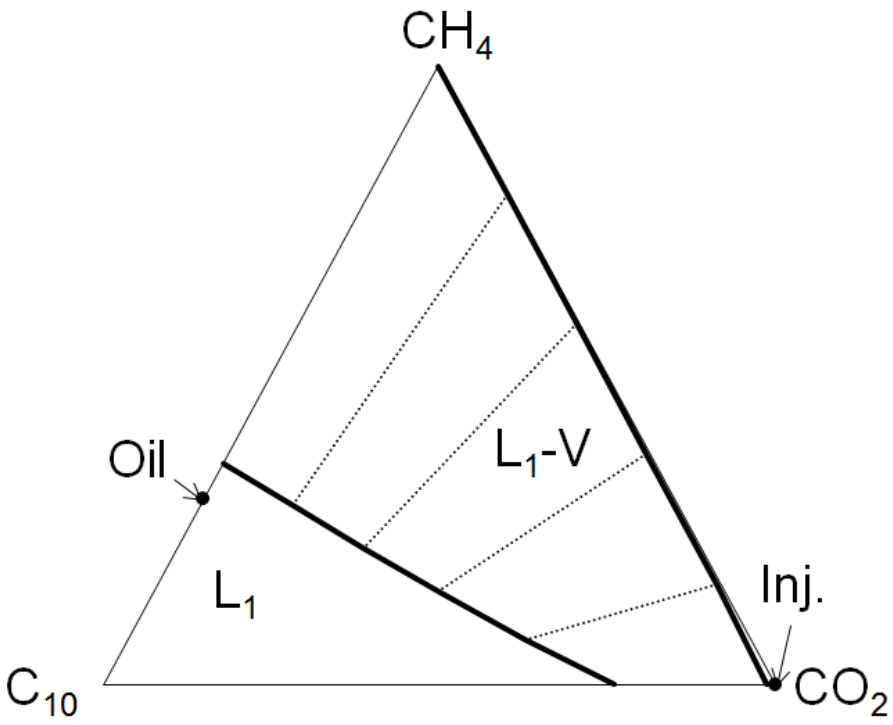

Figure C-2. Ternary diagram for the three-component system (Johns 1992) at reservoir temperature of 160 ºF and 1600 psia.

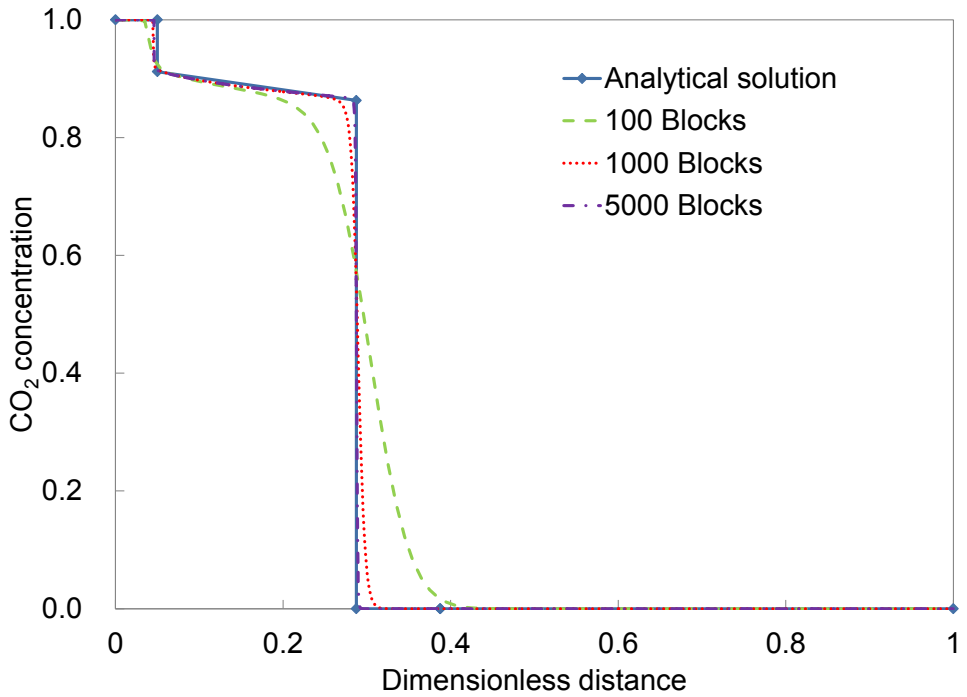

Figure C-2. CO_2 concentration profiles at 0.25 PVI for the displacements of the three-component system (Johns 1992) at reservoir temperature of 160 ºF and 1600 psia.

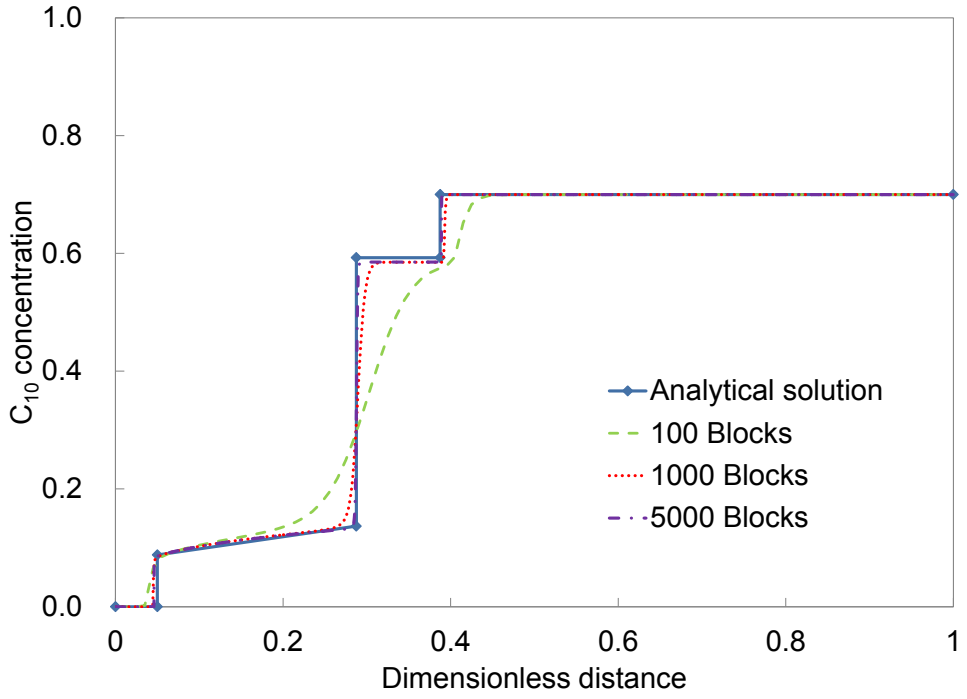

Figure C-3. C_{10} concentration profiles at 0.25 PVI for the displacements of the three-component system (Johns 1992) at reservoir temperature of 160 ºF and 1600 psia.

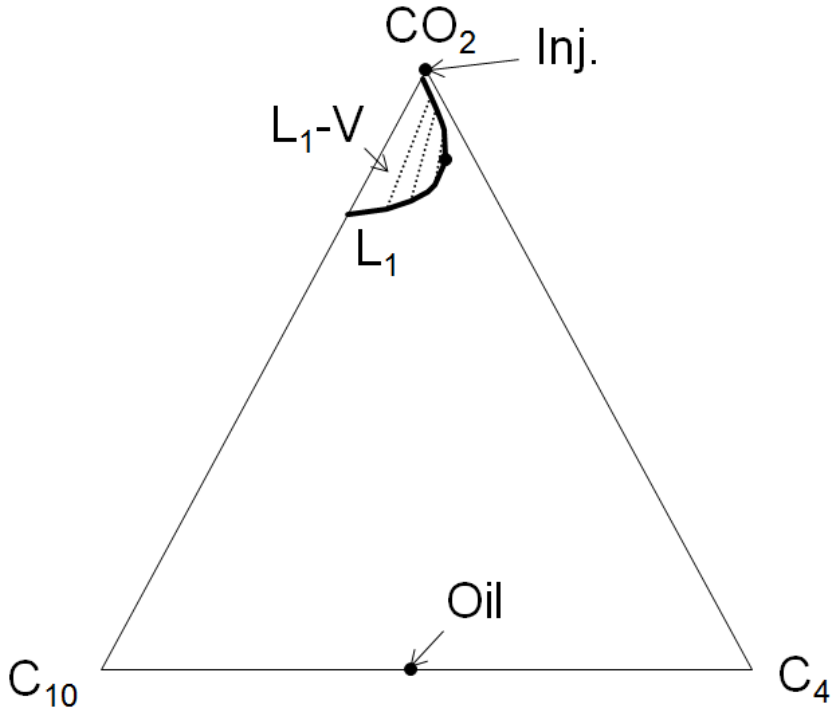

Figure C-4. Ternary diagram for the three-component system (Orr 2007) at reservoir temperature of 160 ºF and 1600 psia.

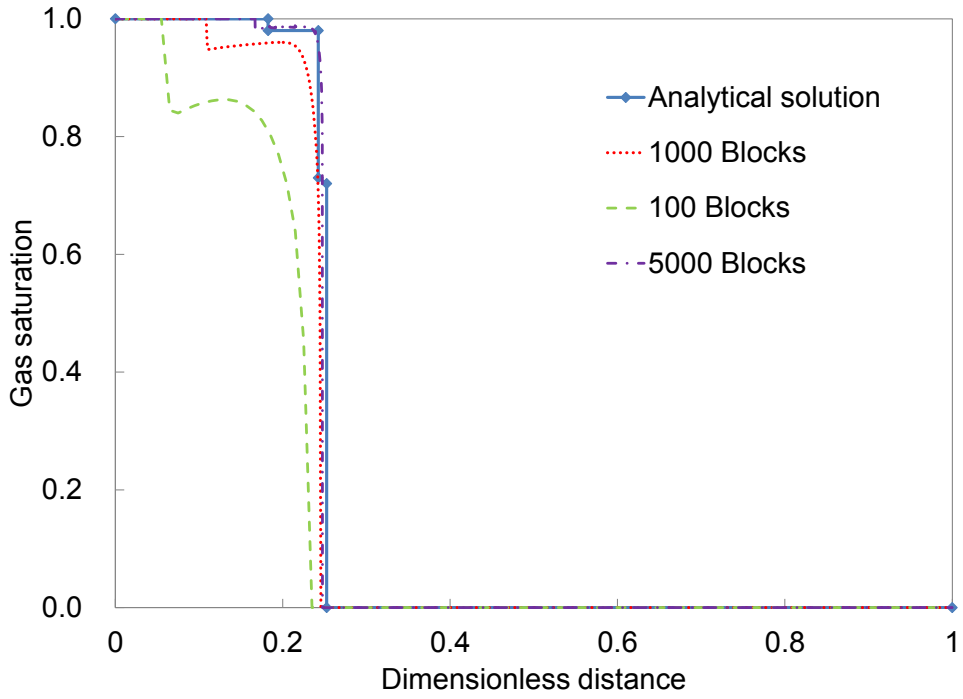

Figure C-5. Gas saturation profiles at 0.25 PVI for the displacements of the three-component system (Orr 2007) at reservoir temperature of 160 ºF and 1600 psia.

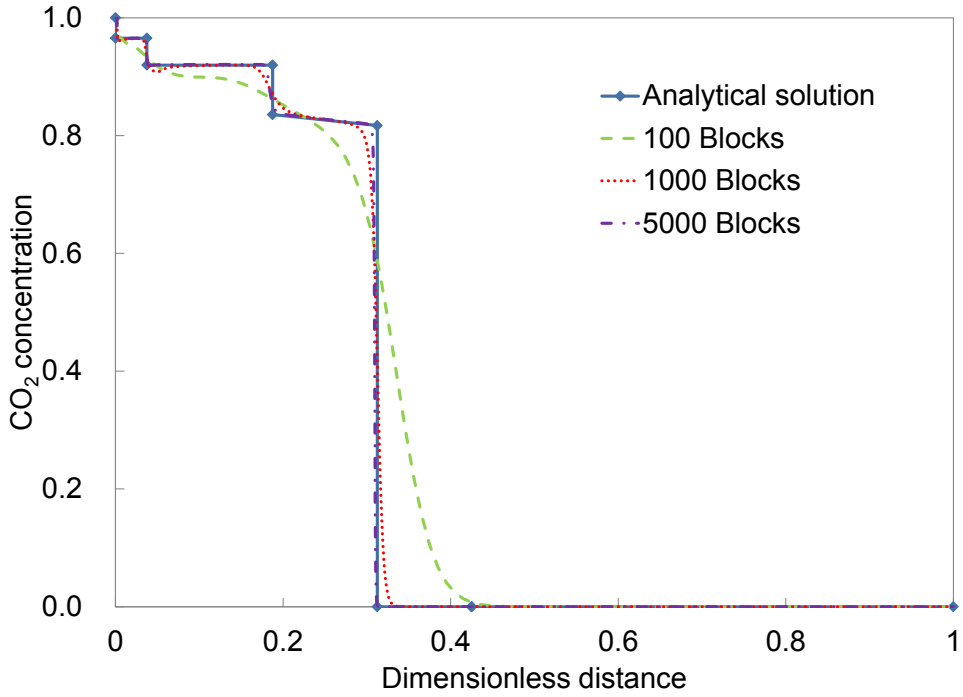

Figure C-6. CO_2 concentration profiles at 0.25 PVI for the displacements of the five-component system (Johns 1992) at reservoir temperature of 160 ºF and 1600 psia.

Appendix D: Phase Identification Algorithm

This appendix is to explain the tabulation procedure that is required prior to the phase identification algorithm. The step-by-step tabulation procedure is explained as follows:

Step 1: Initial simulation run is performed and terminated at a specified time, such as 0.1 PVI.

Step 2: Save $\underline{x}_j^{ini}$ (j $= L_1, V, and\ L_2$) in the 3-phase region from the initial run.

Step 3: Calculate the distances $d_j^{k,k+1}$ for the same phase in neighbouring triangles. Note that k is the index for the tabulated triangle.

Step 4: Calculate the length of all triangles' edge d_{m-n} that approaches to zero as to CEPs (i.e. d_{L1-L2} for LCEP, d_{L2-V} for UCEP). Note that m and n are phase indices. If direction=1, $d_{m-n} = d_{L2-V}$, if direction=2, $d_{m-n} d_{L1-L2}$. Initially, direction=1.

Step 5: Set $\underline{x}_j^{ini}$ as $\underline{x}_j^F$ for the triangle corresponding to the smallest d_{m-n}, Set $\underline{x}_j^{ini}$ as $\underline{x}_j^B$ for the triangle corresponding to the second smallest d_{m-n}. Note that F stands for 'front', and B stands for 'back'.

Step 6: Calculate the compositions of phases after moving a specified step, such as $\mathrm{l} = 0.01$, by use of the equation: $\underline{X}_j^N = \left(\underline{x}_j^F - \underline{x}_j^B\right) \frac{d_j^{F,B}}{l} + \underline{x}_j^F$. Note that N means 'next'.

Step 7: Calculate the composition of the central point $\underline{X}_c^N$ of the triangle determined by $\underline{X}_j^N$. Note that c here means 'central'.

Step 8: Phase equilibrium calculation is performed for $\underline{X}_c^N$. Save the phase compositions from flash calculation as $\underline{x}_j^N$.

Step 9: If the equilibrium phases are 3-phase region, go to step 10, otherwise, $\mathrm{l} = 0.1 * \mathrm{l}$, go to step 6.

Step 10: Calculate the distance d_{m-n}^N. Check if $d_{m-n}^N < \varepsilon$. Yes, go to step 11, otherwise, set $\underline{x}_j^F$ as $\underline{x}_j^B$, and set $\underline{x}_j^N$ as $\underline{x}_j^F$, go to step 6.

Step 11: If direction=1, set direction=2, go to step 4. If direction=2, go to step 12.

Step 12: Calculate the normal vector v^k of all triangles with unit length in the direction from UCEP to LCEP.

Step 13: Calculate the distances of all tabulated triangles to UCEP extension by $D^k = \left(L_1^k - L_1^{UCEP}\right) \cdot v^{UCEP}$.

Step 14: Calculate the rate of changes of tabulated triangles' edges by $u_{i-j}^k = |\frac{d_i^k - d_j^{k-1}}{D^k - D^{k-1}}|$.

Step 15: Define the composition region into two sub-sections: normal region for $\max\left(u_{i-j}^k\right) < \theta$ and refined region for $\max\left(u_{i-j}^k\right) > \theta$, where θ is a given value by user.

Step 16: Calculate the number of triangles in different regions by $N^T = (D^p - D^q)\rho^T$, where p, and q are index for triangles, ρ^T is the density of triangles in composition space. Note that ρ^T is different for normal region and refined region. ρ^T is a value given by user.

Step 17: Save the target triangles by the calculated number of triangles with equal space.